Christian-Albrechts-Universität zu Kiel

Master Thesis

Importance of the Stratosphere for North Atlantic Climate: A Model Study

Author:
Sabine Haase
945327

Supervisor:
Prof. Dr. Katja Matthes

Second Supervisor:
Prof. Dr. Mojib Latif

A thesis submitted in fulfillment of the requirements for the degree

Master of Science (M.Sc.)
Climate Physics: Meteorology and Physical Oceanography

Faculty of Mathematics and Natural Sciences
Christian-Albrechts-Universität zu Kiel

May 2014

Abstract

Anomalies of the winter stratospheric polar vortex can propagate down to tropospheric levels and modulate variability patterns, such as the North Atlantic Oscillation (NAO), which is the leading mode of variability in the North Atlantic (NA) sector during boreal winter. Not only is the NAO important for European winter weather conditions, but the NAO related heat and freshwater fluxes, and the associated changes in westerly wind over the NA region, also influence the formation of deep water masses in the NA basin and can thereby influence the variability of the Atlantic meridional overturning circulation (AMOC). The northward transport of heat by the AMOC is very important for European climate and the variability of the AMOC is therefore of great interest.

To investigate the role of the stratosphere for variability over the North Atlantic sector, two state-of-the-art ocean-atmosphere general circulation models are used: a high-top model (CESM1(WACCM)) and a low-top model (CCSM4). For each model, a Control simulation is analyzed and compared to a simulation under the Intergovernmental Panel on Climate Change (IPCC)'s RCP8.5 scenario, which represents the worst case scenario of greehouse gas (GHG) emissions.

Strong and weak vortex events are defined using the Northern Annular Mode (NAM), which is also used to describe the downward propagation of these anomalies. In the low-top model the downward propagation of stratospheric NAM anomalies to the surface is not well captured, but it is very well represented in the high-top model. This simulated difference in stratosphere-troposphere coupling is also reflected in the simulated effects of the stratosphere on the surface atmosphere and ocean parameters. While stratospheric vortex events in the high-top model are connected to NAO-like anomalies at the surface (in sea level pressure, turbulent heat flux and surface wind stress), in the low-top model this connection is less pronounced. No significant changes in mixed layer depth (MLD), which is used as an indicator for deep water formation, are found in the low-top model. The high-top model, on the other hand, shows a strong connection between stratospheric polar vortex events and MLD anomalies (strong (weak) vortex events are connected to deeper (shallower) MLDs), especially in the Labrador Sea, which is an important area of deep water formation in the NA region.

A cross-correlation analysis of the NAM/NAO and AMOC shows that the NAO leads the AMOC by about 4 years in both, the high and low-top model Control simulations. While the stratospheric NAM is also highly correlated with the AMOC in the high-top model (peaking when the NAM leads the AMOC by 2 years), there is no resonable correlation between NAM and AMOC in the low-top model. Under global warming the correlation between the AMOC and NAO decreases for both models. In the case of the high-top model, the NAM and AMOC are more strongly correlated than the NAO and AMOC under the GHG scenario.

Zusammenfassung

Anomalien im Polarwirbel können von der Stratosphäre in die Troposphäre propagieren. Damit beeinflussen sie die Dynamik in der Troposphäre, im Besonderen beispielsweise die Nord Atlantische Oszillation (NAO), die das dominante Variabilitätsmuster im Nordatlantik darstellt. Die Phase der NAO ist ausschlaggebend für das Wetter in Europa im Winter und beeinflusst ebenfalls die Verhältnisse von Wärme- und Frischwasserfluss als auch die Ausprägung des Westwindes über dem Nordatlantik. Diese Parameter sind wichtig für die Produktion von Tiefenwasser im Nordatlantik und haben dadurch ebenfalls einen Einfluss auf die Variabilität der Umwälzbewegung im Atlantik (AMOC - von (engl.) Atlantic Meridional Overturning Circulation). Die AMOC stellt einen sehr wichitgen Bestandteil im globalen Wärmetransport dar und prägt das Klima Europas, daher ist es von großem Interesse die Variabilität der AMOC besser zu verstehen.

Um die Rolle der Stratosphäre für die Variabilität über dem Nordatlantik zu untersuchen, werden hier zwei der aktuellsten gekoppelten Ozean-Atmosphären Modelle verwendet. Ein high-top Modell (CESM1(WACCM)), welches stratosphärische Prozesse sehr gut darstellt, und ein low-top Modell (CCSM4), welches die stratosphärische Dynamik nicht korrekt simuliert. Für beide Modelle wird eine Kontrollsimulation analysiert und mit einer Treibhausgassimulation (GHG - von (engl.) greenhouse gas) verglichen, die auf dem RCP8.5 Szenario beruht, dem aktuellen Worst-Case-Szenario des Intergovernmental Panel on Climate Change (IPCC).

Starke und schwache Polarwirbel werden mit Hilfe des Northern Annular Mode (NAM) definiert und die Propagation von Anomalien im Polarwirbel in Schichten der Troposphäre wird ebenfalls über die Anomalien der NAM beschrieben. Die Übertragung von stratosphärischen Anomalien in der NAM auf die oberflächennahen Schichten der Troposphäre werden im low-top Modell nicht erfasst. Im Gegensatz dazu wird diese Kopplung im high-top Modell sehr gut simuliert. Dieser Unterschied zwischen high- und low-top Modell findet sich auch in der Verbindung zwischen stratosphärischen Anomalien und oberflächennahen Parametern in der Troposphäre als auch im Ozean. Im high-top Modell stehen Anomalien im Polarwirbel in Verbindung mit NAO-ähnlichen Anomalien (im Druck auf Meereshöhe, Windstress und turbulenten Wärmefluss) an der Oberfläche. Diese Verbindung ist im low-top Modell weitaus schwächer ausgeprägt. Es findet sich im low-top Modell keine signifikante Verbindung zwischen Anomalien im Polarwirbel und der Tiefe der Durchmischungsschicht (MLD - von (engl.) Mixed Layer Depth) im Nordatlantik, die als Indikator für die Tiefenwasserproduktion verwendet wird. Dieser Zusammenhang ist hingegen im high-top Modell deutlich ausgeprägt, besonders in der Labradorsee, die ein wichtiges Gebiet für die Tiefenwasserproduktion im Nordatlantik darstellt. Starke Polarwirbel stehen hier in Verbindung mit einer tieferen MLD, schwache Polarwirbel hingegen mit einer flacheren MLD.

Eine Kreuzkorrelation von NAM/NAO und AMOC zeigt, dass die NAO in den Kontrollsimulationen von high- und low-top Modell die AMOC mit 4 Jahren anführt. Während die stratosphärische NAM im high-top Modell ebenfalls stark mit der AMOC korreliert, gibt es im low-top Modell keine Hinweise auf den Einfluss der Stratosphäre auf die AMOC. In den Treibhausgassimulationen nimmt die Korrelation zwischen NAO und AMOC für beide Modelle ab. Im Falle des high-top Modells ist die Korrelation zwischen NAM und AMOC im GHG Szenario stärker als die Korrelation zwischen NAO und AMOC.

Contents

List of Figures

Abbreviations

AMOC	**A**tlantic **M**eridional **O**verturning **C**irculation
AMV	**A**tlantic **M**ultidecadal **V**ariability
AO	**A**rctic **O**scillation
CESM	**C**ommunity **E**arth **S**ystem **M**odel
CICE	**C**ommunity **I**ce **C**od**E**
CAM	**C**ommunity **A**tmosphere **M**odel
CLM	**C**ommunity **L**and **M**odel
CMIP	**C**oupled **M**odel **I**ntercomparison **P**roject
CCSM	**C**ommunity **C**limate **S**ystem **M**odel
DJFM	**D**ecember-**J**anuary-**F**ebruary-**M**arch
DSOW	**D**enmark-**S**trait **O**verflow **W**ater
DWBC	**D**eep **W**estern **B**oundary **C**urrent
ECMWF	**E**uropean **C**entre for **M**edium-**R**ange **W**eather **F**orcasts
ERA	**E**CMWF **R**e-**A**nalysis
EOF	**E**mpirical **O**rthogonal **F**unction
ESM	**E**arth **S**ystem **M**odel
GCM	**G**eneral **C**irculation **M**odel
GHG	**G**reen**h**ouse **G**as
IR	**I**nfra**r**ed
IPCC	**I**ntergovernmental **P**anel on **C**limate **C**hange
ISOW	**I**celand-**S**cotland **O**verflow **W**ater
LANL	**L**os **A**lamos **N**ational **L**aboratory
LSW	**L**abrador **S**ea **W**ater
MLD	**M**ixed **L**ayer **D**epth
NA	**N**orth **A**tlantic
NAC	**N**orth **A**tlantic **C**urrent

NAM	**N**orthern **A**nnular **M**ode
NADW	**N**orth **A**tlantic **D**eep **W**ater
NAO	**N**orth **A**tlantic **O**scillation
NH	**N**orthern **H**emisphere
PNA	**P**acific **N**orth **A**merican Pattern
POP	**P**arallel **O**cean **P**rogram
RCP	**R**epresentative **C**oncentration **P**athways
SAT	**S**urface **A**ir **T**emperature
SLP	**S**ea **L**evel **P**ressure
SST	**S**ea **S**urface **T**emperature
TMS	**T**urbulent **M**ountain **S**tress
UV	**U**ltra**v**iolet
WACCM	**W**hole **A**tmosphere **C**ommunity **C**limate **M**odel
WMO	**W**orld **M**eteorological **O**rganisation

Chapter 1

Introduction

The connection between stratosphere and troposphere has become an intensively studied research field in the last decade. Already in the 1980s a mechanism for the downward propagation of zonal mean zonal wind anomalies within the stratosphere was suggested by *Hines* [1974]. This led to the question whether stratospheric anomalies could as well propagate into the troposphere and influence its variability. In 1994/95 *Baldwin et al.* [1994] and *Perlwitz and Graf* [1995] correlated stratospheric anomalies to the North Atlantic Oscillation (NAO) and with the work of *Baldwin and Dunkerton* [1999, 2001] the downward propagation of stratospheric anomalies into tropospheric layers was demonstrated.

The stratospheric influence on tropospheric conditions is now considered an important part of the climate system and great effort is taken in investigating this relationship. By incorporating atmospheric model components into general circulation and earth system models (GCMs and ESMs) that are capable of representing stratospheric chemistry and dynamics, the representation of the Earth's climate in these models is improved. Also the stratospheric effect on weather prediction became an important issue (e.g. *Baldwin et al.* [2003]).

Recently, *Reichler et al.* [2012] connected stratospheric anomalies to the oceanic circulation, arguing that stratospheric anomalies, which influence surface conditions in an NAO-like way, can influence the strength of the overturning circulation in the Atlantic Ocean. They used the fact that the connection between an NAO-like heat flux forcing and Atlantic Meridional Overturning Circulation (AMOC) varibility was already shown using ocean models by *Eden and Jung* [2001] and *Eden and Willebrand* [2001]. In these

models the NAO led the AMOC by 5 to 10 years. *Reichler et al.* [2012] used a coupled GCM that is regarded as a low-top model, a model that does not represent stratospheric dynamics and chemistry in a reasonable way as its upper boundary is too low to allow for the observed radiative processes or for a reasonable wave-mean flow interaction.

In this thesis the connection between stratospheric polar vortex events and the variability of North Atlantic climate and oceanic circulation shall be investigated using a high-top model, that does represent stratospheric dynamics and includes fully-interactive chemistry. To better isolate the effect of the stratosphere, a low-top model is used for comparison. Additionally, a climate change scenario is investigated to classify the stratospheric influence on the North Atlantic climate under global warming.

The following Chapter introduces the stratospheric, tropospheric and oceanic dynamics that are important for the connection between these compartments. It is followed by a description of the climate models, the data and the methods used in this work. Chapter 4 gives an overview about how the dynamics introduced in Chapter 2 are represented in the models compared to reanalysis and observations. Afterwards the connection between the stratosphere and different atmospheric surface parameters and oceanic variables in the models is shown. A discussion at the end summarizes and concludes the results.

Chapter 2

Introduction to North Atlantic Climate Variability

Anomalies in the winter stratospheric polar vortex can propagate down into the troposphere and influence the circulation at the surface (*Baldwin and Dunkerton* [2001]). This has an effect on the main pattern of variability in the North Atlantic sector, the North Atlantic Oscillation, that is known to influence the circulation in the North Atlantic Ocean, which is of great importance for the world wide oceanic heat transport.
This chapter introduces the basic atmospheric and oceanic features important for North Atlantic mean climate and its variability. First an overview about the mean tropospheric and stratospheric dynamics is given and the connection between stratosphere and troposphere is described. The Atlantic Meridional Overturning Circulation is introduced and causes for its variability revealing the importance of the troposphere are given.

2.1 Stratospheric Dynamics

2.1.1 Temperature Structure of the Earth's Atmosphere

The atmosphere is separated into different layers based on its vertical temperature characteristics. Figure 2.1 shows an average profile of the standard atmosphere. From the Earth's surface up to about 12 km height atmospheric temperatures decrease. This lowest layer of the Earth's atmosphere is referred to as the troposphere, its upper boundary is

the tropopause. The decrease in temperature with height in this layer is mainly due to the emission of infrared (IR) radiation by water vapor and clouds.

The stratosphere is the second layer of the Earth's atmosphere. It covers the altitude range from about 12 km (tropopause) to about 50 km height (stratopause). The temperature in the stratosphere increases with height peaking at the stratopause (Figure 2.1). The increase in temperature is due to the presence of ozone (O_3) in the stratosphere

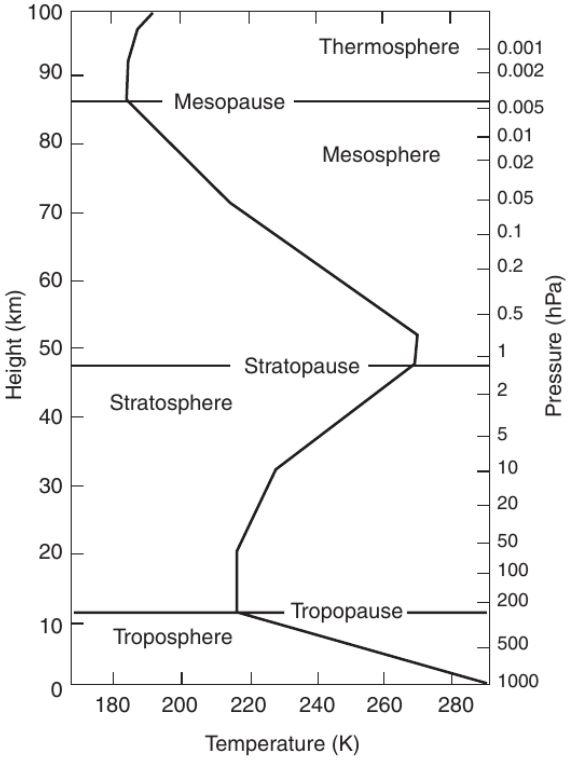

FIGURE 2.1: Midlatitude mean temperature profile based on the U.S. Standard Atmosphere (1976) from *Holton* [2004].

with a maximum at about 10 hPa (*Brasseur and Solomon* [2005]). It absorbs high energetic solar irradiance, i.e. ultraviolet (UV) radiation, and thereby leads to radiative heating. As shown in Figure 2.2 ozone is the major contributor to radiative heating in the stratosphere. The ozone layer is therefore not only important for its well known effect of protecting the biosphere from UV radiation at the surface but also plays an important role in stratospheric dynamics as the stratospheric temperature profile is directly influenced by the distribution and concentration of ozone in the stratosphere (*Andrews et al.* [1987]). Radiative cooling in the stratosphere is partly due to the presence of water vapor and ozone but mainly due to that of carbon dioxide (CO_2) (Figure 2.2). Therefore, the current anthropogenic increase of atmospheric CO_2 concentrations leads to a cooling in

the stratosphere, in contrast to the troposphere, where the net effect of CO_2 is a warming one (*IPCC* [2013]).

The layer above the stratosphere, referred to as the mesosphere (50 to about 85 km), is again characterized by a decrease in temperature. In this layer ozone concentrations decrease with height leading to a reduced radiative heating and therefore to the observed temperature decrease. Above the mesopause, the thermosphere follows. It is characterized by a rapid temperature increase with height due to the photodissociation of oxygen and nitrogen (*Brasseur and Solomon* [2005]).

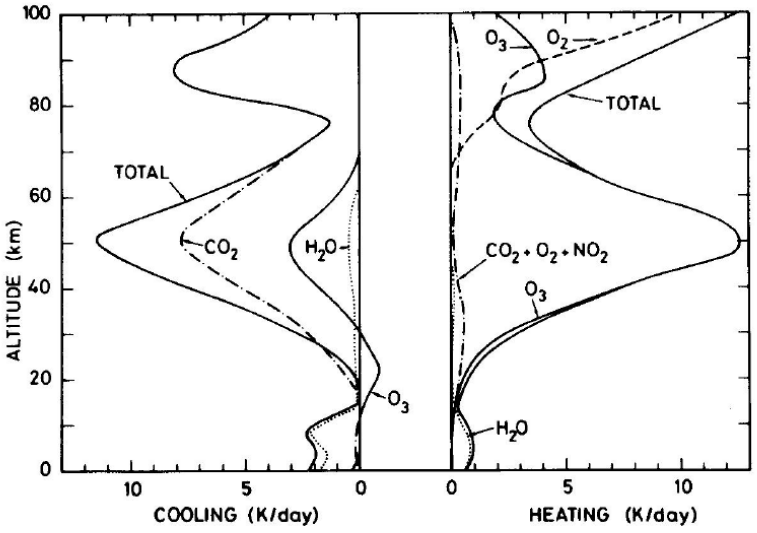

FIGURE 2.2: Vertical distribution of cooling due to emission of infrared radiation (left) and heating due to absorption of solar radiation (right) from *Brasseur and Solomon* [2005].

2.1.2 Characteristics of the Stratosphere

As already mentioned the stratospheric temperature profile is largely influenced by trace gases, especially ozone and carbon dioxide. Stratospheric temperatures increase with height leading to a strong stratification (Figure 2.1). Considering the meridional dimension as well, Figure 2.3 shows that there are significant differences in the meridional distribution of stratospheric temperatures between tropics, middle latitudes and high latitudes as well as between the winter and the summer hemisphere. In the lower stratosphere a distinct minimum in temperature is found over the equatorial region (in the tropical tropopause layer), whereas in the middle and upper stratosphere temperatures gradually decrease from the summer to the winter pole.

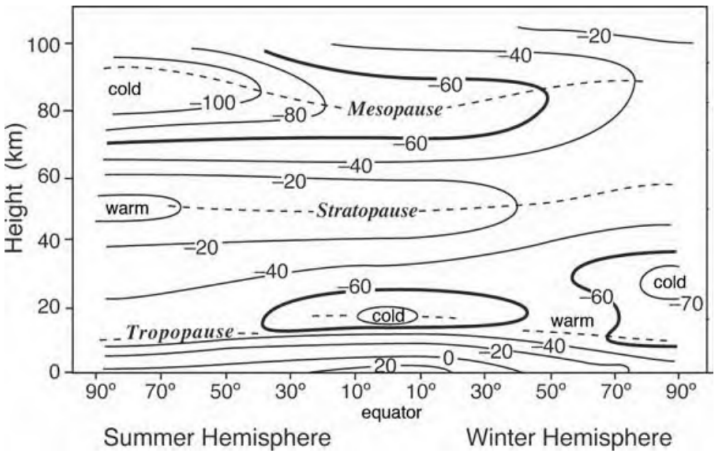

FIGURE 2.3: Observed, zonally averaged temperature distribution from the surface to a height of 100 km. Altitudes at which the vertical temperature gradient vanishes are marked by dotted lines. The -60°C isopleth is represented by the thick line. Figure from *Marshall and Plumb* [2008].

The large scale temperature gradients on the meridional plane (and the accompanied pressure gradients) lead to the establishment of a zonal mean wind field following geostrophic balance (*Andrews et al.* [1987]), which is shown in Figure 2.4. The middle and upper stratosphere are characterized by mean zonal mean westerlies in the winter hemisphere and mean zonal mean easterlies in the summer hemisphere. The lower stratosphere is characterized by a zonal wind pattern that is more or less symmetric around the equator. It is dominated by westerly flow on both hemispheres (compare Figure 2.4 below 20 km height). This symmetric structure of westerly flow reaches down into the troposphere and

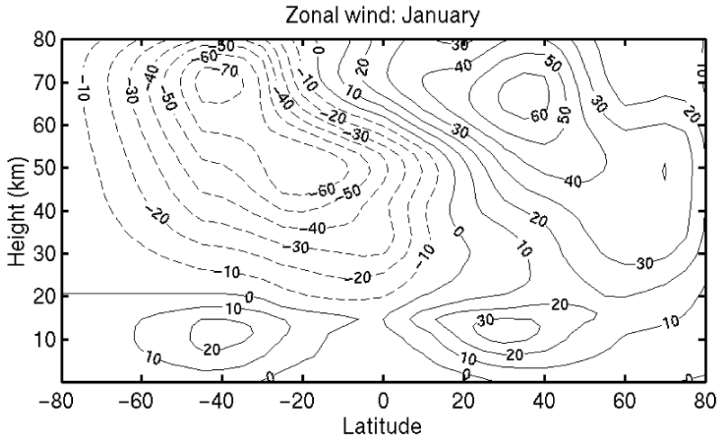

FIGURE 2.4: Observed monthly and zonally averaged zonal wind in [m/s] for January. Figure from *Holton* [2004].

peaks in the tropospheric jet streams.

The strong zonal wind field in the stratosphere is accompanied by a residual flow - the global meridional circulation. The meridional circulation is driven by extratropical wave forcing (termed the *extratropical pump* by *Holton et al.* [1995]). It is characterized by an ascending of air masses over the tropics, poleward motion and a descending of air masses over the poles during autumn and spring. During winter and summer the upward motion is shifted towards the summer pole and the meridional motion is predominantly directed towards the winter pole. This circulation is called Brewer-Dobson-Circulation (BDC) after *Brewer* [1949] and *Dobson* [1956] who found that a meridional transport would be necessary to establish the observed tracer distribution in the stratosphere. The main characteristics and ongoing research on the BDC have been recently summarized in a review paper by *Butchart* [2014].

In the winter hemisphere the establishment of a strong westerly flow leads to the development of a stratospheric jet at high latitudes also called the *polar night jet* as it developes only during polar winter. This jetstream builds the outer edge of the polar stratospheric vortex (which is centered at the pole) separating polar air masses from lower latitude air masses.

The winter stratosphere is exposed to much higher variability compared to the summer stratosphere. This is due to wave-mean flow interaction, which is dependent on strength and sign of the mean zonal wind field. Following *Charney and Drazin* [1961], stationary planetary waves can only exist in a westerly wind field with wind speeds lower than a critical value. Therefore, stationary planetary waves can only propagate into stratospheric layers during the extended winter season (November to March) as the mean zonal windfield in the stratosphere is westerly only during that time.

The dissipation of upward propagating planetary waves disturbes the mean zonal wind field and thereby increases variability. It can lead to a shift and/or to a decrease in strength of the jetstream and therefore to a disturbance of the stratospheric polar vortex culminating in its breakdown. The breakdown is either hallmarked by a displacement or by a splitting of the vortex (*Andrews et al.* [1987]). It takes only a few days and is accompanied by dynamical heating. Therefore, the breakdown of the winter stratospheric polar vortex is referred to as a sudden stratospheric warming (SSW). The occurence of a stratospheric warming was first discovered by *Scherhag* [1952].

There are different kinds of SSWs, described for example in *Labitzke and Naujokat* [2000]. A warming event in general as defined by the World Meteorological Organisation (WMO), for example in *Andrews et al.* [1987], is an event for which the latitudinal gradient in zonal

mean temperature between 60°N and the pole is positive at 10 hPa or below (i.e. the zonal mean temperature at 10 hPa increases from 60°N towards the pole). If, additionally, the zonal mean wind reverses its sign at 60°N and 10 hPa, i.e. changes from westerly to easterly, the event is called a *major warming*. If the westerly flow at 60°N and 10 hPa is preserved, the event is called a *minor warming*. The transition of the zonal mean flow from winter (westerly) to summer (easterly) conditions is called the *final warming*. The WMO definition of SSWs has been adapted, extended or simplified (see for example *Charlton and Polvani* [2007]). Depending on the research question also other defintions to describe such events or anomalies of the stratospheric polar vortex strength in general can be used. A widespread method, also used in this thesis, is to define weak and strong vortex events, where an SSW would be part of the weak vortex events, using the Northern Annular Mode or Arctic Oscillation patterns. This method is described in detail in Section 3.3.1.

As already mentioned by *Hines* [1974] the interaction between upward propagating planetary waves and the zonal mean flow leads to a downward phase propagation of zonal mean zonal wind anomalies within the stratosphere. The question arose whether the anomalies in zonal mean zonal wind can also propagate as far as to reach the troposphere and influence conditions there. *Baldwin et al.* [1994] and *Perlwitz and Graf* [1995] connected anomalies in the northern winter hemisphere polar vortex with anomalies in the troposphere. Both found a correlation between the North Atlantic Oscillation (NAO - see Section 2.2.1) in the troposphere and the strength of the stratospheric polar vortex. Their analyses did not allow to judge whether this relation was forced by the stratosphere or the troposphere. In 1999, Baldwin and Dunkerton used the definition of the Arctic Oscillation (AO - see Section 3.3.1) to investigate the coupling between stratosphere and troposphere. They found that AO signals can propagate down from the stratosphere into the troposphere (Figure 2.5) and concluded that stratospheric events are precursors to tropospheric events when the stratospheric AO amplitude is large and persistent (*Baldwin and Dunkerton* [1999]). This is valid only for low-frequency variability (timescales larger than a month) and not for day-to-day variability.

Baldwin and Dunkerton [2001] extended this analysis using the AO index for characterizing the strength of the polar stratospheric vortex. They defined weak and strong vortex events and used composite analysis to show the downward propagation of the signal as well as the strong persistence of the anomalies (of about 60 days) in the troposphere. They did also find a shift in the probability density function of the NAO connected to

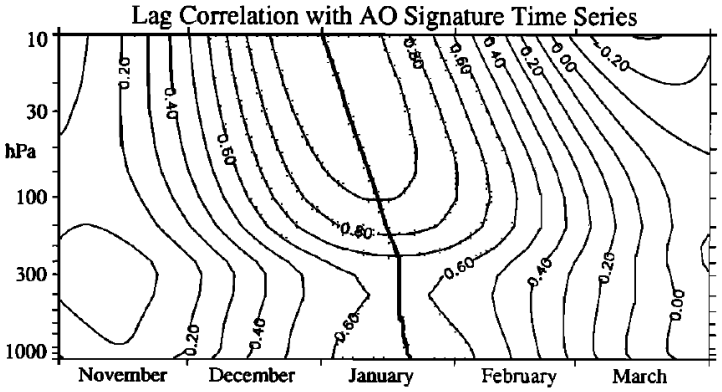

FIGURE 2.5: Correlations between the 90-day low-pass filtered AO timeseries at 10 hPa on January 1^{st} with the AO timeseries at all levels for November to March. Figure from *Baldwin and Dunkerton* [1999].

stratospheric polar vortex events. For strong (weak) vortex events the possibility of a positive (negative) NAO increases. This is consistent with the findings of *Baldwin et al.* [1994] and *Perlwitz and Graf* [1995], only now the direction of the forcing is downward (from the stratosphere to the troposphere). This finding is of great importance for the coupling between stratosphere and ocean and will therefore also be analyzed in this work.

2.2 Troposphere-Ocean-Interaction

As the troposphere is the communicating layer between stratosphere and ocean its dynamics and variability are of great importance for analyzing the stratospheric impact on the North Atlantic circulation. It will therefore shortly be described in the following.
The troposphere is a highly dynamic layer of the atmosphere. Tropospheric dynamics are driven by the absorption of solar radiation at the surface as well as within the tropospheric column mainly by water vapor and clouds but also influenced by greenhouse gases (GHGs) and aerosols. A temperature gradient between equator and pole on both hemispheres drives a meridional circulation (from equator to pole) that is devided into two thermally direct circulation cells (Hadley cell in the tropics and polar cell at high latitudes) and one thermally indirect circulation cell in the middle latitudes (the Ferrel cell). Between Hadley and Ferrel cell a westerly wind jet stream develops - the subtropical jet. Its maximum is located at about 30° latitude and 200 hPa height of the respective winter hemisphere (Figure 2.4). On the summer hemisphere the jet is shifted poleward

and the amplitude is smaller compared to the winter hemisphere. Although the maximum is located at about 10 km height the westerly orientation of the wind field is sustained at lower altitudes. Therefore, especially during winter, the zonal mean zonal wind in the middle latitudes is characterized by westerly flow.

As the troposphere is connected to the Earth's surface, it is also influenced by boundary processes exchanging momentum, heat and trace species. The evaporation of water is an important feature of energy transfer between atmosphere and land as well as between atmosphere and ocean. The ocean does also play an important role in heat redistribution, especially at low latitudes. It is known to integrate high-frequency variability of the atmosphere serving as a long-term memory of tropospheric conditions that can feed back on the atmosphere, e.g. through reemergence of previous winter conditions (*Alexander and Deser* [1995]) but also on longer timescales for example through the variability of the meridional overturning circulation (MOC) in the ocean.

The next sections will focus on tropospheric and oceanic conditions in the North Atlantic (NA) sector as this is the region of interest in this thesis: the North Atlantic Oscillation (NAO) and the Atlantic Meridional Overturning Circulation (AMOC) are described and a link between both is drawn.

2.2.1 North Atlantic Oscillation

The North Atlantic Oscillation (NAO) is the leading mode of sea level pressure (SLP) anomalies in the North Atlantic (NA) region during winter. It was first described by *Walker and Bliss* [1932]. Since then a tremendous amount of research addressing the definition of the NAO and its influences on European weather was carried out (for a review see *Hurrell et al.* [2003]).

The NAO can be regarded as the Atlantic part of a seesaw in atmospheric pressure between polar and middle latitudes on the Northen Hemisphere (*Thompson et al.* [2003]). The hemispheric mode is characterized by the Arctic Oscillation (or Northern Annular Mode), which is described in more detail in Section 3.3.1. This pattern does also affect higher altitudes and is therefore of importance considering the connection between stratospheric levels and the surface anomaly pattern (the NAO).

There are basically three different methods to define the spatial signal of the NAO: Empirical Orthogonal Function (EOF) analysis, one-point correlation and cluster analysis. An overview of these methods can be found for instance in *Hurrell and Deser* [2010]. The

according timeseries (an NAO index) can be derived from the results of an EOF analysis as well as from a cluster analysis. It can also be defined as a station based index, like, for example, in *Hurrell* [1995], who defined the winter mean NAO index as the difference of the normalized December to March (DJFM) SLP difference between Lisbon (Portugal) and Akureyri (Iceland).

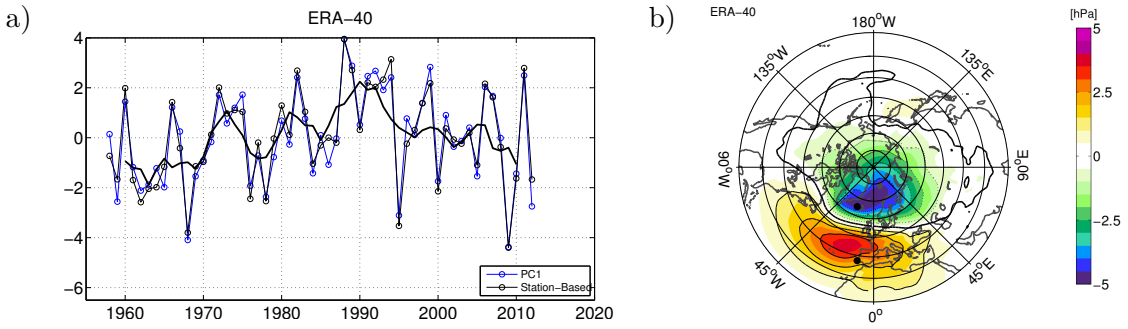

FIGURE 2.6: NAO in ERA-40 data. a) Station-based (black), as well as EOF-based (blue) indices are depicted. The 5-year running mean is calculated from the station based index (bold line), b) NAO pattern as received from regression of the EOF-based NAO index onto NH SLP data in [hPa]. Contour interval is 0.3 hPa with negative values being represented by dashed lines. The black dots indicate the grid point locations used to calculate the station-based NAO Index.

Figure 2.6 features an example for the NAO index and NAO SLP pattern for 1958 to 2012 in ERA-40 data (for more details on ERA-40 see Section 3.2). The NAO index (Figure 2.6a) is shown for a station based and for an EOF based analysis. For the EOF analysis the NA region between 20 and 70°N and between 90°W and 40°E (*Hurrell et al.* [2003]) is used. The resulting pattern explains about 50% of the NA variability. The difference between the methods is very small, suggesting that the NAO index is not sensitive to the method. The SLP pattern (Figure 2.6b) is derived by projecting the northern hemisphere SLP anomaly onto the EOF derived NAO index. It shows that a positive NAO (positive NAO index) is characterized by a negative SLP anomaly over the Greenland Sea and by a positive SLP anomaly over the middle latitude NA region covering also southern Europe. So, during a positive (negative) phase of the NAO the SLP gradient between Iceland and Portugal is stronger (weaker) than usual. This leads to stronger (weaker) than normal westerlies over the NA ocean, which is connected to a shift in the stormtrack influencing winter weather conditions over Europe (*Visbeck et al.* [2001], *Hurrell and Deser* [2010]). During the positive (negative) phase of the NAO the anomalous westerly flow transports relatively warm (cold) and moist (dry) air over central and northern Europe, leading to mild (cold) and wet (dry) winter conditions in northern Europe (Figures 2.7 and 2.8,

Hurrell et al. [2003]). Southern Europe is characterized by drier (wetter) than normal

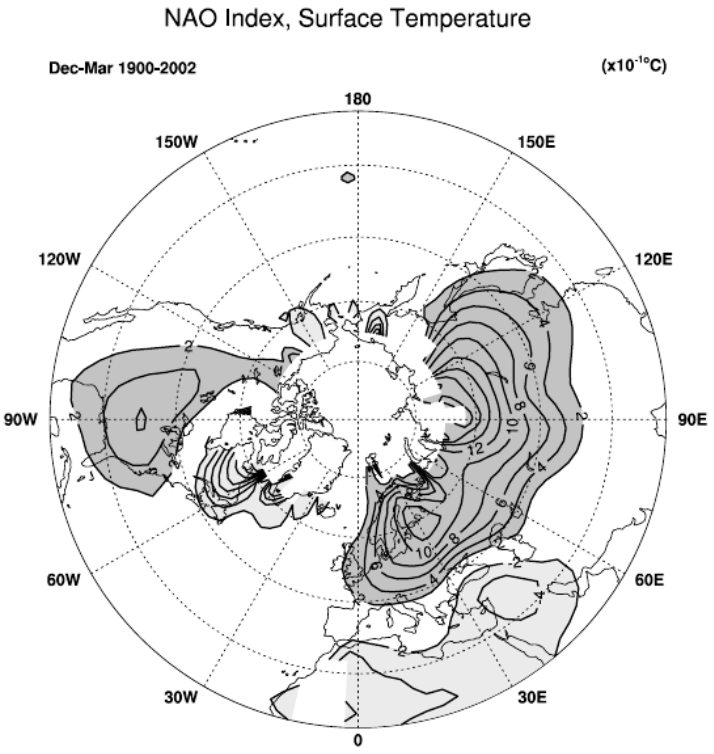

FIGURE 2.7: NAO surface air temperature pattern in [10^{-1} °C] corresponding to a positive phase of the NAO index. The contour increment is 0.2°C. Temperature changes greater than 0.2°C are indicated by dark shading, and those smaller than -0.2°C are indicated by light shading. Regions of insufficient data are not contoured, and the zero contour has been excluded. Figure from *Hurrell et al.* [2003].

conditions. An unusual northerly flow over Greenland and Northeast Canada during the positive phase of the NAO transports cold air masses southward influencing sea surface temperatures (SSTs) in the western Atlantic, especially over the Labrador Sea region (*Hurrell et al.* [2003]). Apart from that temperature anomaly, evaporation anomalies exceed precipitation anomalies over the Labrador Sea region during a positive NAO. A negative NAO phase is characterized by higher than normal temperatures and by a lower than normal evaporation minus precipitation anomaly over the Labrador Sea region (Figures 2.7 and 2.8).

The sea surface temperature (SST) pattern connected to the NAO is characterized by a tripolar structure (Figure 2.9, *Visbeck et al.* [2003]). During a positive phase of the NAO positive SST anomalies are found between 28°N and 45°N, while south and north of these latitudes negative anomalies are found. This pattern explains 8 to 25 % of the winter SST variability.

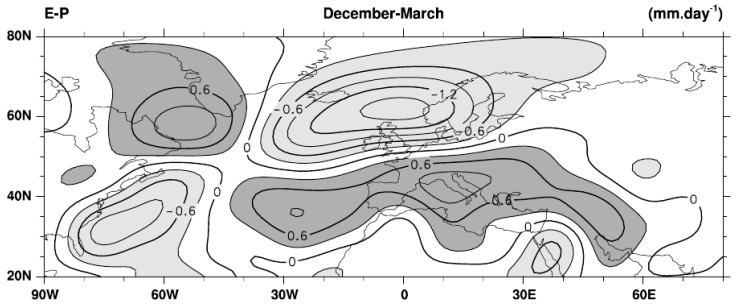

FIGURE 2.8: NAO evaporation (E) minus precipitation (P) pattern corresonding to a positive phase of the NAO. The contour increment is 0.3 $^{\text{mm}}/_{\text{day}}$, differences greater than 0.3 $^{\text{mm}}/_{\text{day}}$ (E exceeds P) are indicated by dark shading, and differences less than -0.3 $^{\text{mm}}/_{\text{day}}$ (P exceeds E) are indicated by light shading. Figure from *Hurrell et al.* [2003].

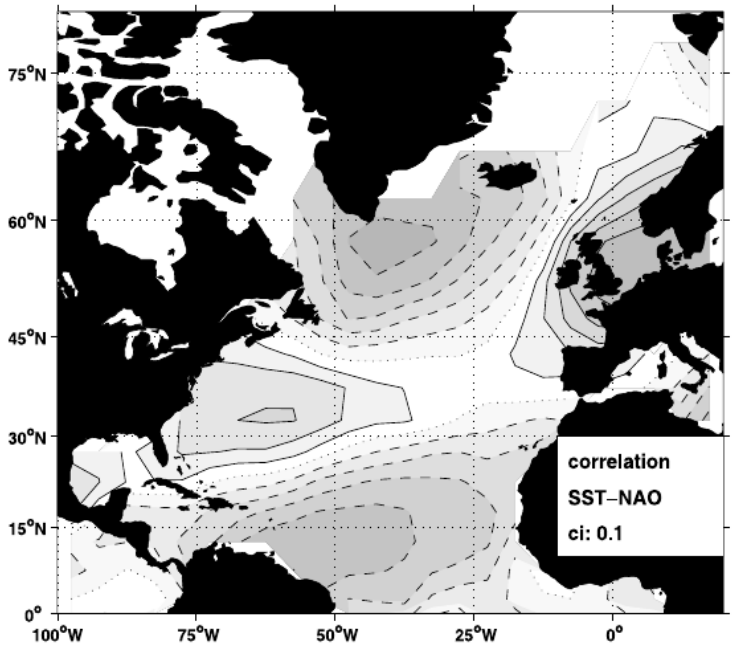

FIGURE 2.9: Correlation of reconstructed SST data set with normalized NAO index for 1900–2000 (December to March season only). Positive values are shown with solid contours, negative values with dashed contours, and zero correlation is represented by a dotted line. Maximum values are on the order of 0.3 to 0.5, which means that the NAO explains about 8–25 % of the total winter SST variance. Figure from *Visbeck et al.* [2003].

To sum this up, wind stress, heat flux and freshwater flux changes associated with a certain phase of the NAO influence not only weather conditions over Europe but also surface ocean conditions. This has an influence on the sea surface density distribution and affects open ocean convection.

2.2.2 Atlantic Meridional Overturning Circulation

The ocean plays an important role in redistributing heat on Earth. Together with the atmospheric circulation, the oceanic circulation transports heat from tropical to polar regions. Figure 2.10a depicts the difference in transport between ocean and atmosphere. On a global average the ocean transport is most important in the tropical regions whereas the heat transport via the atmosphere peaks in middle latitudes (*Trenberth and Caron* [2001]). The largest amount of heat transport is due to atmospheric transport. But nevertheless the influence of the oceanic transport is not negligible. Within the different ocean basins transport of heat differs tremendously (Figure 2.10b). In the Atlantic Ocean the transport of heat is directed towards the north in the whole basin, so that heat is transported from the southern hemisphere (SH) over the equator into the northern hemisphere (NH). The heat transport in all basins together sums up to the mean meridional transport depicted also in Figure 2.10a.

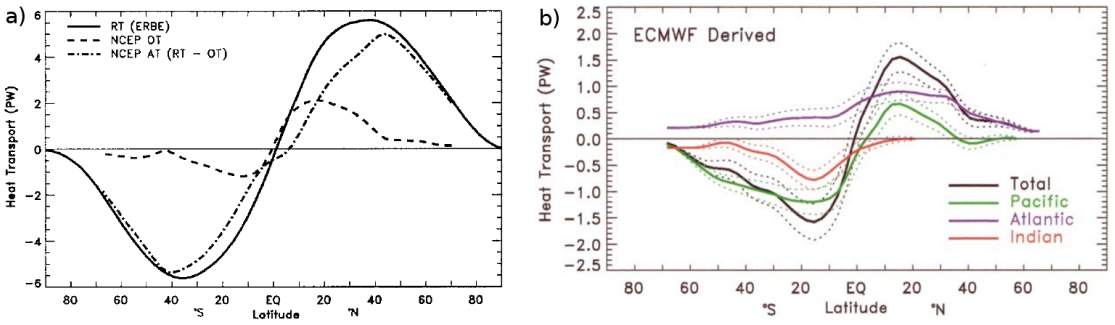

FIGURE 2.10: a) Required total heat transport from the top of the atmosphere radiation (RT: solid line), estimated ocean heat transport (OT: dashed line), implied atmospheric transport (AT: dashed-dotted line); b) Implied zonal annual mean ocean heat transports for the total (black), Atlantic (violet), Indian (red), and Pacific (green) basins. The dashed curves depict 1 std of the transports. Heat transport is given in [PW]. Figure from *Trenberth and Caron* [2001].

A very famous concept describing the transport of heat within the ocean as a whole is the "great ocean conveyer". It was first proposed by *Broecker and Peng* [1982] and revised afterwards (for a detailed historical overview on the global ocean circulation see

Richardson [2008]). In Figure 2.11 the schematic of the ocean conveyor as described by Broecker in 1987 is shown. It gives a very simplified picture of the ocean's overturning and should not be regarded as truth. Nevertheless, as already indicated in this simple schematic, the North Atlantic (NA) Ocean plays an important role in the overturning circulation as it is the only region on the NH where deep water masses are formed. There is no deep water formation in the Pacific Ocean nor in the Indian Ocean. Deep waters are formed via open-ocean convection in the NA and Arctic Seas and via shelf convection around Antarctica.

As this work focuses on the NA region the process of open-ocean convection will be looked at in more detail. Figure 2.12 shows a schematic overview on how open-ocean

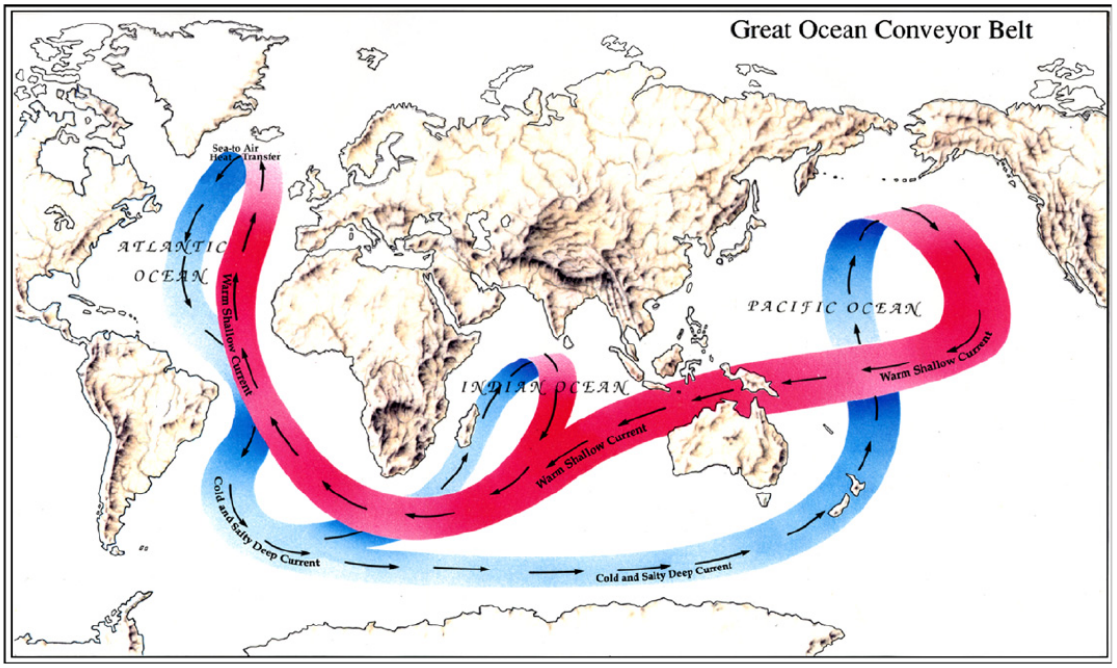

FIGURE 2.11: The Great Ocean Conveyor as described by Broecker in 1987. Figure from *Richardson* [2008].

deep convection takes place. The first phase is the preconditioning (Figure 2.12a), which is necessary to destabilize the water column. This is a large-scale (in the order of 100 km) process (*Marshall and Schott* [1999]). The next phase is the deep convection itself (Figure 2.12b), which takes place in plumes in the order of 1 km. Lateral exchange and spreading (Figure 2.12c and d) eventually leads to the formation of a volume of water at depth with homogenous characteristics (a water mass - shaded volume of fluid in Figure 2.12). The water column is restabilized separating the deep water mass from the surface after the convection.

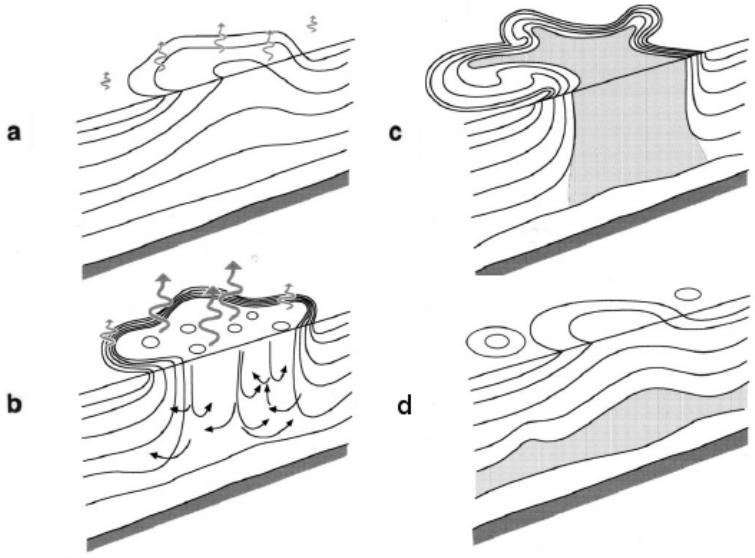

FIGURE 2.12: Schematic diagram depicting the phases of open-ocean deep convection: (a) preconditioning, (b) deep convection, (c) - (d) lateral exchange and spreading. Buoyancy flux through the sea surface is represented by curly arrows, and the underlying stratification/outcrops is shown by continuous lines. The volume of fluid mixed by convection is shaded. Figure from *Marshall and Schott* [1999].

To allow for the preconditioning a strong heat flux from the ocean towards the atmosphere is necessary. This is the case only during winter especially for regions where cold and dry winds from land or ice surfaces blow over water (*Marshall and Schott* [1999]). These winds enhance latent and sensible heat fluxes leading to an oceanic loss of heat (which increases surface density) and favoring an oceanic loss of freshwater (also increasing surface density). Second, to allow for deep convection the deep layers of the water column should be of low stratification (e.g. due to last winter convection). The third prerequisite is the doming of the isopycnals (*Marshall and Schott* [1999]), which brings deep waters towards the surface exposing them directly to strong surface forcings. The doming is favored by cyclonic ciculation (of atmosphere and ocean). The number of regions that cover all of the prerequisites is limited. In the NA region the Labrador and Greenland Seas fulfill these prerequisites, the Irminger Sea is also thought to be of importance in the formation of deep water masses (*Marshall and Schott* [1999], *Pickart et al.* [2003]).

Deep convection can be characterized by the mixed layer depth (MLD). The maximum MLD is reached during March. Therefore, this month is used to investigate the strength of winter deep convection. In Figure 2.13a the observed[1] March MLD and in Figure 2.13b

[1] World Ocean Database 2005 (WOD05) - a gridded monthly hydrographic database of the world ocean, *Boyer et al.* [2006]

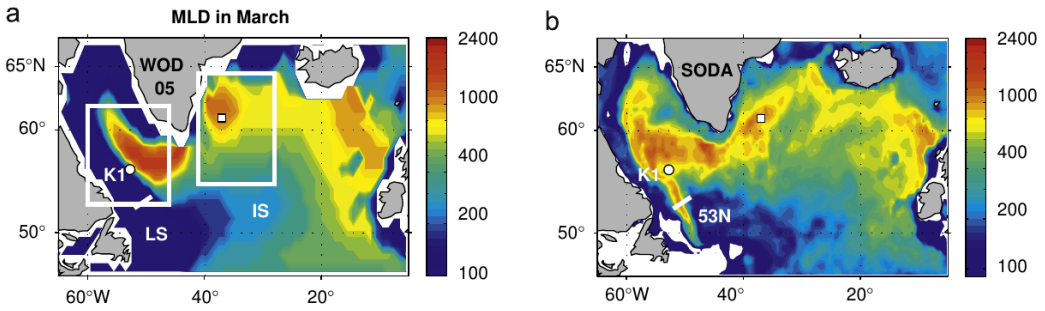

FIGURE 2.13: March Mixed Layer Depth in [m] in a) WOD05 and b) SODA. Figure from *Schott et al.* [2009].

the March MLD from an ocean assimilation product (SODA[2]) are depicted. The MLD is in this case defined as the depth at which the density exceeds the surface density by 0.1 $^{kg}/_{m^3}$ (*Schott et al.* [2009]). Comparing the MLD inferred from hydrographic data and the result from SODA shows that there are some differences in the maximum depth reached. This becomes also obvious in Figure 2.14 which shows the temporal evolution of the MLD at one location in the Labrador Sea (K1 - indicated in Figure 2.13) for observations (dots) and SODA (thick line). In SODA maximum depths of about 1000 m (peaking in 2006 with a maximum depth of about 1500 m) are reached. The observations

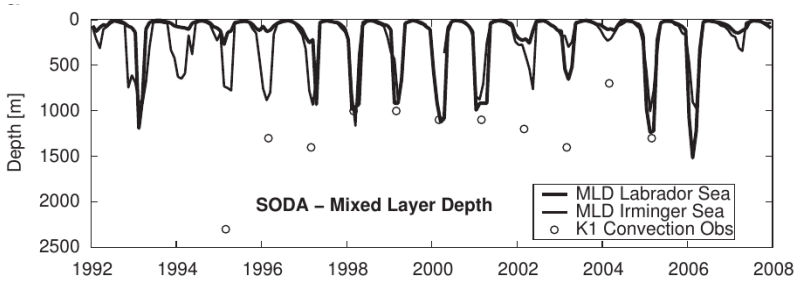

FIGURE 2.14: MLD timeseries in SODA (lines) and observations (dots) in the Labrador Sea (thick black line) and in the Irminger Sea (thin black line) - locations are indicated in Figure 2.13. Figure from *Schott et al.* [2009].

on the other hand show maximum values, that exceed those of SODA in almost all cases, peaking in 1995 with a MLD greater than 2000 m. The regions of maximum MLD though are very similar between observations and SODA (Figure 2.13). They are to find in the Labrador Sea, the Irminger Sea and between Iceland and the British Isles. These deep convection sites, especially the Labrador Sea, serve as regions for deep water formation. These deep waters are transported south at depth and build the lower limb of the Atlantic Meridional Overturning Circulation (AMOC).

[2]Simple Ocean Assimilation Model, *Carton and Giese* [2008]

The AMOC transports warm water masses northward (at upper layers) and cold water masses southward (at deep layers). It is defined as the zonally integrated volume flux in the Atlantic Ocean as a function of latitude and depth (*Lozier* [2012]) and can be represented by a meridional stream function. Figure 2.15 features the meridional stream

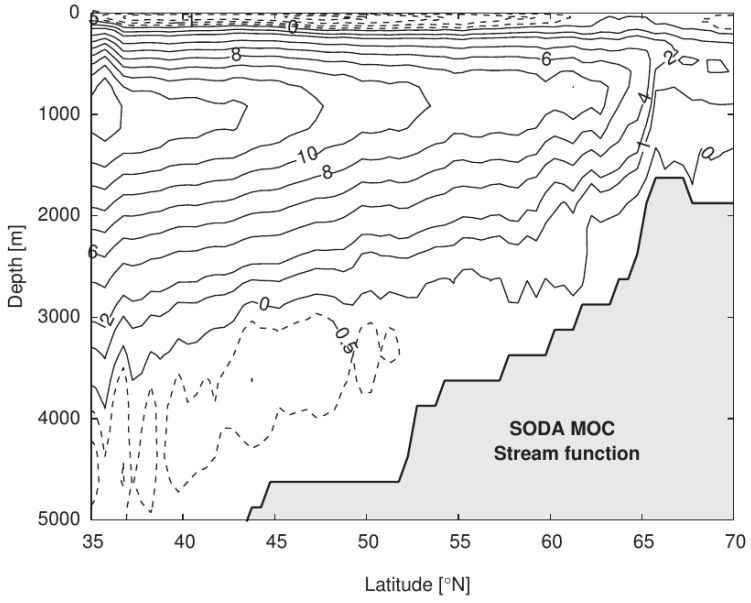

FIGURE 2.15: Atlantic meridional overturning streamfunction for the Simple Ocean Assimilation Model (SODA) in [Sv]. (1 Sv = 10^6 m^3/s). Positive values with contour intervals of 2 Sv, negative values with contour intervals of 0.5 Sv. Figure from *Schott et al.* [2009].

function in the NA Ocean based on SODA. The maximum of the stream function is located at a depth of about 1000 m and a latitude of about 35°N. The maximum is slightly larger than 16 Sv and lies within the observation-based estimates from *Schott and Brandt* [2007] and *Kanzow et al.* [2010] (compare the following sections).

Figure 2.15 shows the AMOC north of 35°N only. To get an impression on how the water mass distribution and meridional circulation looks like in the Atlantic ocean from the south to the north pole, Figure 2.16 shows a salinity section of the whole western Atlantic ocean. The spreading of the different water masses is indicated by arrows. The meridional circulation of the whole Atlantic Ocean can be summarized as follows: Deep water masses, summarized as the North Atlantic Deep Water (NADW), are formed in the NA region (in deep convection zones in the Arctic Ocean as well as in the Labrador Sea). These water masses are transported south in the deep ocean. Part of it is upwelled in the southern ocean, the rest is redistributed into the other basins. Surface currents transport warm and salty waters northward (balancing the southward transport in the

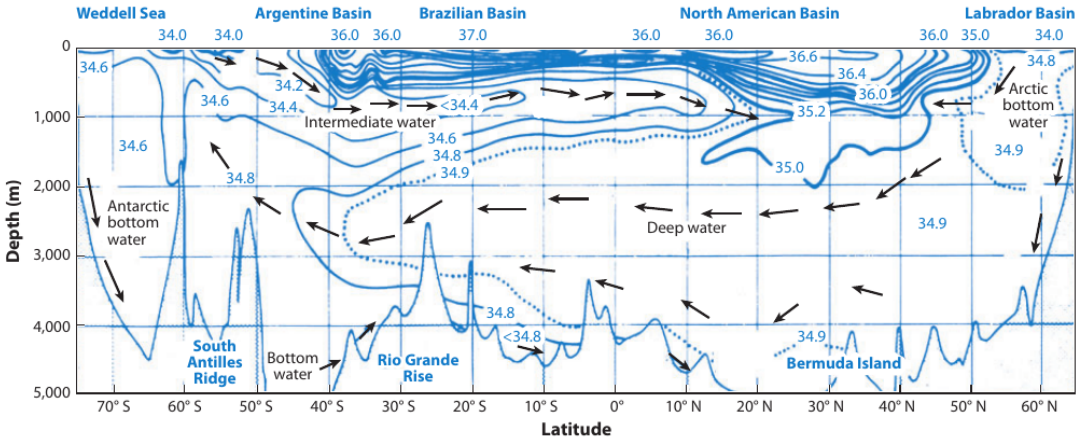

FIGURE 2.16: Meridional Cross Section of Salinity in the western Atlantic Ocean. Water masses as well as their pathways are indicated. Figure from *Lozier* [2012].

interior). This influence on the surface temperatures in the NA basin leads to the fact that the variability of the AMOC can also be connected to a variability pattern called the Atlantic Multidecadal Variability (AMV)[3]. It describes anomalies of the NA sea surface temperatures (SSTs) on a multidecadal timescale (*Kushnir* [1994], *Sutton and Hodson* [2005]) and is connected to the strength of the AMOC. This connection can be described as follows: An increase in AMOC strength leads to a stronger transport of subtropical warm water masses towards the North influencing the overall NA SST characteristics with a certain timelag. In the low-top model used in the present study the AMV lags behind the AMOC by 2 years (*Danabasoglu et al.* [2012a]).

In the NA basin the currents that transport warm subtropical water northward are called the *Gulf Stream* and the *North Atlantic Current* (NAC). They highly influence near surface air temperatures, especially in Europe. Therefore it is of great interest to understand how AMOC variability is driven.

The next section will give a short overview on how the circulation in the subpolar NA region looks like and how deep water masses that form the deep branch of the AMOC are generated.

[3]The Atlantic Multidecadal Variability (AMV), also referred to as the Atlantic Multidecadal Oscillation (AMO), is defined by *Sutton and Hodson* [2005] as the average of the detrended annular mean SST anomalies over the region 0° to 60°N and 75°W to 7.5°W. A low-pass filtered timeseries is usually used as an AMO index.

2.2.2.1 Ocean Circulation in the Subpolar North Atlantic and NADW Formation

The circulation in the subpolar NA basin is illustrated schematically in Figure 2.17. Warm and salty subtropical waters are transported north via the NAC, which is represented by the red arrows in Figure 2.17. Further north it transforms into the Irminger Current (orange arrows) and splits into a northward and an eastward propagating branch. Some of the Irminger Water (still relatively warm and salty) is transported into the Norwegian Sea, another part is recirculated along the coast of Greenland into the Labrador Sea. Deep water masses, depicted in blue, are generated in the Arctic Sea and transported into the subpolar NA as overflow water over the Denmark Strait (Denmark Strait Overflow Water - DSOW) as well as over the Iceland Scotland throughflows forming the Iceland Scotland Overflow Water (ISOW). The formation of overflow water and the transport of these dense water masses are also shown schematically in Figure 2.18. Part of the ISOW is directly transported towards the south, whereas the larger part of the ISOW reaches the western part of the basin and propagates cyclonically along the topography (*Schott and Brandt* [2007]). It merges with the DSOW at the southern tip of Greenland. On their way DSOW as well as ISOW entrain water and increase their volumes (indicated in Figures 2.17 and 2.18). They circulate around the Labrador Sea and form the lower part of the Deep Western Boudary Current (DWBC), which forms the main pathway for southward transport. An additional contribution to the DWBC is the Labrador Sea Water (LSW) which is formed by deep winter open-ocean convection in the center of the Labrador Sea. LSW is represented by white arrows in Figure 2.17. Part of it is recirculated within in the subpolar NA basin while the other part builds the upper layer of the DWBC transporting cold and dense waters south along the coast of North America. Figure 2.17 includes transport estimates for the different ocean currents in Sv ($1\,\mathrm{Sv} = 10^6\,\mathrm{m^3\,s^{-1}}$). The total volume transport of cold and dense waters at depth (in the form of the North Atlantic Deep Water - NADW, which is a combination of ISOW, DSOW and LSW) towards the south is estimated to be about $16\,\mathrm{Sv} \pm 2\,\mathrm{Sv}$ (*Schott and Brandt* [2007] and references therein). This number represents the strength of the AMOC at about 43°N (section A2 in Figure 2.17). The estimated contribution of the different water masses to the total southward transport are indicated in Figures 2.17 and 2.18. The DWBC transports about 13 Sv of NA waters south, the remaining 3 Sv are transported south in the interior of the ocean basin. Approximately 4 Sv of the DWBC are made up of LSW, the remaining 9

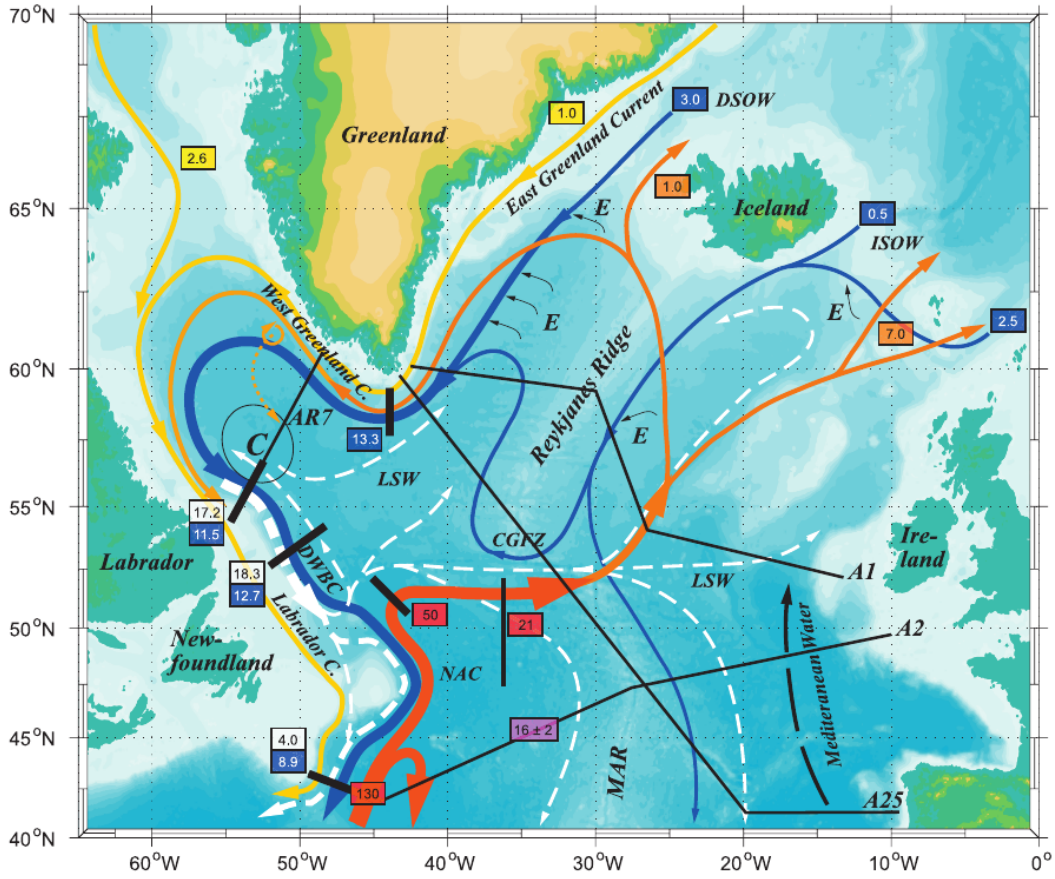

FIGURE 2.17: Circulation in the subpolar North Atlantic. Topographic features and current branches are indicated (CGFZ = Charlie Gibbs Fracture Zone, MAR = Mid-Atlantic Ridge; DWBC = Deep Western Boundary Current, NAC = North Atlantic Current, DSOW and ISOW = Denmark-Strait and Iceland-Scotland Overflow Water, LSW = Labrador Sea Water; C = Convection, E = Entrainment. Locations of moored current-meter arrays are marked by heavy black bars. WOCE Hydrographic Program lines A1, A2, A7 and A25 are incdicated (thin black lines).Transports are marked for the mean DWBC (LSW layer = white box, deeper layers = blue box), for the NAC (red box) and extensions (orange box) as well as for the shallow Arctic inflow (yellow box); Meridional Overturning Circulation across A2 (magenta box). Figure from *Schott and Brandt* [2007].

Sv are made up overflow water masses, which include waters that were entrained on their path through the subpolar NA basin (Figure 2.17).

2.2.2.2 Variability of the AMOC

As the transport of cold waters towards the south depends on the formation rate of NADW, the variability of the export of cold water masses should also be connected to the variability of deep water mass formation. Unfortunately, the estimation of AMOC variability from observations as well as the direct measurement of deep water formation

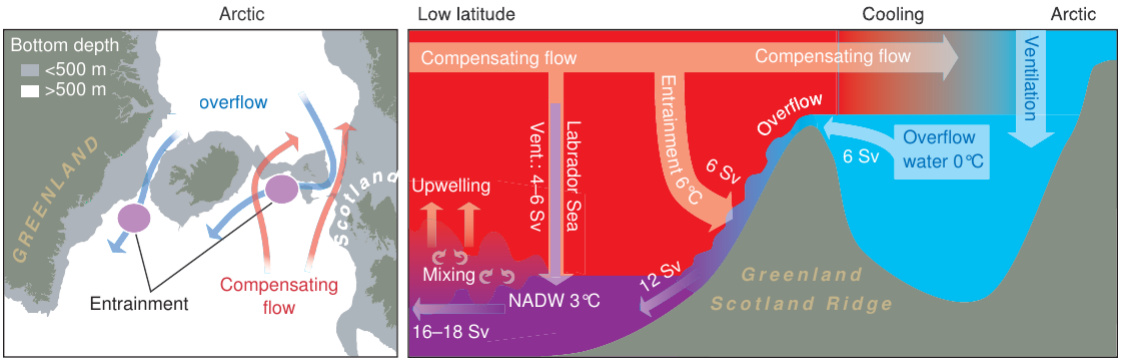

FIGURE 2.18: Scheme of the formation of North Atlantic Deep Water. Arrows on the map (left) indicate the overflow (blue) and compensating inflow (red). On the schematic section (right), temperatures in [°C] and volume transports in [Sv] are approximate values. Figure from *Hansen et al.* [2004].

is difficult (*Schott and Brandt* [2007], *Lozier* [2012]). Measurements of the deep water formation rate, which is restricted to the winter season, are compromised by sea ice and unhospitable weather conditions, that make it impossible to carry out measurements using research vessels during that period. Measurements are therefore either carried out during summer or via the installation of moorings (allowing only point measurements). Nevertheless, NA deep convection zones (such as the Labrador Sea) have been a focus of physical oceanographic studies in the last decades. The contribution of overflow variability to the variability of the AMOC is less well studied (*Lozier* [2012]). The variability in LSW formation is regarded as a very important component to the variability of DWBC transport and the total overturning circulation variability. The relationship between LSW formation and the transport in the DWBC was shown in model experiments (e.g. *Böning et al.* [2006]) but are hard to confirm with observations. *Dengler et al.* [2006] found a contradiction between LSW formation rates and the strength of the DWBC at the exit of the Labrador Sea using observational data (from 1996 to 2005). As the formation rate of LSW decreased during this period, the strength of the Deep Labrador Current increased. Measuring the strength of the AMOC is not easy as well. Historically, the DWBC was regarded as the pathway, that deep water masses take when travelling south. This is now questioned as different experiments, releasing floats within the density range of the LSW core in the DWBC (see for example *Schott and Brandt* [2007] or *Lozier* [2012] for an overview), could not support this hypothesis. The floats would rather recirculate into the interior of the subpolar North Atlantic than drift southward. This implies that measuring the DWBC transport alone does not represent the total southward transport of NADW.

Therefore, the interior of the Atlantic ocean gained a lot of interest in recent years. In 2004, the first project to monitore the basin-scale overturning circulation in the Atlantic Ocean was initiated. The program is called RAPID-MOC (Rapid Climate Change Program - Atlantic Meridional Overturning Circulation). To monitore the overturning circulation meridional velocities were measured along 26.5°N covering boundary currents as well as the interior ocean transport across this latitude. The program is described in *Cunningham et al.* [2007]. It provides the first continuous basin scale time series of the AMOC to the scientific community. *Rayner et al.* [2011] give an overview about the main results gained from the first four deployment years. They detected a strong intraseasonal variability in the AMOC from April 2004 to April 2008. The mean meridional transport at 26.5° N was estimated to be 18.7 ± 2.1 Sv (*Kanzow et al.* [2010]). This is about 2 Sv stronger compared to the estimate of *Schott and Brandt* [2007] at 43°N. The strength of the AMOC ranged from a minimum of 5 Sv to a maximum of 30 Sv during one year. This finding makes it hard to use short time measurements or point measurements for the evaluation of the total transport as the seasonal cycle masks the low-frequency variability. Long time series would be necessary to investigate the influence of different deep water formation regions on the variability of the AMOC.

Additionally, the variability of the AMOC is found to be a function of latitude (*Lozier et al.* [2010], *Biastoch et al.* [2008]). *Lozier et al.* [2010] found that variability of the AMOC is much higher in the subtropics compared to the subpolar region. This means that the only long-term measurement of the AMOC covering the whole Atlantic basin is characterized by larger variability than that expected at higher latitudes. The amount of variabilty influenced by deep water formation in the Labrador Sea compared to the variability in the overflow is therefore not easy to estimate from direct observations.

In this work the overflow rate will not be used. The focus will rather lie on the influence of stratospheric events on anomalies in maximum MLD in the NA region and the potential effect on the variability of the AMOC through deep water formation in general.

2.3 Stratosphere-Troposphere-Ocean Coupling

AMOC variability is at least partly driven by variability in the formation of deep water masses in the North Atlantic. As the export of overflow waters from the Arctic Seas into the North Atlantic is hypothesized to be stable (*Lozier* [2012]), the largest source of

variability comes from the formation of LSW. The formation of deep waters in general depends on the stability of the water column. To initiate deep convection (reaching depths of 1500 to 2500 m) a few prerequisites have to be fulfilled: low stratification at depth, doming of the isopycnals due to Ekman pumping initiated by cyclonic wind anomalies and an intense buoyancy loss due to heat and freshwater fluxes that increases the sea surface density. Without a sufficient buoyancy loss convection will not start. Therefore atmospheric variability is a very important driver of deep convection and eventually of the AMOC. In the North Atlantic region the NAO is the dominant atmospheric variability pattern (compare Chapter 2.2.1). It influences heat and freshwater flux as well as wind stress over the region of interest. A positive NAO phase is associated with negative SST anomalies over the Labrador Sea (compare Figure 2.7) and with a larger evaporation than precipitation rate (compare Figure 2.8). Both anomalies lead to an increase of density (temperature decrease and increase of salinity due to a loss of freshwater). *Eden and Jung* [2001] forced an Ocean General Circulation Model (OGCM) solely by NAO related surface fluxes (heat, wind and freshwater fluxes). They found that interdecadal North Atlantic circulation variability can be described as the lagged response to interdecadal NAO-like surface heat flux variability. So, NAO-related surface fluxes are connected to the variability in the AMOC.

As the NAO can be regarded as part of the hemispheric seesaw in atmospheric mass between pole and middle latitudes, and as the stratosphere is known to influence this pressure pattern, stratospheric anomalies that penetrate into tropospheric layers could influence the variability of the AMOC through influencing the NAO. This response will be looked at in more detail in this thesis.

Chapter 3

Data and Methods

3.1 Model description and experimental design

In this thesis two coupled climate models of the same model family from the National Center of Atmospheric Research (NCAR) are investigated. They were chosen to allow for a comparison between a stratosphere resolving (high-top) and a stratosphere not resolving (low-top) model as land, ocean and sea ice components are identical and the underlying physics in the atmosphere components is the same (*Hurrell et al.* [2013]). Both models are part of the Coupled Model Intercomparision Project Phase 5 (CMIP5), though the runs from the high-top model used in this work were not carried out as part of CMIP5 but by the group of Katja Matthes using the CMIP5 recommendations (*Hansen et al.* [2014]). An overview about the models and experiments used in this thesis can be found in Table 3.1.

3.1.1 CESM1(WACCM)

The high-top model is an Earth System Model and part of the first version of the Community Earth System Model (CESM1) family, which is a state-of-the-art coupled model system including an interactive ocean, land, sea ice and atmosphere component. In the model version used here, the Whole Atmosphere Community Climate Model (WACCM) is incorporated as the atmosphere component (*Marsh et al.* [2013]). WACCM is a high-top fully-intercative chemistry-climate model extending up into the thermosphere. Its model top is at 5.1 10^{-5} hPa, which is about 140 km height. It has 66 vertical levels

TABLE 3.1: Models and Experiments used in this Thesis

Model	**Atm. Component**	**Model Top**	**Runs**	**Time Span**
CESM1(WACCM)	WACCM4	140 km	Natural	1955 to 2099
			RCP8.5	1955 to 2099
CCSM4	CAM4	40 km	Control	1053 to 1108
			RCP8.5	1955 to 2099

and a horizontal resolution of 1.9° latitude by 2.5° longitude. It is designed to represent stratospheric dynamics, including radiative processes due to stratospheric trace species such as ozone (recall Figure 2.2). Parameterizations of non-orographic gravity waves are included, as well as surface stress due to unresolved topography, called *turbulent mountain stress* (TMS). Incorporating TMS improved the simulated frequency of SSWs in CESM1(WACCM) (*Marsh et al.* [2013]).

The ocean component is version 2 of the Parallel Ocean Program (POP2) from the Los Alamos National Laboratory (LANL). It has 60 vertical levels and a horizontal grid with a nominal 1° resolution, which is described in *Danabasoglu et al.* [2006]. A detailed description of POP2 is given in *Danabasoglu et al.* [2012b].

The sea ice component is version 4 of the LANL Community Ice CodE (CICE4), the land component is version 4 of the Community Land Model (CLM4). Both of these are described shortly in *Hurrell et al.* [2013].

Two runs from CESM1(WACCM) are used: a control run and a GHG run that span a period from 1955 to 2099 (145 years). The GHG scenario investigated here is the RCP8.5 scenario from the 5^{th} Assessment Report of the Intergovernmental Panel on Climate Change (IPCC). RCP stands for Representative Concentration Pathways (*Meinshausen et al.* [2011]). The RCP8.5 scenario is the worst case scenario of these GHG projections. It is characterized by an increase of CO_2 concentrations from 379 ppm in 2005 to 936 ppm until 2100. Apart from CO_2, also the concentrations and/or emissions of other GHGs as well as of ozone depleting substances (ODSs) are included in the scenario. For detailed information see *Meinshausen et al.* [2011]. The GHG and ODS concentrations of the period before 2005 are covered by the Historical scenario, which is based on observations (*Meinshausen et al.* [2011]). The run used here as a control run follows a *Natural* setup with GHG and ODS concentrations kept constant at the 1960 level (*Hansen et al.* [2014]). Spectrally resolved solar variability is included in this experiment following *Lean et al.*

[2005].

3.1.2 CCSM4

The Community Climate Sytem Model Version 4 (CCSM4) is a low-top coupled general circulation model. Its atmosphere component is the Community Atmosphere Model Version 4 (CAM4) with a horizontal resolution of 0.95° latitude by 1.25° longitude and 26 vertical levels (*Hurrell et al.* [2013], *Gent et al.* [2011]). It has therefore a higher horizontal but lower vertical resolution compared to CESM1(WACCM). The model top reaches a height of 3.54 hPa, which is at about 40 km and lies within the middle stratosphere. The ocean, land and sea ice components are the same as in CESM1(WACCM).
A control as well as a GHG run are used from CCSM4. The GHG run has the same boundary conditions as the one for CESM1(WACCM) (RCP8.5 scenario) and to allow for a better comaprison between low and hig top model, the same period (1955 to 2099) is chosen. The control run in this case is a simulation with constant GHG and ODS concentrations and no solar variability. It covers a period of 55 years, which is roughly one third of the period covered by the other model runs.

3.2 Observational Data

The 40-year European Centre for Medium-Range Weather Forecasts (ECMWF) Re-Analysis (ERA-40) dataset (*Uppala et al.* [2005]) is used to compare the model results to data close to observations. The ERA-40 data spans the period 1958–2002. It is extended until 2012 using ERA-Interim data (*Dee et al.* [2011]). In the following the designation ERA-40 is used for the extended ERA-40 set (spanning the period 1958 to 2012). The resolution of the data used in this thesis is 2.5° × 2.5° in the horizontal and 23 levels in the vertical, with the highest level being 1 hPa. The quality of the data changes with the quality of the observations; strong improvements were achieved with the beginning of the satellite era in the 1970s.

3.3 Methods

3.3.1 Definition of Polar Vortex Events

In this thesis strong as well as weak polar vortex events are investigated. To define these events the definition of the Northern Annular Mode (for December to February) is used, based on the method of *Baldwin and Dunkerton* [2001]. The designation *Northern Annular Mode* (NAM) is used as an equivalent for the term *Arctic Oscillation* (AO). It was introduced by *Thompson and Wallace* [2000] to point out the similarities with the Southern Annular Mode (in the southern hemisphere). In general NAM or AO illustrate the seesaw of atmospheric mass between the pole and the middle latitudes. It was first defined for the surface only (*Thompson and Wallace* [1998]) and later extended to all levels of the atmosphere (*Baldwin and Dunkerton* [1999]).
In this work the nomenclature NAM is used. For each vertical level, the NAM is here defined as the first Empirical Orthogonal Function (EOF1) of geopotential height (GPH) anomalies north of 20°N for the winter period (December to February). Following the work of *Baldwin and Thompson* [2009] the zonal mean of the GPH anomalies was used for the EOF analysis. The EOF analysis was carried out as described in Chapter 3.3.1.1. The resulting pattern was projected onto the daily GPH anomaly data to get a NAM index for each level. The NAM index at 10 hPa (NAM_{10hPa}) was used to define weak and strong events, respectively. The first day of a sequence of at least 5 days with $NAM_{10hPa} \leq -3$ is defined as the central date for a weak vortex event, whereas for a strong vortex event a threshold of $NAM_{10hPa} \geq 2.5$ is required (*Reichler et al.* [2012]). To select an event, at least 5 consecutive days meeting/exceeding the threshold are needed. An interruption of the threshold by 3 days is allowed to exclude interpreting an event that shows some variability as two individual events. The threshold definition for weak and strong vortex events differs in absolute value as the distribution of the NAM is negatively skewed (*Baldwin* [2001]).

3.3.1.1 Empirical Orthogonal Function Analysis

The empirical orthogonal function analysis (short EOF analysis) is a statistical method used to evaluate variability patterns and their temporal evolution in, for example, geophysical scalar fields. The dataset is separated into different variability patterns from

which each explains a certain amount of the total variability of the investigated scalar field. These different variability patterns are by definition orthogonal to each other. The demanded orthogonality has to be kept in mind when interpreting the results of an EOF analysis.

EOF analysis is sometimes also referred to as Principle Component (PC) analysis. This leads to different designations for patterns and timeseries among publications. In this thesis the patterns of variability are referred to as EOFs, whereas the according timeseries are referred to as PCs (or indices).

The EOF analysis applied here is based on the covariance matrix, $\mathbf{V}$, of the detrended anomalies from dataset $\mathbf{D}$. It is defined in equation 3.1.

$$\mathbf{V} = \mathbf{D}\,\mathbf{D^T} \tag{3.1}$$

The solution of the eigenvalue problem in equation 3.2

$$\mathbf{V}\,\mathbf{C} = \mathbf{C}\,\mathbf{\Lambda} \tag{3.2}$$

gives the eigenvalues, $\lambda_\mathbf{i}$, as the diagonal of $\mathbf{\Lambda}$ and the corresponding eigenvectors, $\mathbf{c_i}$, that form the matrix $\mathbf{C}$. The eigenvectors represent the variability patterns. Using the eigenvalues one can calculate the proportional variance that each eigenvector explains compared to the total variance. The explained variance (EV) is defined in equation 3.3.

$$\mathbf{EV_i} = \frac{\lambda_\mathbf{i}}{tr(\mathbf{\Lambda})} \tag{3.3}$$

The variability patterns that are given by the eigenvectors are now referred to as EOFs. EOFs are stationary variability patterns that do not change their shape with time. The temporal change of the pattern is described by the PC timeseries, which is calculated by multiplying the scalar field of interest with the eigenvectors (equation 3.4).

$$\mathbf{PC_i} = \mathbf{D}\,\mathbf{c_i} \tag{3.4}$$

The EOF with the highest EV is referred to as EOF1, the one with the second highest EV is referred to as EOF2 until EOFN, where N is the number of eigenvectors. The according PCs are referred to as PC1, PC2 ... PCN.

In case of calculating the Northern Annular Mode, $\mathbf{D}$ represents the December to February

(DJF) mean of the detrended zonal mean GPH anomaly at a certain level. The leading EOF, EOF1, is referred to as the NAM pattern for each level individually. They are normalized using standard deviation. The positive phase of the NAM is defined by a negative anomaly over the pole and a positive anomaly over the middle latitudes. For the calculation of the PCs a daily resolved year round dataset of the detrended zonal mean GPH anomalies is used. Thereby a daily NAM index for each level is derived.

3.3.2 Index Definitions

3.3.2.1 North Atlantic Oscillation

Following *Hurrell* [1995] the NAO index is defined as the difference in normalized SLP anomaly between Iceland and the Azores. According to the resolution of the data the grid points closest to the stations Akureyri (65.7°N, 18.1°W) and Lisbon (38.8°N, 9.1°W) were used. Anomalies were calculated and the DJF mean was derived. After that the indices were detrended and normalized using their standard deviation. The station data is normalized to avoid differences in variability (which is much greater for the Iceland station compared to Portugal). As the last step the difference between both indices was calculated (Akureyri minus Lisbon), resulting in the station-based NAO index.
For comparison also an EOF based index was calculated by carrying out an EOF analysis for detrended SLP anomalies in the North Atlantic region between 20 and 70°N and between 90°W and 40°E (*Hurrell et al.* [2003]).

3.3.2.2 Atlantic Meridional Overturning Strength

For the description of the strength of the Atlantic Meridional Overturning Circulation (AMOC) the meridional stream function of the Atlantic basin was used. The AMOC strength is defined as the maximum of this stream function. An index is generated using the meridional stream function at about 40°N and 1000 m depth. This region was chosen as it displays a region close to the maxima of the stream functions for the models used in the analysis (Figure 4.10).

3.3.3 Anomaly Calculation and Detrending

When referring to anomalies in this thesis, the climatology was removed from the data for two distinctive periods individually: period 1 being 1955 to 2026, period 2 being 2027 to 2099. This was done due to the non-linear character of the global warming trend (*McLandress and Shepherd* [2009]). Linear trends were also removed for these two period independently. This differentiated climatology calculation and detrending was also applied to the CESM1(WACCM) Natural experiment (although a trend in this dataset was not expected) to avoid differences in the results between GHG and control experiment that are due to the detrending method. For the CCSM4 Control experiment and for the ERA-40 data no differentiating between periods was applied due to the shorter timespans these datasets cover.

3.3.4 Composite Analysis

To connect stratospheric events to anomalies at the surface and in the ocean composite analysis was used. Composite analysis, in general, is based on calculating the mean over certain events in time. These special points in time are chosen according to a certain criteria. In this thesis, the central dates of weak and strong vortex events respectively were selected in time according to the criteria given in Section 3.3.1. First, the mean of these events including 90 days before and after the central date were calculated resulting in composites that show the evolution of an average vortex event (weak and strong) on a height-lag plain with the central date of a vortex event being lag zero. Second, the means of different atmosphere and ocean parameters following the central dates (3 months) were calculated, resulting in longitude-latitude composites that show the average state of a certain parameter within the 3 months after a stratospheric vortex event.

3.3.4.1 Significance Testing

To test the composites for significance a bootstrapping (Monte Carlo) approach was applied (similar to *de la Torre et al.* [2012]). Therefore 1000 randomly produced central dates are used to calculate random composites. The randomly selected central dates are designed to lie in those months in which the real central dates occur. The tested hypothesis is whether the real composites are significantly different from the set of random

composites. Significance is reached when the real composites lie within the lowest or highest 5% of the distribution drawn from the random composites.

Chapter 4

Atmospheric and Oceanic Conditions in Model Simulations and Reanalysis

In this Chapter the mean conditions of atmosphere and ocean that were adressed in Chapter 2 are presented for the CESM1(WACCM) and CCSM4 data. The results are compared to ERA-40 data in the case of atmospheric variables and to other observations (SODA and WOD05) that were presented in Chapter 2.2.2 regarding the maximum mixed layer depth (MLD) anomalies.

4.1 Stratospheric Polar Vortex Events

As explained in Chapter 3.3.1 the occurence of stratospheric polar vortex events is defined using the Northern Annular Mode (NAM) for the boreal winter season (December to February). To give an example on how the NAM looks like in the model data this section will give a short overview on the structure of the NAM in the model data compared to the ERA-40 reanalysis data set and will then proceed with the characteristics of weak and strong polar vortex events.

The positive phase of the NAM is characterized by a negative anomaly in zonal mean geopotential height (GPH) over the pole and a positive anomaly in zonal mean GPH over the middle latitudes (Figure 4.1). It is therefore connected to a strengthening of the

westerly wind regime, that dominates during winter, and consequently to a strengthening of the stratospheric polar vortex. The characteristics of the negative phase are opposite to that of the positive phase.

The comparison between model data and reanalysis (Figure 4.1a and b) shows a good agreement in the mean structure of the NAM. The strongest anomaly is found over the

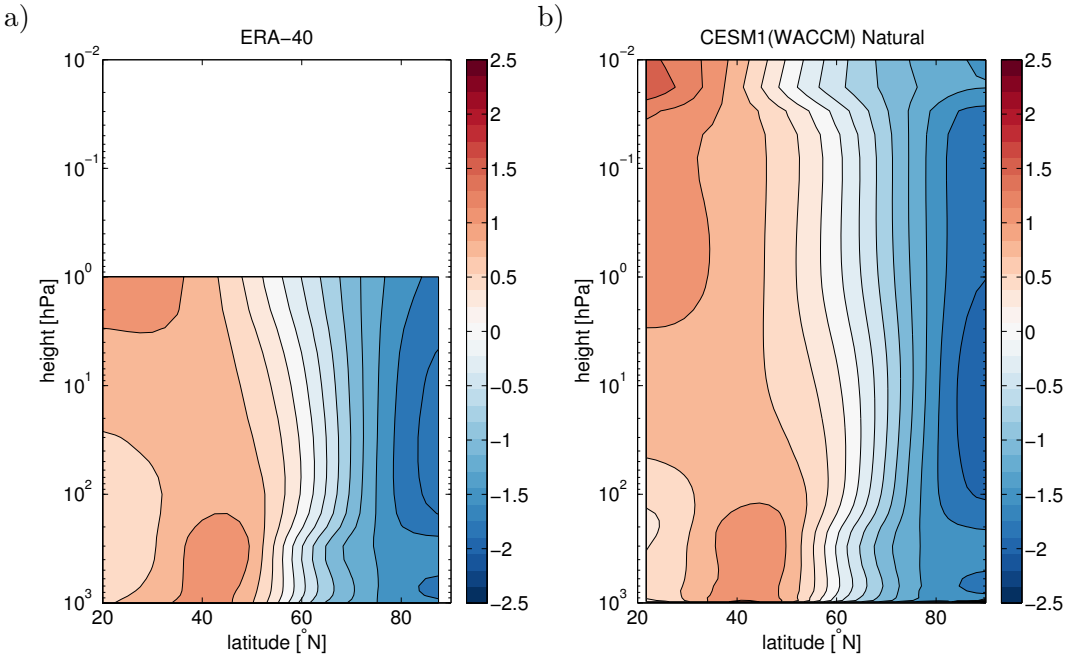

FIGURE 4.1: Vertical profile of the Northern Annular Mode in a) ERA-40 data and b) CESM1(WACCM) Natural. Each level is normalized by its standard deviation. Contour interval is 0.25. Dimensionless.

pole ranging from about 100 hPa to 1 hPa in CESM1(WACCM). In the ERA-40 data this region is smaller and shifted to lower altitudes.

The highest values of explained variance are found in the stratosphere (Figure 4.2), with percentages exceeding 80%. This indicates that the NAM is by far the most important variability pattern in the stratosphere. In the troposphere the maximum explained variance (about 55%) is reached between 600 and 700 hPa in the model data and at about 850 hPa in the ERA-40 data. The minimum of explained variance can be found at the 300 hPa level, with values of 52% for the model data and 46% for the ERA-40 data. This minimum can be explained by the large influence of other variability patterns, such as the Pacific North American Pattern (PNA) that was shown to influence atmsopheric variability especially around the 300 hPa level in *Baldwin and Thompson* [2009]. Nevertheless, also in the troposphere a high amount (about 50%) of variance in zonal mean GPH anomaly is explained by the first EOF, namely the NAM. The structures of the NAM in the other

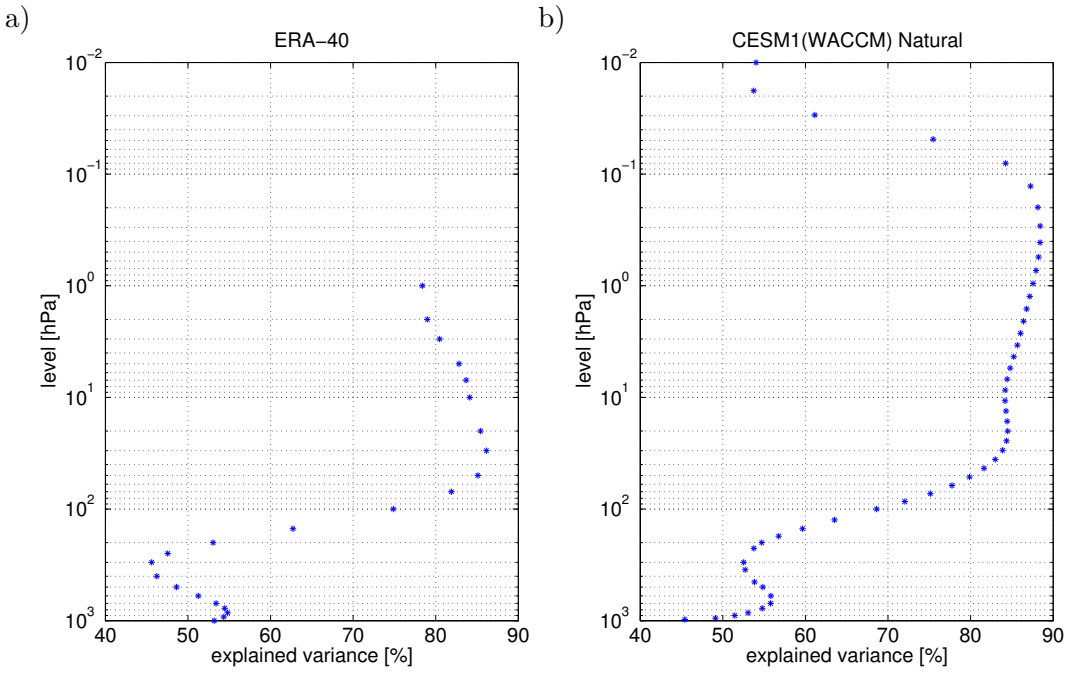

FIGURE 4.2: Explained Variance of the Northern Annular Mode for each level in a) ERA-40 and b) CESM1(WACCM) Natural.

model data do not differ much from the results shown here. The explained variances in the low-top model, though, differ from the high-top model and the reanalysis results (see Appendix Figure A.2) as far as they are higher than observed in the troposphere and lower than observed in the stratosphere.

To identify weak and strong vortex events the NAM index at 10 hPa was used (see Chapter 3.3.1 for more details). Figure 4.3 shows the evolution for weak (Figure 4.3a) and strong (Figure 4.3b) vortex events in ERA-40. Following *Baldwin and Dunkerton* [2001], the colorcoding (red is used for negative and blue is used for positive NAM anomalies) is used to indicate that the weakening of the vortex is connected to a warming.

There are some differences between the downward propagation of weak and strong vortex events. For the weak vortex event the signal clearly originates in the stratosphere and propagates downward. It reaches the surface after about 2 weeks and the tendency for a negative NAM at the surface persists for more than 50 days. The strong vortex event on the other hand does not show the downward propagation in such a distinct way. Significant anomalies reaching the surface are not apparent but they persist for about 50 days at the 200 hPa level. Strong as well as weak vortex events are followed by an anomaly of opposite sign, originating above the 1 hPa level. This anomaly can be recognised at the 1 hPa level approximately 30 days after the central date.

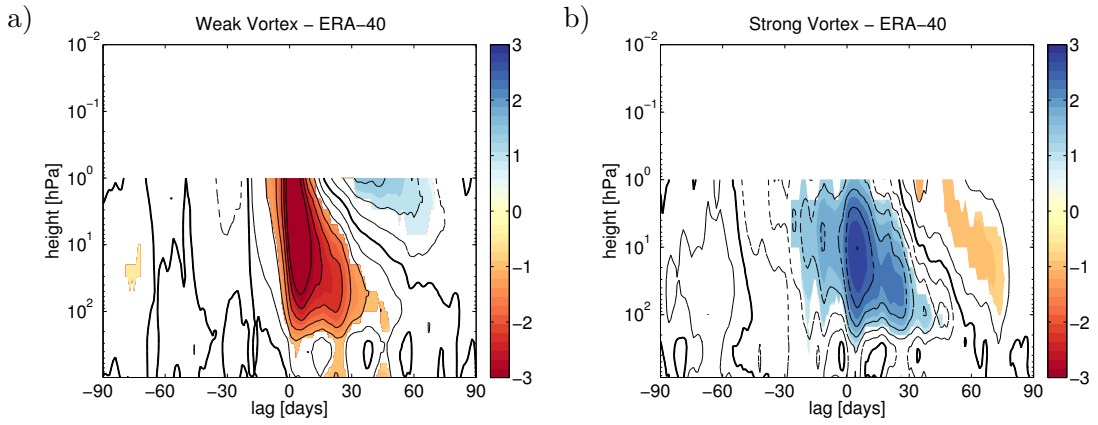

FIGURE 4.3: Composites of the NAM for a) weak and b) strong vortex events in ERA-40. The definition of the central date (Lag 0) is based on the NAM_{10hPa}, which is ≤ -3 for weak events and ≥ 2.5 for strong events. Colored regions are significant at the 90% level. Contour interval is 0.5. The zero contour line is indicated by a bold line, negative values are presented by dashed contours. Dimensionless.

In Figure 4.4 the persistence of weak and strong events in ERA-40 is depicted. In general one can see that the frequency of weak vortex events exceeds that of strong vortex events. The amount of weak and strong vortex events does of course vary with the threshold used

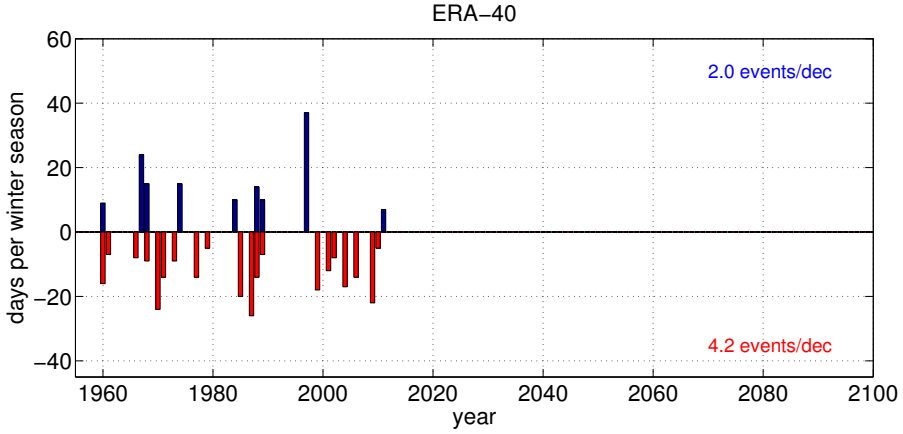

FIGURE 4.4: Persistence of vortex events in ERA-40. Weak events are colored red, strong events are colored blue. The bars show the number of days per winter season that are identified as being part of a vortex event. The year indicates the start of the winter season. The frequency of weak (red) and strong (blue) events is given in [events/decade].

to define weak and strong vortex events. Here, the thresholds used by *Reichler et al.* [2012] are used. It has to be mentioned here that although one could suppose that a weak vortex event is equal to a sudden stratospheric warming (SSW), the definiton for weak vortex events used here results in a frequency that is lower than the frequency of observed major SSWs (which was estimated by *Charlton and Polvani* [2007] to be approximately 6

events per decade using a comparable reanalysis data set). This departure is due to the differing definitions.

4.1.1 Polar Vortex Events in CESM1(WACCM)

Figure 4.5 shows NAM composites for weak and strong vortex events in both runs of CESM1(WACCM). The vortex events in CESM1(WACCM) are very similar to those in ERA-40. But, in contrast to the ERA-40 data, the strong events in the Natural run connect significantly to the surface (Figure 4.5b) and the anomlies persist there for more than 50 days. In the RCP8.5 run the signal is not as persistent. The anomaly of opposite

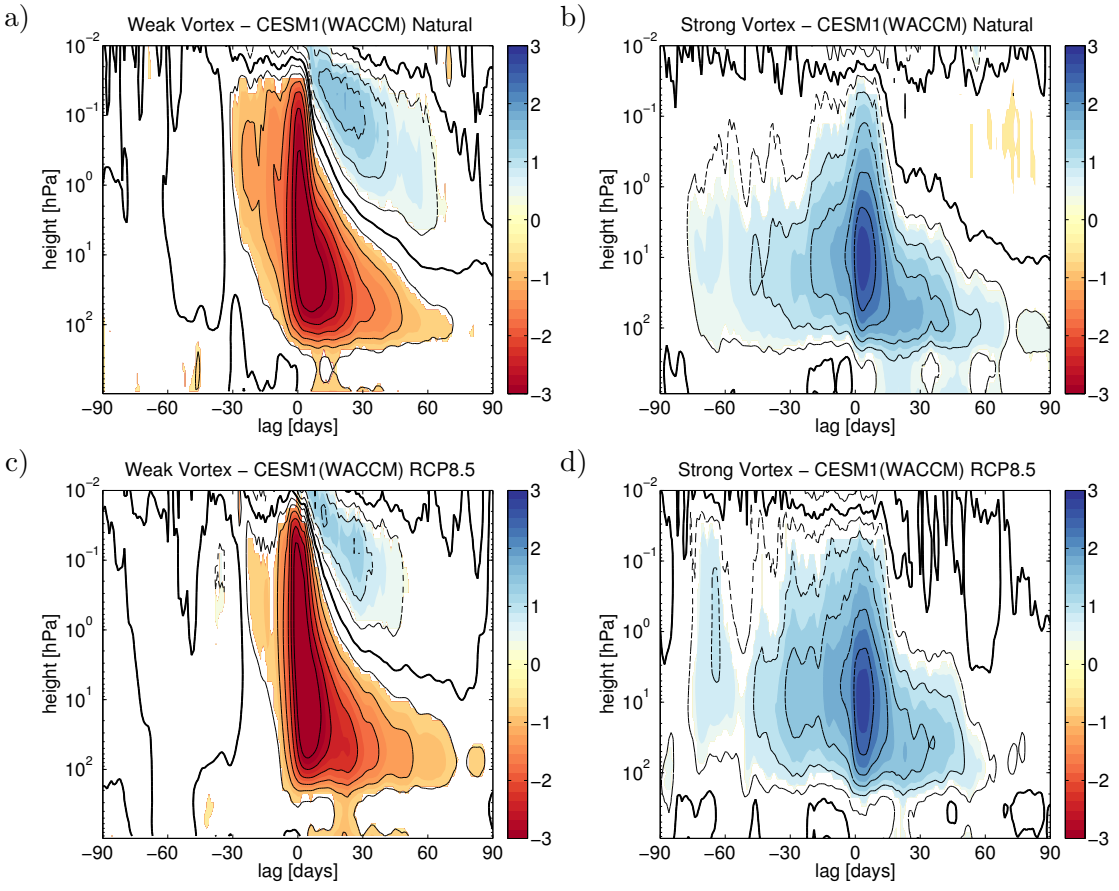

FIGURE 4.5: Composites of the NAM as in Figure 4.3 but for CESM1(WACCM) Natural (a and b) and CESM1(WACCM) RCP8.5 (c and d). Weak events in a) and c), strong events in b) and d).

sign following the weak and strong vortex events seen in ERA-40 is not significant in the composites of strong vortex events in CESM1(WACCM), but it is apparent for the weak vortex events (compare Figures 4.3b and 4.5a and c).

The weak events in the two CESM1(WACCM) simulations differ from each other in strength: the Natural experiment shows a stronger signal in the first two weeks (down to the 100 hPa level) compared to the RCP8.5 experiment (Figure 4.5a and c). Another difference can be found in the period before the central date. In the Natural experiment the central date is led by a negative anomaly appearing in the mesosphere already 20 days before the central date. In the RCP8.5 simulation this anomaly is also apparent but of much lower strength compared to the Natural run. This feature was also described in *Hansen et al.* [2014].

The frequency of weak events in CESM1(WACCM) is higher than that of strong events (Figure 4.6) and although the frequency of weak events does not differ much between the Natural and the RCP8.5 run, the frequency of strong events is much lower for the RCP8.5 run compared to the Natural run. The difference in frequency between strong and weak

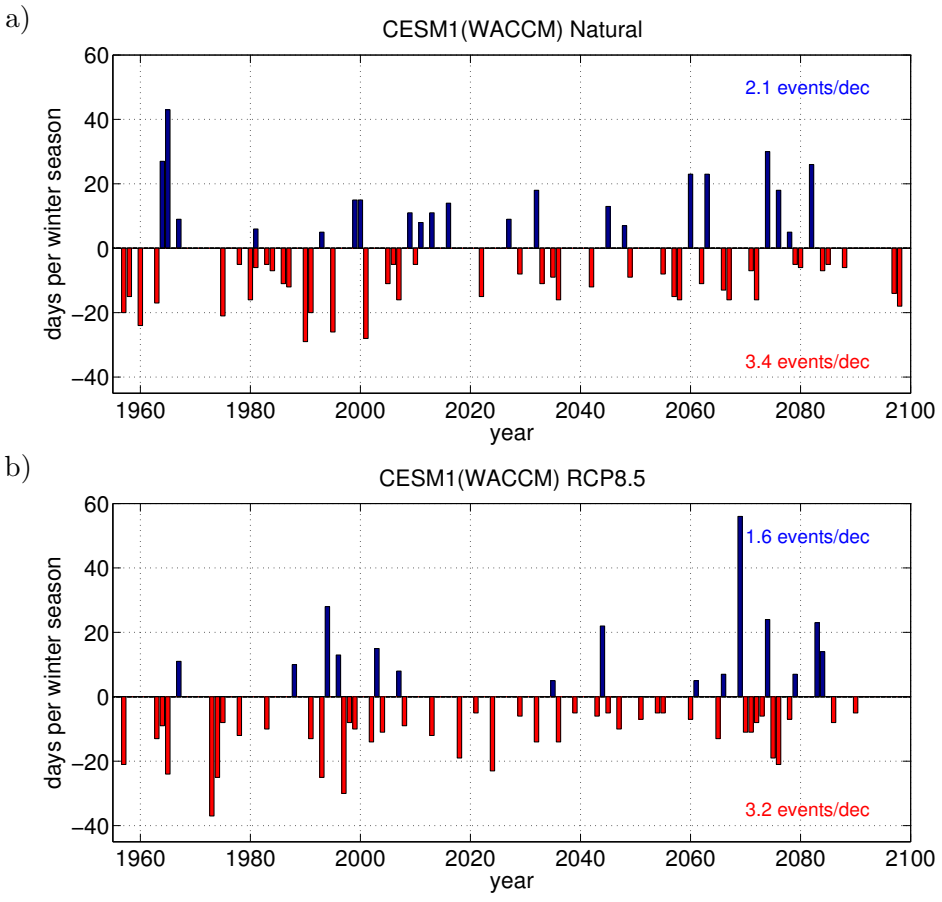

FIGURE 4.6: Persistence of vortex events as in Figure 4.4 but for a) CESM1(WACCM) Natural and b) CESM1(WACCM) RCP8.5.

events, though, is consistent with the results from ERA-40 although the frequency of weak events is lower in the model simulations compared to the reanalysis data.

The length of the timeseries of the model simulations makes it possible to take a look at changes in persistence of the events with time. For the RCP8.5 run (Figure 4.6b) the tendency for strong events increases from the 20^{th} to the 21^{st} century. In the Natural run (Figure 4.6a) this is not the case, but there are periods in which the occurence of strong or weak events is higher compared to other periods. Periods that are dominated by strong events are for example: 1964-1967, 2009-2017, and 2074-2082; whereas for example the period from the 1970s to the late 1990s is dominated by weak events.

4.1.2 Polar Vortex Events in CCSM4

In CCSM4 the downward propagation of stratospheric weak vortex events is not that distinct. In the Control run the signal in the stratosphere seems to be driven by tropospheric anomalies (Figure 4.7a) as the only significant connection with the troposphere occurs about a week before the central date. In the RCP8.5 run the propagation of the

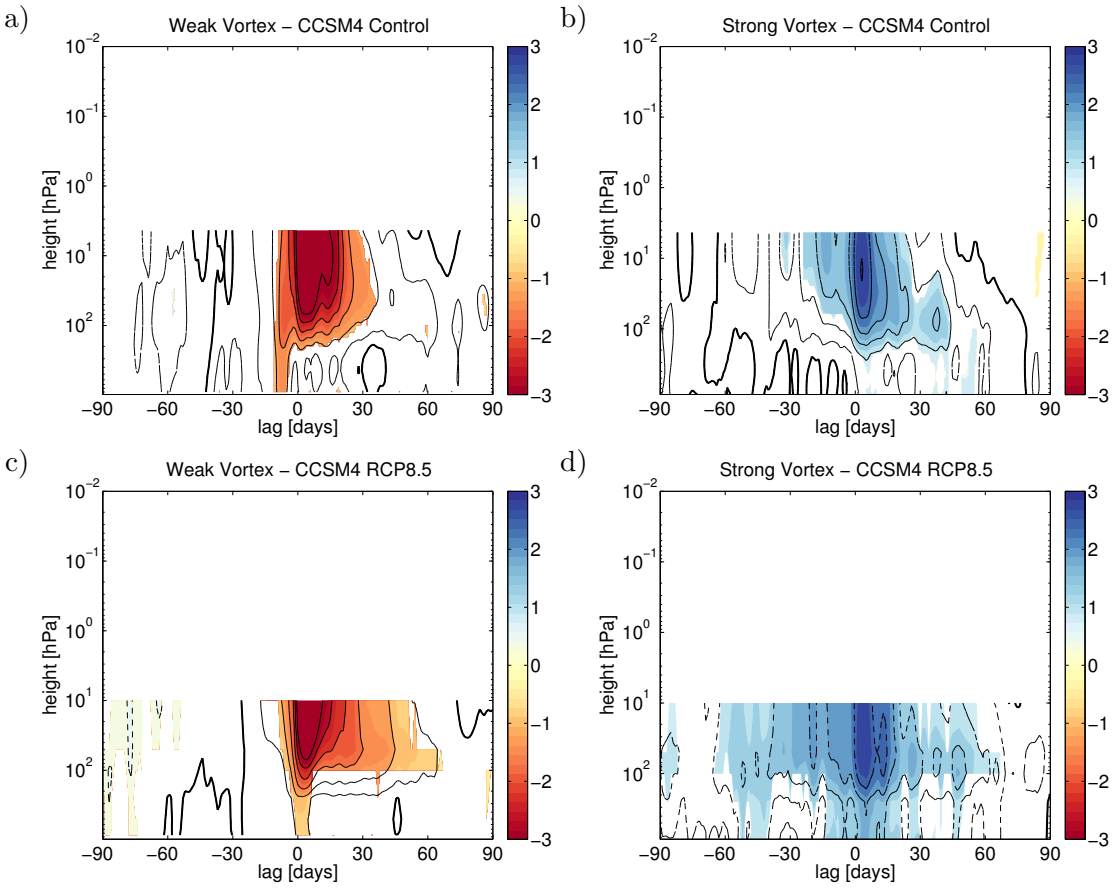

FIGURE 4.7: Composites of the NAM as in Figure 4.3 but for CCSM4 Control (a and b) and CCSM4 RCP8.5 (c and d). Weak events in a) and c), strong events in b) and d).

stratospheric signal down into the troposphere occurs right after the central date (Figure 4.7c). The anomalies of the NAM connected to a weak stratospheric polar vortex above the 100 hPa level are more persistent in the RCP8.5 run compared to the Control run. This is the case for weak and for strong events.

The downward propagation of NAM anomalies connected to strong vortex events is shown in Figure 4.7b and d. For the Control run, the pattern is similar to that from ERA-40, whereas for the RCP8.5 run the pattern looks very different, showing positive tropospheric NAM anomalies starting more than 50 days before the onset of the stratospheric event. This was not observed for the CESM1(WACCM) runs (compare Figure 4.5) and might be due to the very low amount of strong events occuring in the CCSM4 RCP8.5 run (Figure 4.8b). The low frequency of strong events in this run leads to a higher probability for

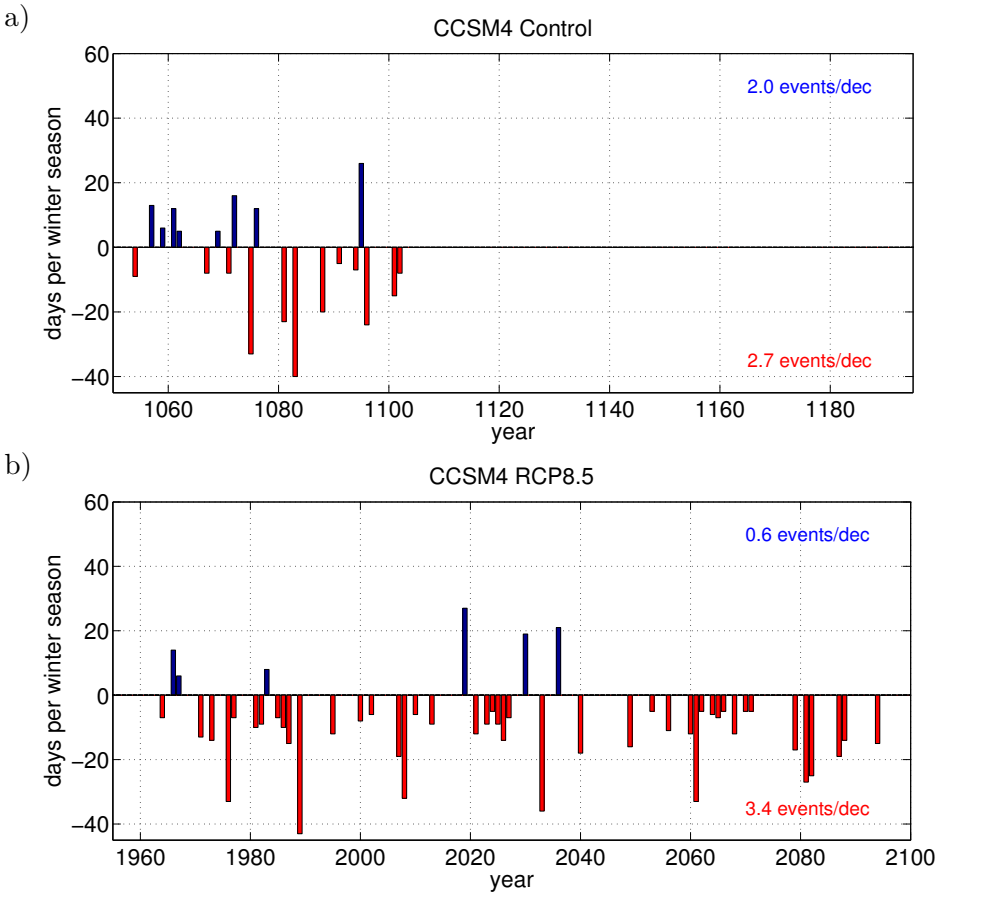

FIGURE 4.8: Persistence of vortex events as in Figure 4.4 but for a) CCSM4 Control and b) CCSM4 RCP8.5.

significance and might falsify the picture of strong events in CCSM4 RCP8.5.

In CCSM4 RCP8.5 a frequency of strong events of only 0.6 events per decade is found, whereas for the other model simulations this frequency ranges between 1.6 events per

decade (CESM1(WACCM) RCP8.5) and 2.1 events per decade (CESM1(WACCM) Natural). The CCSM4 Control run is closest to the ERA-40 data; both having a frequency of 2.0 events per decade (compare Figures 4.4, 4.6 and 4.8). So, the shortage in strong events is not apparent in the low-top model in general - but only in the RCP8.5 run. The method used to define strong events is therefore regarded as suitable also for the low-top model, although the 10 hPa level used for the definition is close to the model top. Due to the low number of strong events in CCSM4 RCP8.5 a difference in occurence between the 20^{th} and the 21^{st} century can not be inferred (Figure 4.8b). The frequency of weak events does not differ very much among the model data. It is higher in the ERA-40 data, though. While in the RCP8.5 run from CESM1(WACCM) a decrease in frequency of weak events between the 20^{th} and 21^{st} century can be found, this is not that obvious for the CCSM4 data.

To sum this up, the downward propagtion of weak and strong polar vortex events is close to reanalysis in CESM1(WACCM). The most striking differences between Natural and RCP8.5 run are: 1) the negative NAM anomaly for the composites of the weak polar vortex events in the mesosphere starting 3 to 4 weeks before the central date is much stronger in the Natural simulation compared to RCP8.5 and 2) the connection to the troposphere is more significant in the Natural run compared to the RCP8.5 run for the composites of strong polar vortex events. Under the global warming scenario the number of strong vortex events inceases from the 20^{th} to the 21^{st} century while the number of weak events decreases. In CCSM4, weak vortex events connect significantly to the troposphere only before the central date in the Control run and only for a few days after the central date in the RCP8.5 run. For the composites of strong polar vortex events the downward propagtion is apparent but significancy is questioned for the RCP8.5 run due to the low amount of strong events in total.

4.2 North Atlantic Oscillation

As described already in Section 3.3.2 the North Atlantic Oscillation (NAO) is the leading mode of SLP in the North Atlantic region during boreal winter. Figure 4.9 shows the regressions of the EOF-based NAO index onto the detrended SLP anomalies for CESM1(WACCM) and CCSM4. During a positive NAO phase the SLP over Iceland is anomalously low, whereas it is anomalously high over the middle latitudes in the North

Atlantic region. But, in contrast to the result for ERA-40 (compare Figure 2.6), the NAO patterns for the model data show an additional strongly significant signal in the Pacific

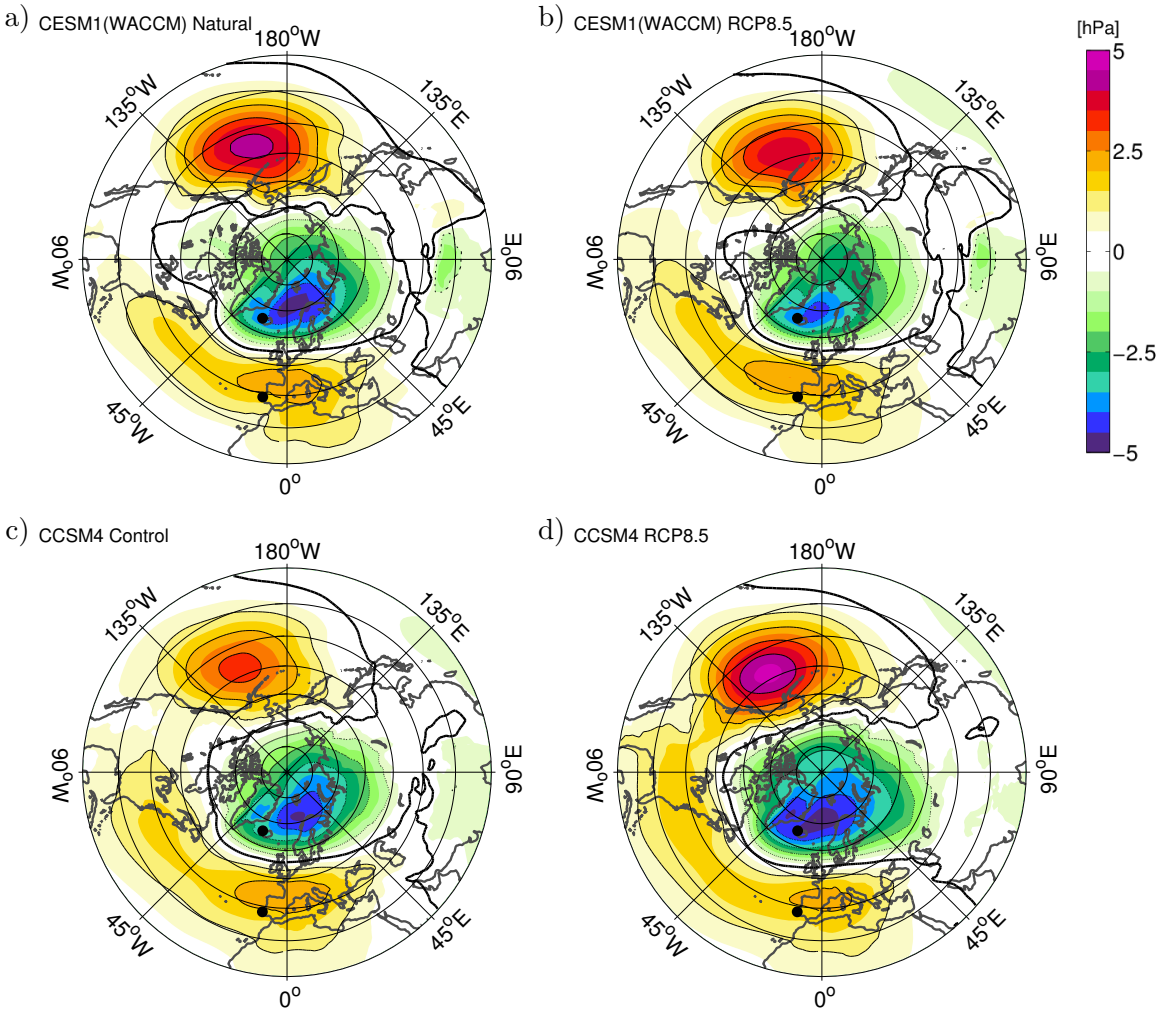

FIGURE 4.9: NAO pattern as received from regression of the EOF-based NAO index onto NH SLP data in [hPa] for a) CESM1-WACCM Natural, b) CESM1(WACCM) RCP8.5, c) CCSM4 Control and d) CCSM4 RCP8.5. The zero contour line is depicted in bold, negtaive values are indicated by dashed contours. The contour interval is 0.3 hPa.

sector. The SLP anomaly in the Pacific is even stronger than the anomaly in the Atlantic Ocean. This signal is apparent in the low-top as well as in the high-top model (Figure 4.9). It might be connected to the strong El Niño Southern Oscillation (ENSO) signal in CCSM4 and CESM1(WACCM) (*Deser et al.* [2012], *Marsh et al.* [2013]).

The corresponding NAO indices are to be found in Appendix A. The indices do not show a trend in the NAO signal but there is one distinctive feature in the CESM1(WACCM) RCP8.5 run: for the period from 2030 to about 2060 the variability of the NAO is very

low compared to the rest of the timeseries. Such a period of low variability is not apparent in the other model runs, nor in the reanalysis data.

4.3 The Atlantic Meridional Overturning Circulation

To characterize the Atlantic Meridional Overturning Circulation (AMOC) in the model data first a look at the mean meridional stream function will be taken. After that the maximum mixed layer depth (MLD) is characterized as it is an important feature for the variability of deep water formation and therefore also for the variability of AMOC strength (as it was pointed out in Chapter 2.2.2).

The mean stream function of the AMOC for the different simulations is presented in Figure 4.10. The maxima of the stream functions are located at a depth of about 1000 m around 35°N for CCSM4 and around 35°N and 40°N for the CESM1(WACCM) runs. The RCP8.5

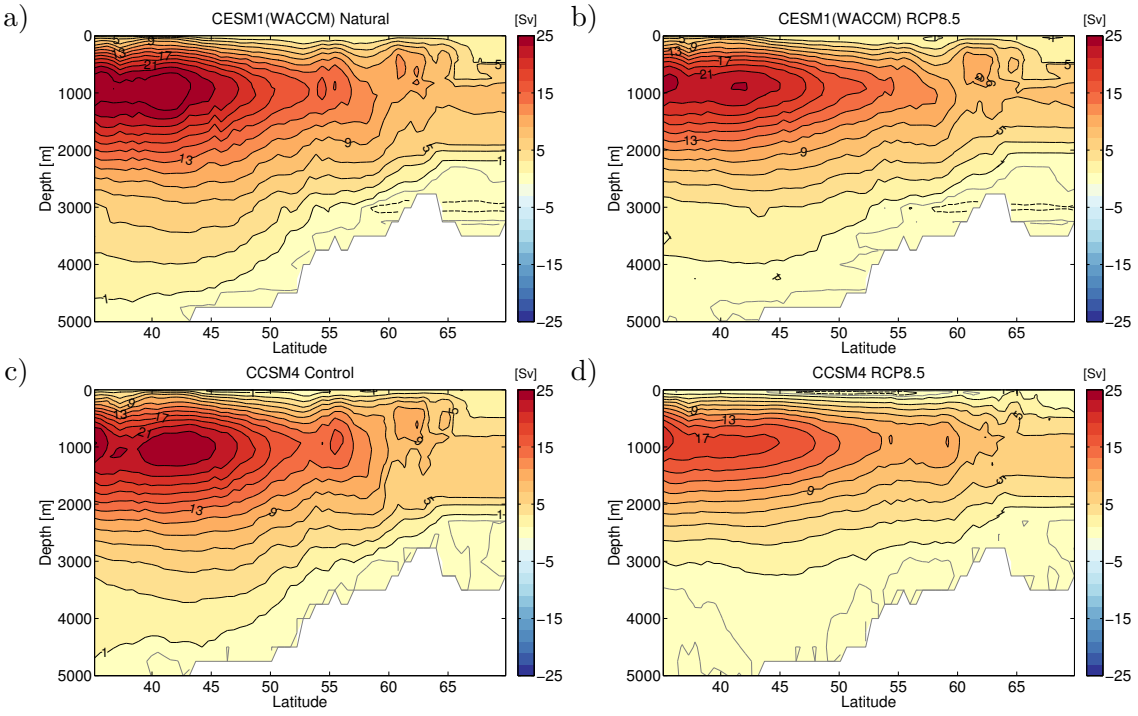

FIGURE 4.10: Meridional Overturning in the Atlantic Ocean represented by the meridional streamfunction in [Sv] (1Sv $= 10^6 \mathrm{m}^3/\mathrm{s}$) for a) CESM1-WACCM Natural, b) CESM1(WACCM) RCP8.5, c) CCSM4 Control and d) CCSM4 RCP8.5. Positive values with contour intervals of 2 Sv, negative values with contour intervals of 0.5 Sv (dashed), the zero contour line is colored in grey.

simulations show a weaker mean overturning compared to the Natural/Control experiments; the CCSM4 runs show a weaker overturning compared to the CESM1(WACCM)

runs. The difference between Natural/Control and RCP8.5 simulations is due to the

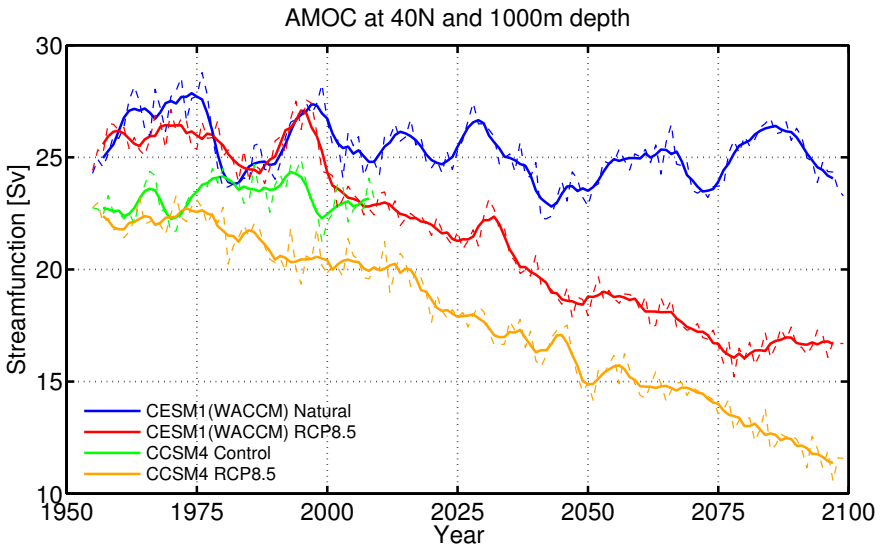

FIGURE 4.11: AMOC strenght in [Sv] at 40°N and 1000 m depth with time for CESM1(WACCM) Natural (blue), CESM1(WACCM) RCP8.5 (red), CCSM4 Control (green) and CCSM4 RCP8.5 (orange). The dashed curves represent annular mean values, the solid lines represent 5-year running means. The time axis does not depict the corresponding years for CCSM4 Control, which would span from 1053 to 1108, it is displayed as starting in 1955.

weakening of the overturning with climate change that is apparent in both models (Figure 4.11).

Comparing these stream functions to SODA (see Section 2.2.2, Figure 2.15) one can see that latitude position and depth of the overturning maxima in the model simulations are very close to reanalysis. The absolute strength, though, is too high in the models. It exceeds 21 Sv whereas the observed AMOC strength is estimated to be about 16 ± 2 Sv at about 43°N (*Schott and Brandt* [2007]).

As the strength of the AMOC is connected to the formation of deep water masses, the representation of winter deep convection in the models is presented in the following. Therefore, the March MLD is considered as the maximum MLD is reached in early spring, usually during March. Figure 4.12 shows the maximum MLD for March in the model data. The March MLD pattern in the model data compares well to the observations (2.13) regarding the spatial distribution. The amplitude can unfortunately not be compared directly as the definitions of the MLD differ between model and observational data. For the WOD05 and SODA data the MLD is defined as the depth at which the potential density exceeds the surface density by 0.1 kg m^{-3} (*Schott et al.* [2009]). The MLD in the model data is defined as the depth at which potential density exceeds the surface density

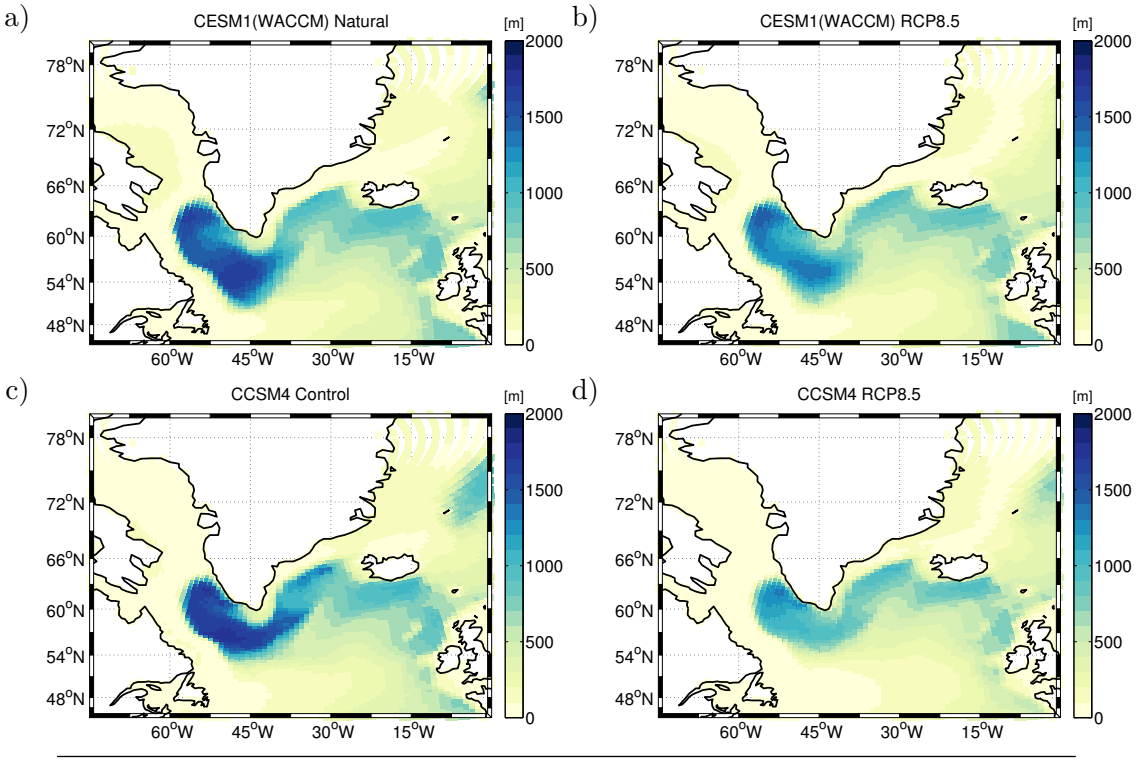

FIGURE 4.12: Maximum March MLD in [m] for a) CESM1-WACCM Natural, b) CESM1(WACCM) RCP8.5, c) CCSM4 Control and d) CCSM4 RCP8.5.

by 0.125 kg m^{-3} (*Danabasoglu et al.* [2012b]). So, the threshold is stricter for the model data. Instead of the mean March MLD that is shown in Figure 2.13, Figure 4.12 shows the maximum MLD during March. For the model simulations the maximum MLD is used because the mean MLD was not available as a variable for all model simulations. For those experiments, where the mean MLD is available, the difference in spatial distribution is very small (not shown).

The temporal evolution in MLD for the model data is shown in Figure 4.13. The region used to calculate these timeseries is based on gridpoints close to region K1 indicated in Figure 2.13, because for this station there are direct measurements available to compare with. Regarding the Natural/Control runs (Figure 4.13a and c), one can see that maximum MLDs close to 2000 m are reached. CESM1(WACCM) shows stronger variability in MLD (700 to 1900 m depth) on the interannual scale compared to CCSM4 (which varies between 1700 to 1900 m). CESM1(WACCM) is thereby closer to observations than CCSM4 (recall Figure 2.14). Another difference between the high and the low-top model can be found in the consistency of MLD between two or more successive years. In CESM1(WACCM), years with a low MLD are followed by years that do also show a relatively low MLD. The maximum depth increases only stepwise. In CCSM4 this is

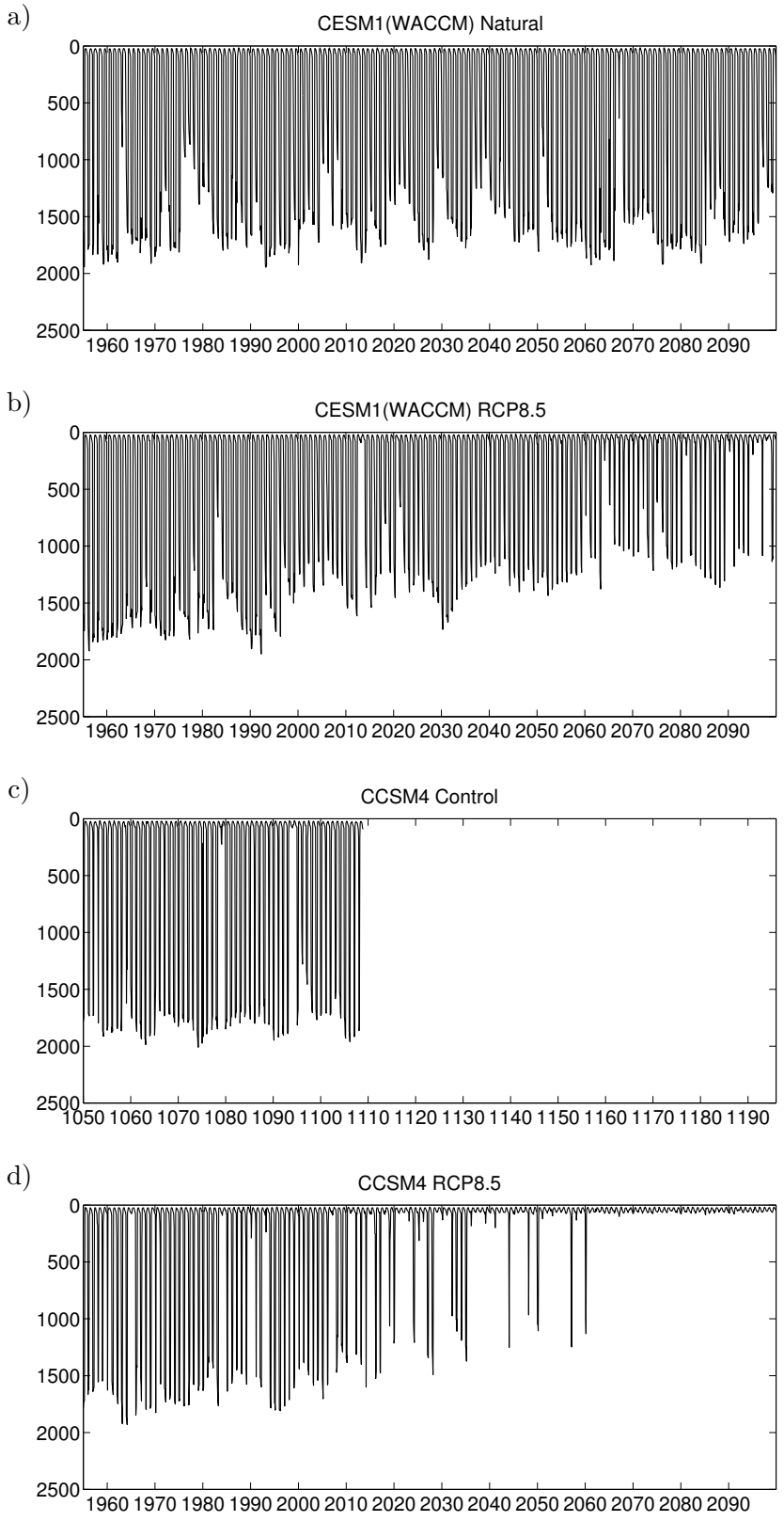

FIGURE 4.13: Maximum MLD at K1 in [m] with time (compare Figure 2.13) for a) CESM1-WACCM Natural, b) CESM1(WACCM) RCP8.5, c) CCSM4 Control and d) CCSM4 RCP8.5.

also the case to some degree, only there are also years where there is no deep convection at all (MLDs of only a few meters), which are followed by years with very high MLDs. This is not very realistic, as the previous winter conditions ifluence the strength of deep convection in the following year (recall the preconditioning phase described in Chapter 2.2.2).

The RCP8.5 runs (Figure 4.13b and d) show a decrease in MLD with time, which is consistent with the decrease in AMOC strength under global warming. For CCSM4 the number of years with deep convection decreases strongly after 2020 and deep convection even stops after about 2060. The reduction of MLD under global warming is much stronger for the low-top compared to the high-top model. A similar reduction in MLD in the Labrador Sea under global warming was also described by *Guemas and Salas-Mélia* [2007]. Deep convection stopped in their setup after the year 2040. They used the coupled model CNRM-CM3[1] (with the atmospheric component run on a horizontal grid of about 2.8° resolution and 45 levels on the vertical) and argued that atmospheric circulation in the lower stratosphere is represented correctly. The GHG scenario they used (SRES-A1B[2]) is characterized by a much lower atmospheric CO_2 increase compared to the RCP8.5 scenario investigated here. Nevertheless, they find an even stronger decrease in deep convection in the Labrador Sea. The reasons for that can not be inferred from the analysis carried out here, but a different representation of the change in sea ice cover and/or change in freshwarter budget under global warming are very likely. The difference between CESM1(WACCM) and CCSM4 in MLD reduction has to be due to the atmospheric forcing as ocean and sea ice componets in both models are identical.

Measurements and SODA simulations of the MLD at K1 are depicted in Figure 2.14. Comparing these with the model results leads to the conclusion that deep convection is overestimated in the model data (at least at K1), which is consistent with the overestimated AMOC strength. In the CCSM4 and CESM1(WACCM) model simulations the mean MLD is too deep but the variability seems to be too weak and is best represented in CESM1(WACCM) Natural. Very deep convection reaching levels below 2000 m is missing in the model simulations but is also not captured in SODA. The regions of deep convection, though, are represented very well in CESM1(WACCM) and CCSM4.

[1] third version of the CNRM (Centre National de Recherches Météorologiques) global atmosphere-ocean-sea ice coupled model (CNRM-CM3)

[2] IPCC special report on emission scenarios A1B scenario

In this chapter it was shown that stratospheric vortex events in CESM1(WACCM) connect significantly to the surface, whereas this link is missing in CCSM4. Under the GHG scenario the significance of downward coupling between the stratosphere and the surface decreased for strong polar vortex events in CESM1(WACCM). In CCSM4 the number of strong vortex events detected for this scenario was very low and the reliability of the information gained from the composite analysis regarding this experiment is questionable. The NAO in CESM1(WACCM) and CCSM4 shows a prominant anomaly in the Pacific section of the NH that is not apparent in ERA-40. This feature does not change under the GHG scenario.

The structure of the AMOC and the regions of deep water formation are represented well in CESM1(WACCM) and CCSM4, but the strength of the AMOC is overestimated in both models. The variability of deep water formation in the Labrador Sea, that was investigated using maximum MLD, is better represented in CESM1(WACCM) than in CCSM4. Under global warming the depth of the MLD decreases with time, indicating a reduction in deep water formation in the Labrador Sea. In CCSM4 deep convection stops in the middle of the 21^{st} century. This is consistent with the observed decrease in strength of the AMOC under the RCP8.5 scenario.

Chapter 5

The Connection of the Stratosphere to North Atlantic Climate

To examine the stratospheric influence on atmospheric and oceanic surface parameters, in this Chapter, the patterns of different atmospheric surface variables as well as of ocean parameters are shown as composites for weak and strong vortex events. In all cases, the mean of three months following the onset of a weak or strong vortex event is shown. For this analysis only monthly mean anomaly data is used to exclude low frequency variability. First the high-top model results will be presented followed by the results for the low-top model.

5.1 CESM1(WACCM)

5.1.1 Atmospheric Patterns

The composites of sea level pressure (SLP) in the high-top model show an NAO-like pattern (Figure 5.1) with significant anomalies confined to the North Atlantic (NA) sector in the CESM1(WACCM) Natural simulation for weak vortex events. For strong events in this experiment there is also a significant signal in the North Pacific. For the GHG run the SLP composite for weak vortex events is comparable to that of the Natural run, although

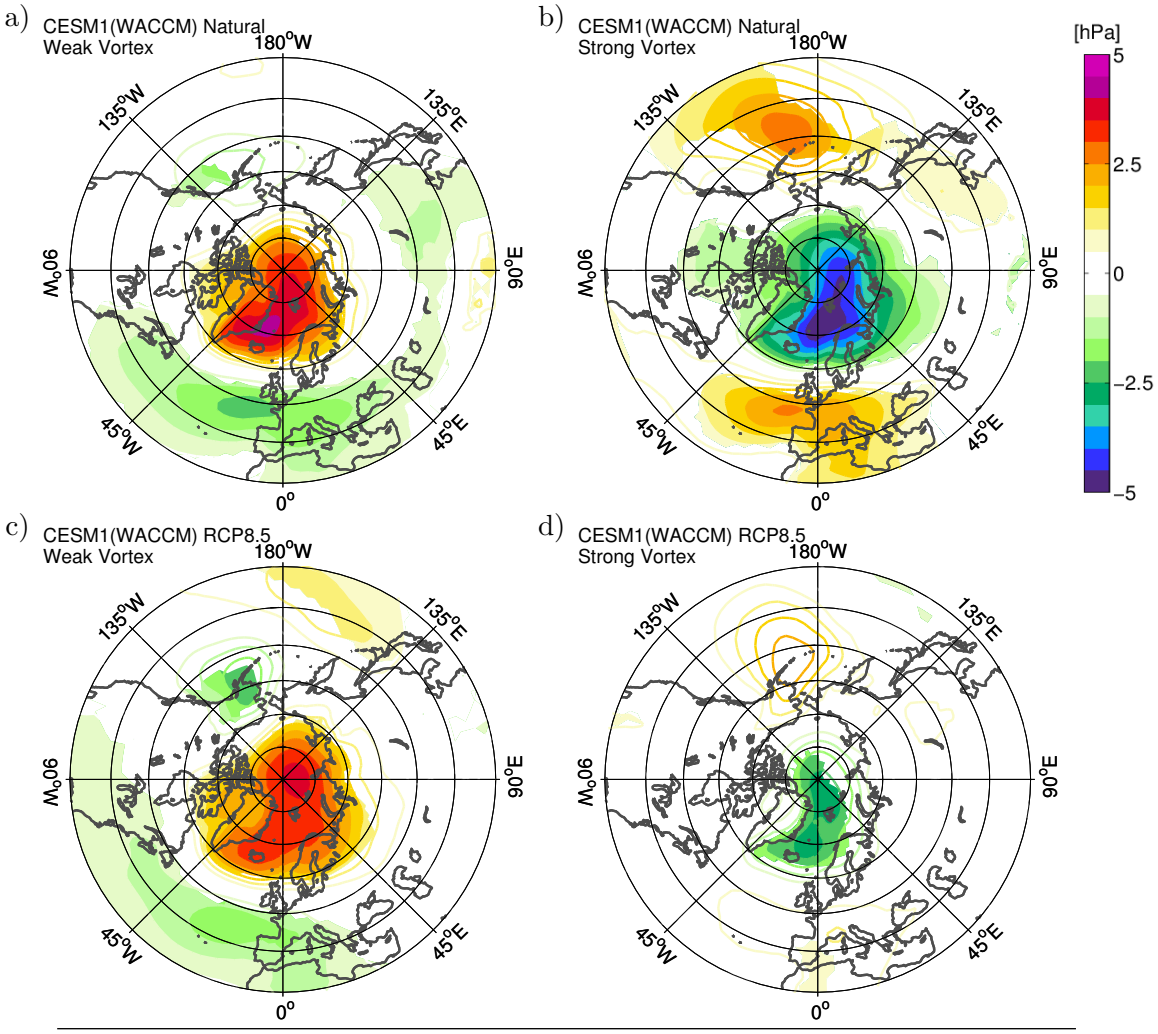

FIGURE 5.1: Composites of Sea Level Pressure in [hPa] for CESM1(WACCM) Natural (a and b) and CESM1(WACCM) RCP8.5 (c and d). Mean of three months after the onset of weak (a and c) and strong (b and d) stratospheric vortex events. Filled contours represent anomalies that are significant at the 90% level. The contour interval is 0.5 hPa.

the anomalies are smaller. In the case of the strong vortex events, the GHG simulation shows significant anomalies in SLP only over the polar region (east of Greenland).

In general, a weak (strong) stratospheric vortex event is connected to a positive (negative) SLP anomaly over the pole and to a negative (positive) anomaly over the middle latitudes. So, the SLP composites of weak (strong) polar vortex events show some similaties to a negative (positive) NAO-like SLP pattern (recall Figure 2.6). The composites for the strong events are not as similar to an NAO-like pattern as the weak events are. In the Natural simulation an anomaly in the Pacific sector is apparent that is even more significant than the anomaly in the NA region. This feature is not common for the NAO in reanalysis data, but it is apparent in the NAO pattern derived for the model data (Figure 4.9). Therefore, one can conclude that the composite of SLP for strong vortex

events does show a positive NAO-like pattern despite the anomaly in the North Pacific. The RCP8.5 simulation on the other hand does not show any significant anomaly in SLP at the middle latitudes for the strong vortex events and is therefore not comparable to a positive NAO phase.

As the composites for weak and strong vortex events show (at least partially) an NAO-like SLP pattern, the parameters that are influenced by the state of the NAO are looked at in more detail in the following. Variability in the SLP, that can be described by the NAO, is connected to changes in wind stress and thereby also in surface heat fuxes over the ocean (see Chapter 2.2.1). Figures 5.2 to 5.5 show the composites for weak and strong vortex events of zonal and meridional wind stress as well as of latent and sensible surface heat fluxes.

The composites of zonal wind stress (Figure 5.2) show that for the Natural as well as for

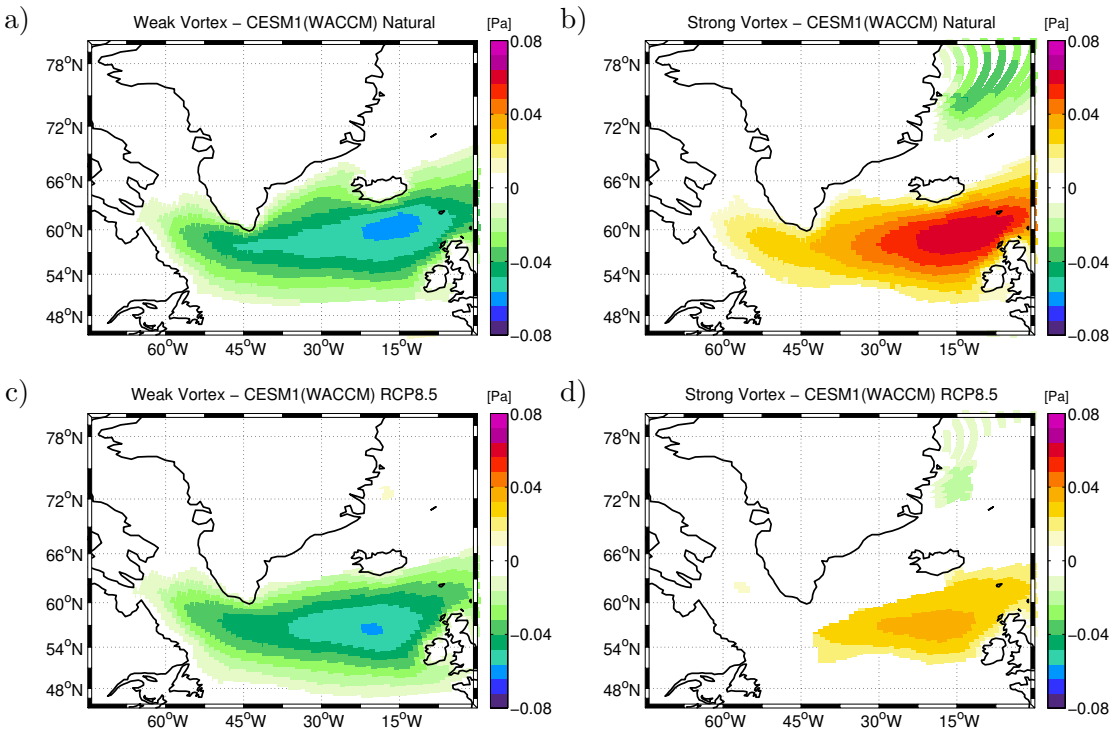

FIGURE 5.2: Composites of zonal wind stress in [Pa] for CESM1(WACCM) Natural (a and b) and CESM1(WACCM) RCP8.5 (c and d). Mean of three months after the onset of weak (a and c) and strong (b and d) stratospheric vortex events. Coloured areas are significant at the 90% level.

the GHG run a weak vortex event (negative NAO) is connected to an easterly anomaly in zonal wind stress (decreasing the strength of mean zonal westerlies) whereas a strong vortex event (positive NAO) is connected to an increase in westerly wind stress over the middle latitudes. The strongest anomaly can be found over the eastern part of the NA

basin between 55 and 65°N. The weakest response is observed for the CESM1(WACCM) RCP8.5 run. This was to be expected from the composites of SLP (Figure 5.1), showing that the pattern that bared the smallest resemblance to the NAO, also featured the smallest anomaly in zonal wind stress (Figures 5.1d and 5.2d). Apart from the main signal in the central NA region, another anomaly is to find north of about 70°N (east of Greenland). It is apparent only in the composites for the strong vortex events. It is an easterly anomaly and thereby of opposite sign compared to the anomaly in the central NA basin. In the Natural run this anomaly is much more significant and of higher amplitude compared to the RCP8.5 run.

The composites of the meridional wind stress are shown in Figure 5.3. In the Natural simulation the composite for weak vortex events reveals a northward wind stress anomaly west of the southern tip of Greenland, decreasing the southward transport of cold air from the North. Between 45 and 15°W a southward anomaly in wind stress is apparent. This feature increases the transport of cold and dry air masses from Greenland over the Irminger Sea. In the composite for strong vortex events there is a significant southward wind stress anomaly located east of Greenland between 66 and 78°N, whereas in the region of the North Atlantic Current (recall Figure 2.17) a northward anomaly in wind stress can be recognized. In the GHG run, the pattern of meridional wind stress anomaly connected to weak and strong stratospheric vortex events cover the same regions as in the Natural run, but significance and amplitude of the anomalies is much smaller.

Anomalies in strength and direction of zonal and meridional wind stress can influence the amount of heat released from the ocean into the atmosphere. The heat fluxes responsible for the transfer of heat from ocean to atmosphere are turbulent heat fluxes that depend on the amplitude of the wind itself and on the difference in temperature (for sensible heat flux) or specific humidity (for latent heat flux) at the interface between ocean and atmosphere. That is why cold and dry winds originating from land or ice surfaces increase the oceanic loss of heat by increasing the gradient in temperature and specific humidity at the atmosphere-ocean interface. As the wind stress anomalies differ considerably from the mean state for strong and weak vortex events also the turbulent heat fluxes should feature significant anomalies connected to stratospheric events.

The latent heat pattern connected to weak vortex events is characterized by a decreased loss of heat from the ocean to the atmosphere in the latitude range from about 50 to 65°N for the Natural as well as for the RCP8.5 experiment (Figure 5.4a and c). This is in line with the decreased westerly wind stress in that region (Figure 5.2a and c). There

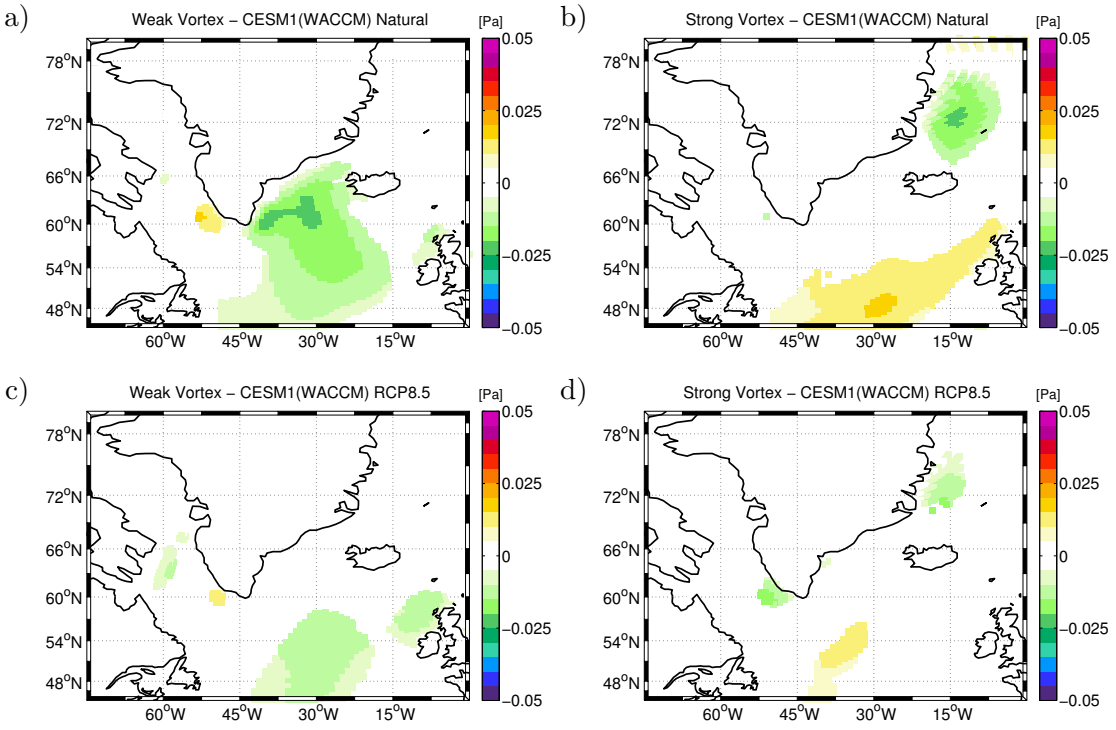

FIGURE 5.3: Composites of meridional wind stress in [Pa] for CESM1(WACCM) Natural (a and b) and CESM1(WACCM) RCP8.5 (c and d). Mean of three months after the onset of weak (a and c) and strong (b and d) stratospheric vortex events. Coloured areas are significant at the 90% level.

is one difference between both experiments, as the negative anomaly in latent heat flux in the RCP8.5 experiment covers a larger area than in the Natural run, in which also a positive anomaly (indicating an enhanced transfer of heat from ocean to atmosphere) can be observed north of Iceland (along about 66°N). This difference might be connected to the different amplitude in merdional wind stress anomaly between the Natural and the RCP8.5 run (Figure 5.3a and c). In the Natural experiment there is a northerly anomaly in wind stress east of Greenland between 60 and 66°N presumably decreasing humidity over the Irminger Sea and thereby counteracting the effect of diminished westerlies in that region.

In the case of the strong vortex events (Figure 5.4b and d), the signal in the RCP8.5 simulation is not as significant as the one in the Natural experiment. It is hallmarked by a stronger than usual latent heat transfer from the ocean towards the atmosphere. The area affected is shifted towards the North by about 1° compared to the weak vortex events. North of 72°N another positive anomaly is apparent signalizing an increase in heat transfer from ocean to atmosphere in the Greenland Sea after the onset of a strong vortex event. This additional anomaly in latent heat flux north of 72°N might be due to

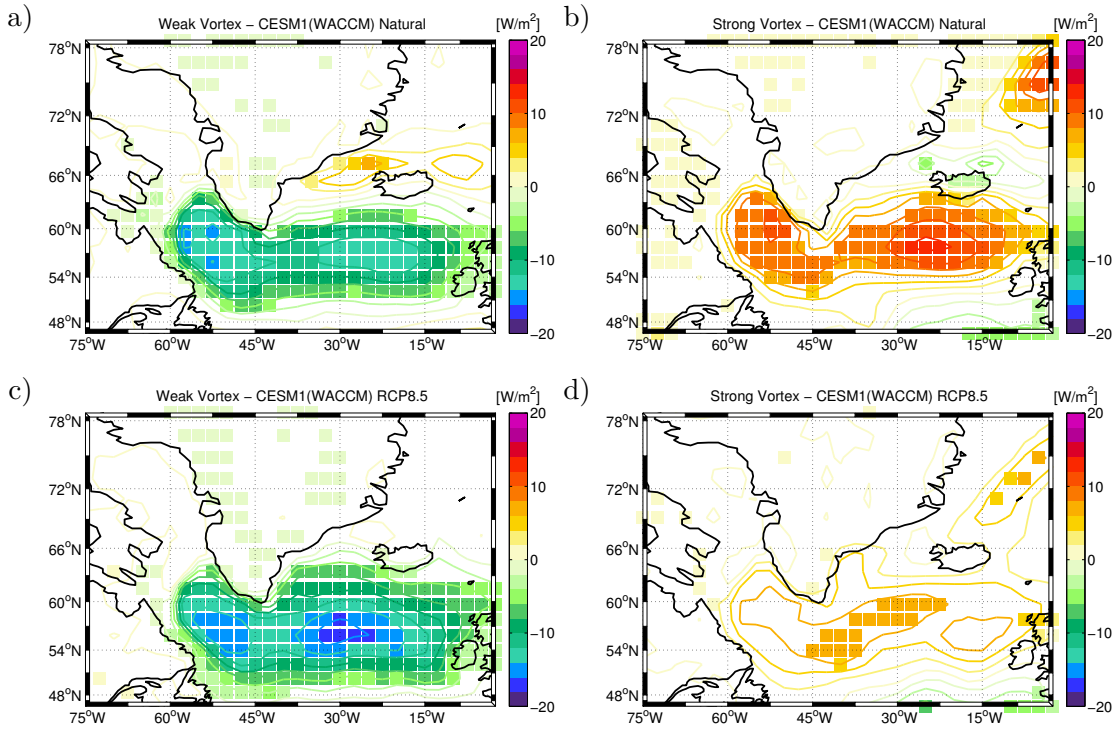

FIGURE 5.4: Composites of latent heat flux in [W/m^2] for CESM1(WACCM) Natural (a and b) and CESM1(WACCM) RCP8.5 (c and d). Mean of three months after the onset of weak (a and c) and strong (b and d) stratospheric vortex events. Filled squares indicate areas that are significant at the 90% level. Contours are depicted in an interval of 2 W/m^2.

the anomaly in zonal wind stress in that region (Figure 5.2b and d).

The anomaly patterns in the case of the sensible heat flux (Figure 5.5) compare well to the ones of the latent heat flux anomalies, in such a way that weak events are connected to a reduced heat transfer from ocean to atmosphere and strong events are connected to an increased oceanic heat loss. These anomalies are confined to the latitude range between about 50 and 66°N. The differences between the Natural and the GHG experiment in the composites for weak vortex events and the difference between strong and weak event composites north of 72°N, that were described for the composites of the latent heat flux are apparent also in the composites of the sensible heat flux. The RCP8.5 simulation does not show any significant anomalies in the composite for strong vortex events (in contrast to the latent heat flux where there were at least a few spots with significance). The sensible heat flux anomalies in the composites for the weak events is wider-stretched in the case of the RCP8.5 simulation compared to the Natural one. As in the latent heat flux anomalies in the Natural experiment a sensible heat flux anomaly of different sign occurs north of 66°N, only now for both, weak and strong events. A difference to the latent

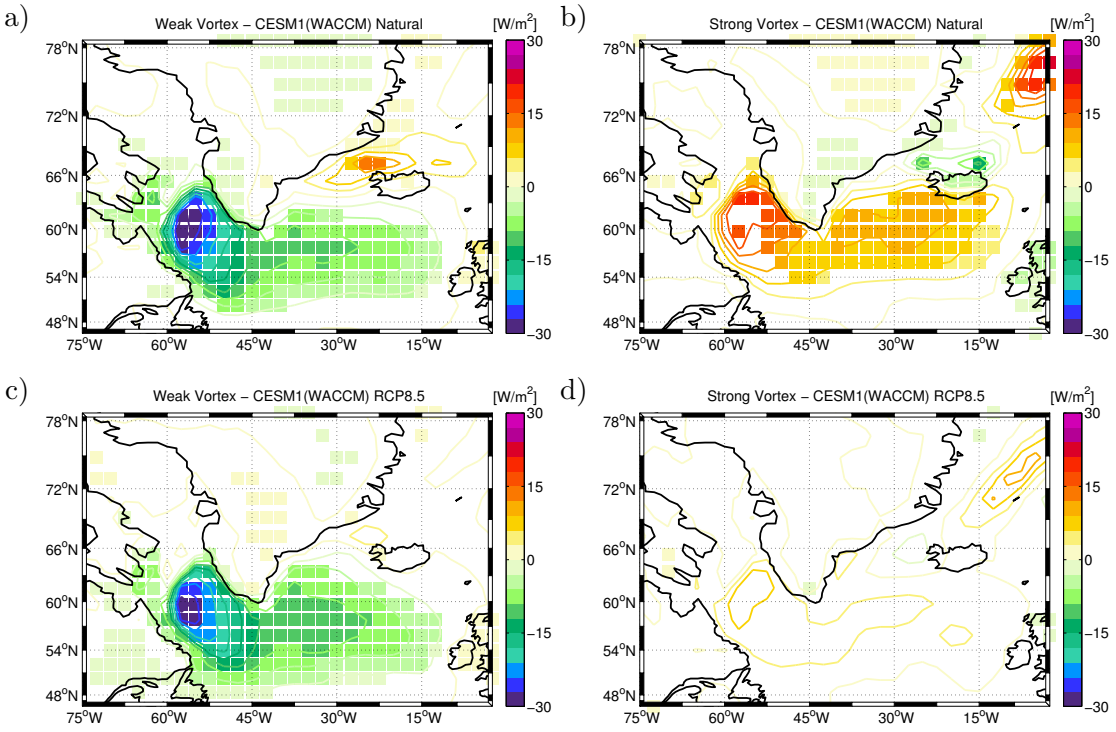

FIGURE 5.5: Composites of sensible heat flux in [W/m^2] for CESM1(WACCM) Natural (a and b) and CESM1(WACCM) RCP8.5 (c and d). Mean of three months after the onset of weak (a and c) and strong (b and d) stratospheric vortex events. Filled squares indicate areas that are significant at the 90% level. Contours are depicetd in an interval of 3 W/m^2.

heat flux composites is that there is a distinct maximum in amplitude in the sensible heat flux anomaly connected to stratospheric vortex events, located in the Labrador Sea. The anomalous sensible heat flux in the Labrador Sea is higher than anywhere else in the NA region (for weak and strong events).

Summerizing, the high-top model showed a response in the NA region to stratospheric voretx events that is comaprable to an NAO anomaly. It affects wind stress as well as surface heat fluxes and can therefore be expected to also have an influence on the production of oceanic water masses.

5.1.2 Ocean Response

As the composites of the atmospheric parameters already suggest, there is a pattern in the ocean mixed layer depth (MLD) that can be connected to stratospheric polar vortex events. These changes in MLD are represented in composites of strong and weak vortex events in Figure 5.6. Again the maxmimum monthly MLD is regarded here (for more

information see Section 4.3).

The preconditioning of open-ocean convection and therefore also of MLD is influenced strongly by bouyancy loss due to turbulent heat fluxes (recall Chapter 2.2.2). As discussed in Chapter 5.1.1 in the pace of a weak vortex event, the wind stress over the NA Ocean is decreased and so is the oceanic heat loss. This leads to a smaller than normal buoyancy loss during winter counteracting deep convection. This reasoning can be supported by the

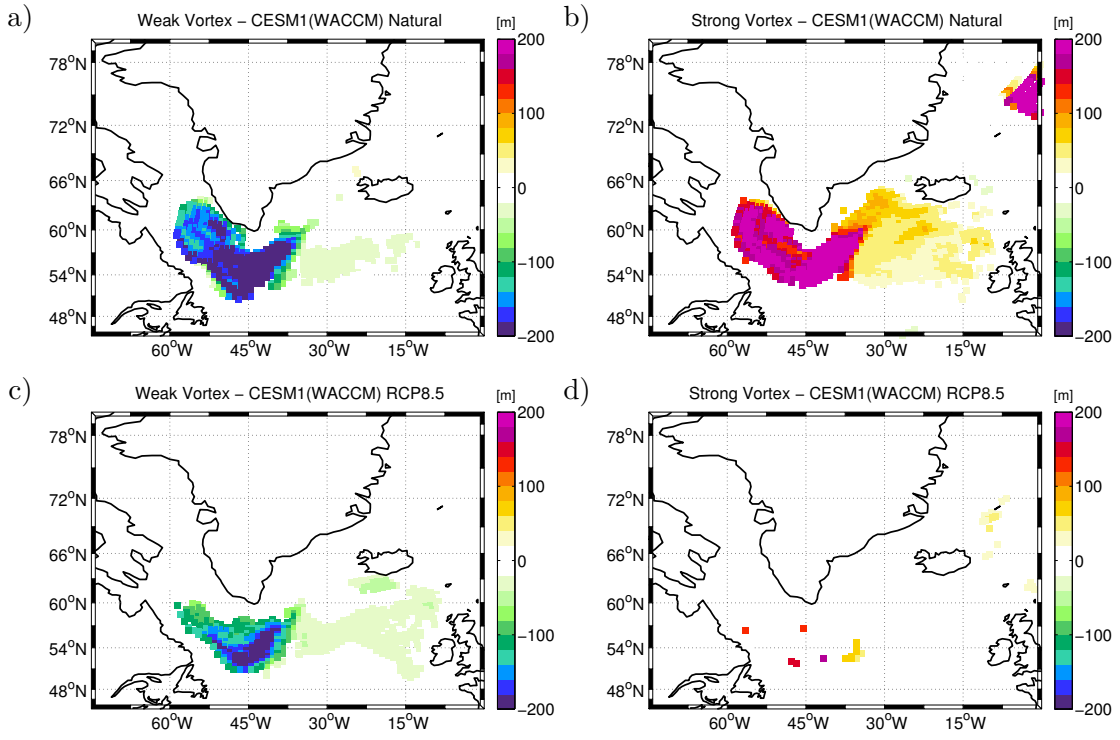

FIGURE 5.6: Composites of Maximum MLD in [m] for CESM1(WACCM) Natural (a and b) and CESM1(WACCM) RCP8.5 (c and d). Mean of three months after the onset of weak (a and c) and strong (b and d) stratospheric vortex events. Coloured areas are significant at the 90% level.

composites of the MLD for weak vortex events (Figure 5.6a and c) showing a shallower MLD than normal. The region most effected is the Labrador Sea as this was also the region most effected by the sensible heat flux anomalies (Figure 5.5). In the RCP8.5 run the region of significant anomalies connected to a weak vortex events is smaller compared to the Natural run. The maximum of MLD anomaly is located south of Greenland in the GHG run, whereas in the Natural run it is wider-spread covering also regions within the Labrador Sea. For strong stratospheric vortex events (Figure 5.6b and d) the MLD signal in the RCP8.5 simulation is not significant, which is due the already discussed lack of NAO-like forcing in this case. In the Natural run the MLD pattern arising from a strong vortex forcing covers a similar region as for the weak vortex events, only spreading a bit

further towards Iceland and not as far south. The anomaly of MLD in the Labrador Sea is larger in amplitude compared to the composites of the weak events. There is also a MLD anomaly north of 70°N in the Natural run that can be connected to the observed anomalies in surface wind stress and turbulent heat flux in that region (Chpater 5.1.1). This suggests an increase in deep water formation also in the Greenland Sea following a strong vortex event in the Natural experiment.
In general, a weak vortex event is connected to shallower than normal MLDs, whereas a strong vortex event is connected to deeper than normal MLDs and can thereby influence the production of North Atlantic Deep Water. This anomaly is mainly found in the Labrador Sea (after weak events in the Natural as well as in the RCP8.5 run and after strong events in the Natural run). Only after a strong polar vortex event an anomaly in MLD in the Greenland Sea can be recognized in the Natural experiment.

5.2 CCSM4

5.2.1 Atmospheric Patterns

In contrast to the high-top model the SLP patterns following weak and strong stratospheric polar vortex events in the low-top model (Figure 5.7) do not show a signal that is as close to the NAO, as the SLP anomaly in the NA sector is diminished or missing.
For the composites of the weak vortex events there is a strong positive SLP anomaly over the pole and a weak negative anomaly over the North Atlantic in the Control run. This pattern is closest to an NAO-like SLP pattern in the CCSM4 data. In the GHG run the anomalies over the pole and over the NA region are weaker compared to the Control run and the negative anomaly over the NA section is confined to the eastern part of the basin.
The composites of the strong vortex events show a negative anomaly over the pole for the GHG and the Control run, a positive anomaly over the North Pacific region for the GHG run and a positive anomaly over Southern Europe for the Control run.
In spite of the diminished SLP anomaly over the NA sector there is a response to weak and strong vortex events in surface wind stress (Figures 5.8 and 5.9) as well as in turbulent heat flux (Figures 5.10 and 5.11).
The composites of zonal wind stress are depicted in Figure 5.8. As in CESM1(WACCM), weak vortex events are connected to diminished westerlies whereas strong vortex events

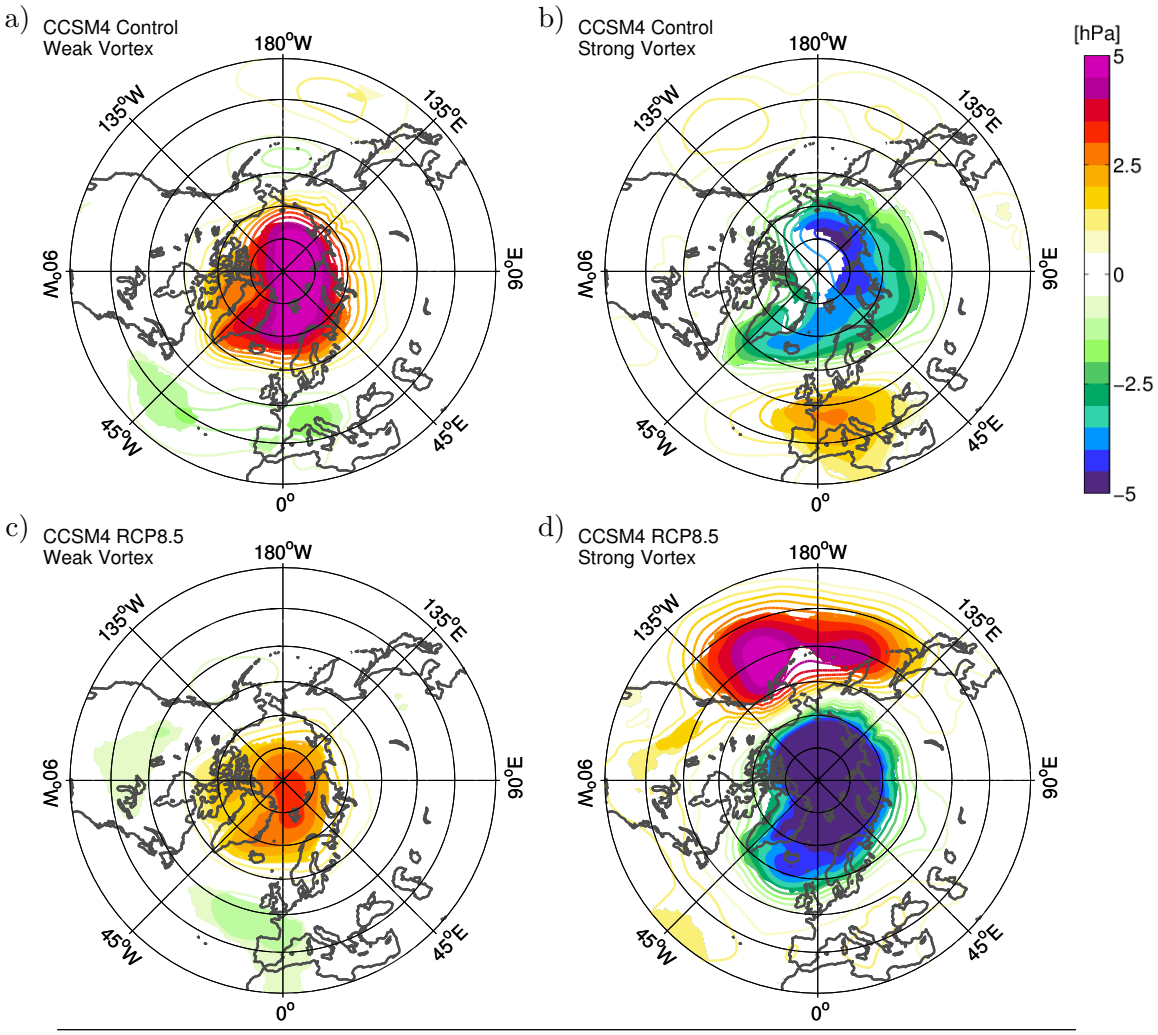

FIGURE 5.7: Composites of the Sea Level Pressure in [hPa] as in Figure 5.1 but for CCSM4 Control (a and b) and CCSM4 RCP8.5 (c and d). Weak events in a) and c), strong events in b) and d).

can be characterized by enhanced westerlies in the central NA region. In the Control run there is another anomaly apparent in the composite for strong vortex events: an easterly anomaly located east of Greenland north of 66°N.

The zonal wind stress anomaly in the composites for weak events spreads further north in the eastern part of the NA basin compared to the anomalies in the composites for strong vortex events. Especially, in the case of the GHG run, the zonal wind stress anomalies connected to a strong vortex event are significant only south of 60°N in the eastern part of the basin. In the western part of the basin they reach further north also covering regions of the Labrador Sea.

The composites of the meridional wind stress anomaly for weak vortex events (Figure

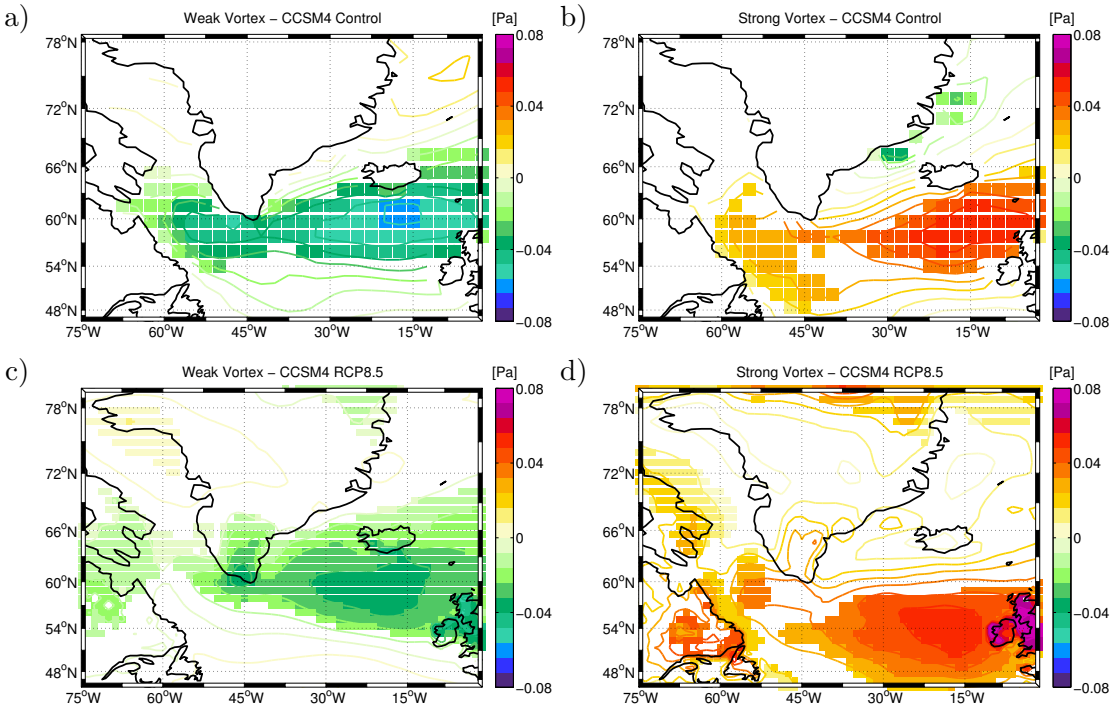

FIGURE 5.8: Composites of zonal wind stress in [Pa] for CCSM4 Control (a and b) and CCSM4 RCP8.5 (c and d). Weak events in a) and c), strong events in b) and d). Filled squares indicate areas that are significant at the 90% level. Contours are depicetd in an interval of 0.008 Pa.

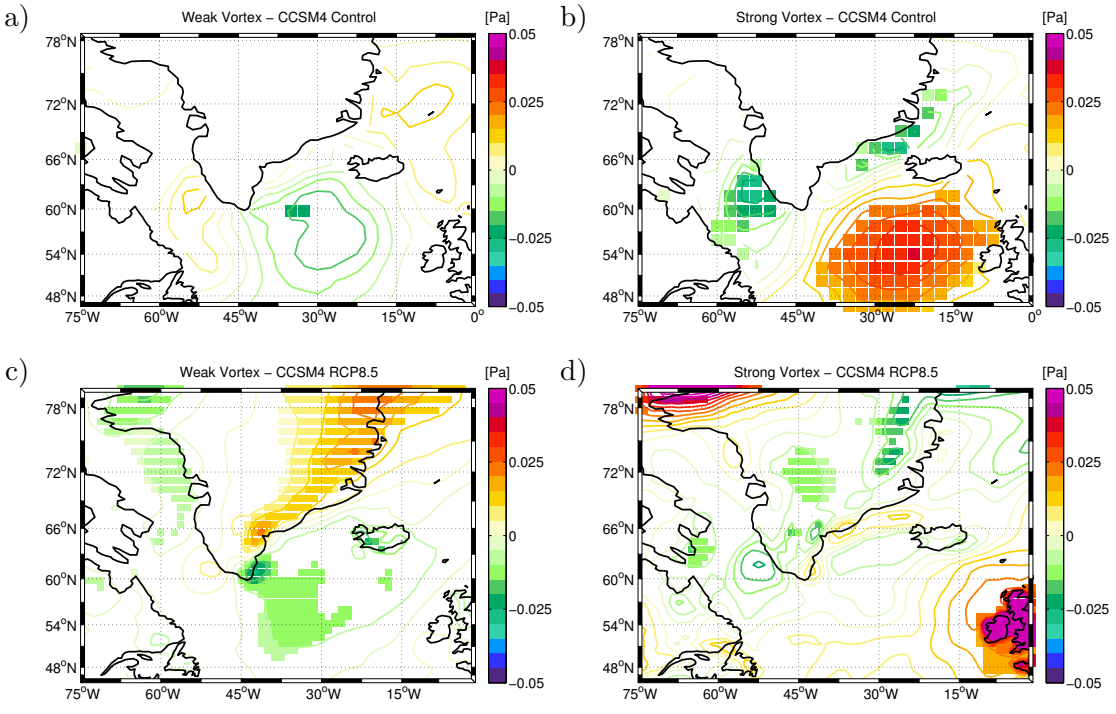

FIGURE 5.9: Composites of meridional wind stress in [Pa] for CCSM4 Control (a and b) and CCSM4 RCP8.5 (c and d). Weak events in a) and c), strong events in b) and d). Filled squares indicate areas that are significant at the 90% level. Contours are depicetd in an interval of 0.008 Pa.

5.9a and c) are close to the pattern described for the high-top model, showing a wide-spread negative (southward) anomaly between 45 and 15°W. Though, a significant positive (northward) anomaly west of Greenland is missing. In the composites for the strong vortex events there is no significant signal in the NA region for the GHG run, but a very strong anomaly pattern is apparent in the Control run. It is characterized by a negative (southward) anomaly west of Greenland (in the Labrador Sea) and east of Greenland (close to the coast, north of 66°N). Additionally, there is a wide-spread positive (northward) anomaly in the eastern part of the basin (south of Iceland).

According to the wind stress pattern there are also significant anomalies in turbulent heat flux in the low-top model connected to weak and strong vortex events. Figure 5.10 shows the latent heat flux anomalies connected to weak and strong events, whereas in Figure 5.11 the sensible heat flux anoamlies are featured. The turbulent heat flux patterns in

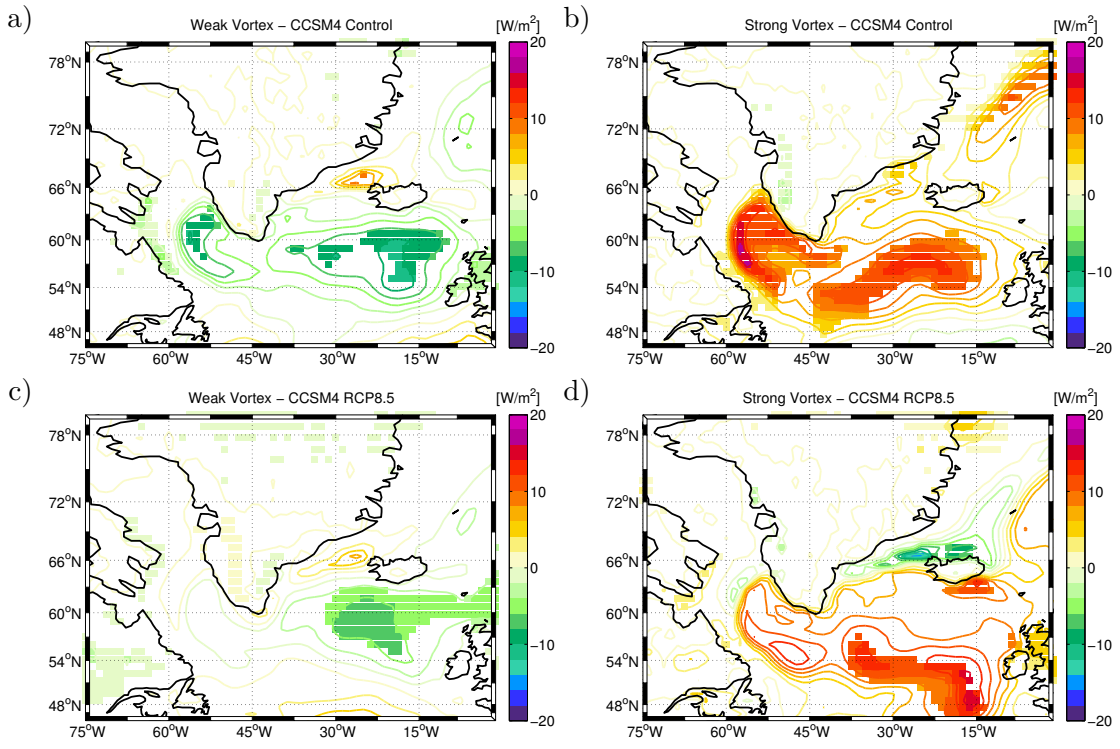

FIGURE 5.10: Composites of latent heat flux in [W/m^2] as in Figure 5.4 but for CCSM4 Control (a and b) and CCSM4 RCP8.5 (c and d). Weak events in a) and c), strong events in b) and d).

general show a negative anomaly (lower than normal oceanic heat loss) for weak stratospheric vortex events and a positive (larger than normal oceanic heat loss) during strong stratospheric vortex events. In the RCP8.5 run significant anomalies occur only in the eastern part of the NA basin except for the sensible heat flux composite of strong vortex

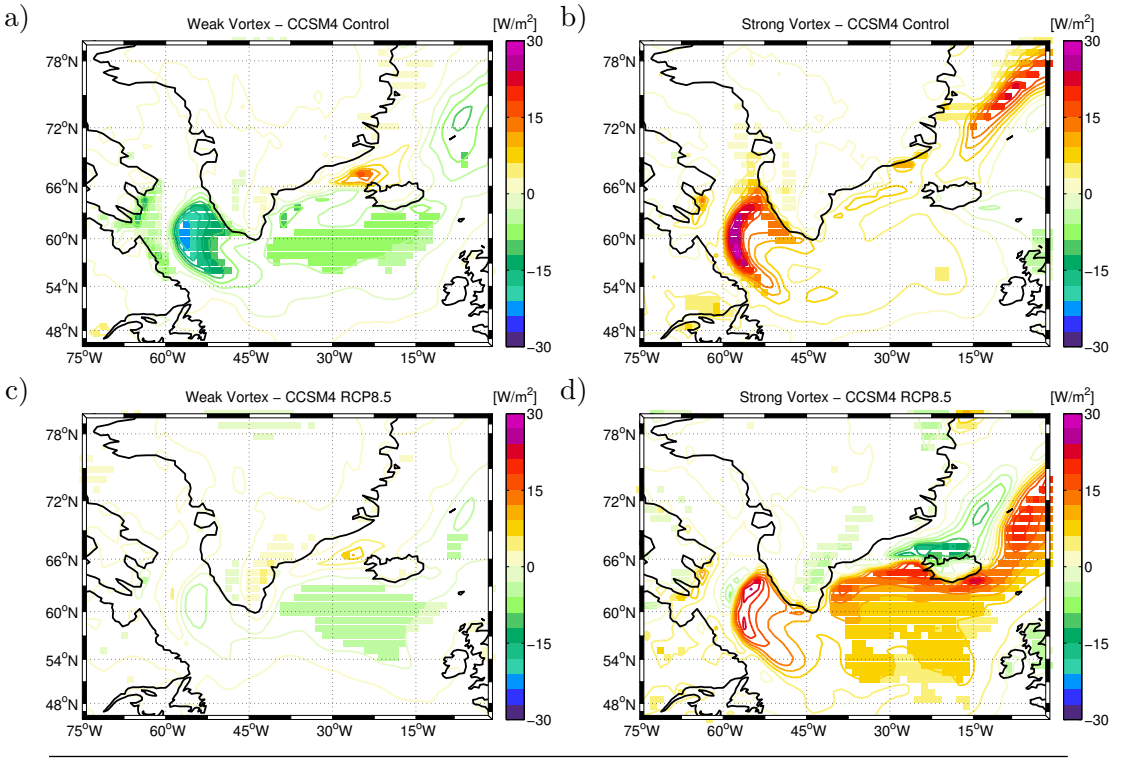

FIGURE 5.11: Composites of sensible heat flux as in Figure 5.5 but for CCSM4 Control (a and b) and CCSM4 RCP8.5 (c and d). Weak events in a) and c), strong events in b) and d). Values are given in $[W/m^2]$.

events, where a very small region in the Larador Sea shows significance. This might be connected to the weak zonal and meridional wind stress anomalies in the western part of the basin for this experiment especially for the composite of the weak vortex events. In the Control run, on the other hand, there are also significant anomalies in the western part of the basin, especially in the Labrador Sea.

In the composites for the strong vortex events there is a positive anomaly (enhanced ocean heat loss) north of 72°N east of Greenland. This signal is not found in the composites for the weak vortex events. The strongest sensible as well as latent heat flux anomalies are found in the Control run over the Labrador Sea region. An execptionally wide-spread positive latent heat flux anomaly over the Labrador Sea in the Control run after a positive vortex event could be connected to the strong southward anomaly in meridional wind stress over that region.

5.2.2 Ocean Response

Although there are some significant heat flux anomalies connected to weak and strong vortex events the significance of the MLD anomalies connected to stratospheric events is very small in CCSM4 (Figure 5.12). It is larger for strong vortex events compared to

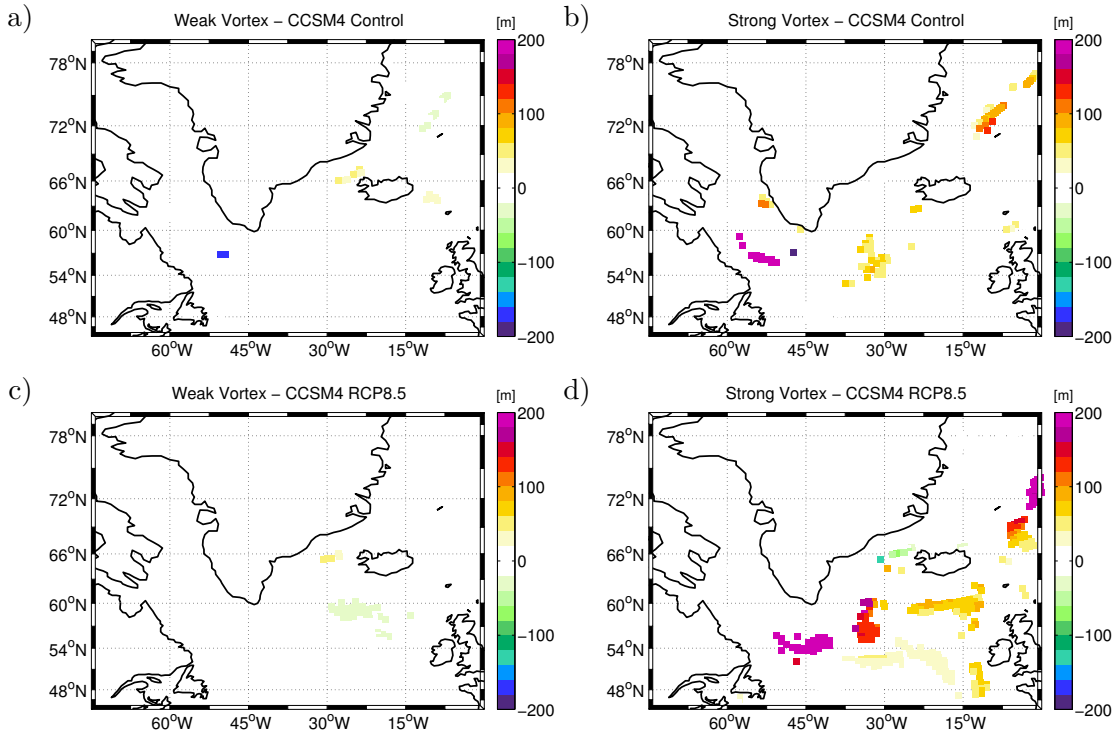

FIGURE 5.12: Composites of Maximum MLD in [m] as in Figure 5.6 but for CCSM4 Control (a and b) and CCSM4 RCP8.5 (c and d). Weak events in a) and c), strong events in b) and d).

weak vortex events. The signal found in the RCP8.5 scenario for strong vortex events can not be connected to the regions of the observed heat flux anaomalies in contrast to the signal in the Control run, where the areas of maximum heat loss after strong events do also show a significant anomaly in MLD although it covers only a very small region.

In summary, it was shown that stratospheric polar vortex events are connected to NAO-like SLP forcings at the surface in CESM1(WACCM). This connection is less pronounced in CCSM4. Changes in wind stress as well as in surface heat fluxes could be found following stratospheric vortex events in both models, although the similarity of the SLP response to an NAO-like pattern in CCSM4 low. The connection of stratospheric events to the oceanic circulation was examined using the maximum MLD. In CESM1(WACCM)

a strong signal in MLD anomalies connected to strong and weak polar vortex events was found, with the largest anomalies in the Labrador Sea. In CCSM4 the significane of MLD anomalies connected to stratospheric vortex events was very low for strong vortex events and even absent for weak vortex events. Under global warming, the composites of atmospheric and oceanic surface parameters showed in general a weaker response to stratopsheric events.
These results lead to the assumption that the strength of the AMOC can be influenced by stratospheric polar vortex events when the stratosphere is reasonalby resolved in a model.

5.3 Lagged Response of the AMOC to NAO and NAM

As a change in the strength of the AMOC due to an NAO-like surface forcing lags about 6-8 years (*Eden and Willebrand* [2001]) behind the surface forcing this section presents a lead-lag correlation analysis linking the AMOC index (maximum of the meridional stream function at 40°N) to the NAO and to the NAM_{10hPA}. The definiton of these indices is described in Chapter 3.3.1 and 3.3.2. For the NAO the station-based index is used. For the correlation 11-year running means are used to investigate the low-frequency relationship between AMOC, NAO and NAM_{10hPA}.
The results of the correlation analysis are presented in Figure 5.13. The blue line represents the auto-correlation of the AMOC. It shows an oscillatory behaviour ranging between periods of 25 to 30 years for the different simulations. The black line indicates the cross-correlation between AMOC and NAM_{10hPA}, the red line the cross-correlation between AMOC and NAO. The AMOC leads for positive lags. The results for the cross-correlations differ between low and high-top model as well as between GHG and Control/Natural experiments. The only similarity can be found between the cross-correlation of AMOC and NAO in CESM1(WACCM) Natural and CCSM4 Control. Both are highly correlated (> 0.7) with the NAO leading the AMOC by 4 years.
In CESM1(WACCM) Natural the NAM_{10hPa} leads the AMOC by 2 years (with a correlation of about 0.6) but as the NAO leads the AMOC with a lag of 4 years, the NAO signal that preceeds the AMOC does not seem to be driven by stratospheric processes. In the case of CESM1(WACCM) RCP8.5 this dependency is not reproduced. Here, the NAM_{10hPa} leads the AMOC by 5 years (with a correlation of about 0.4) followed by the NAO with a lower correlation coefficient (of about 0.3). This indicates that the relation

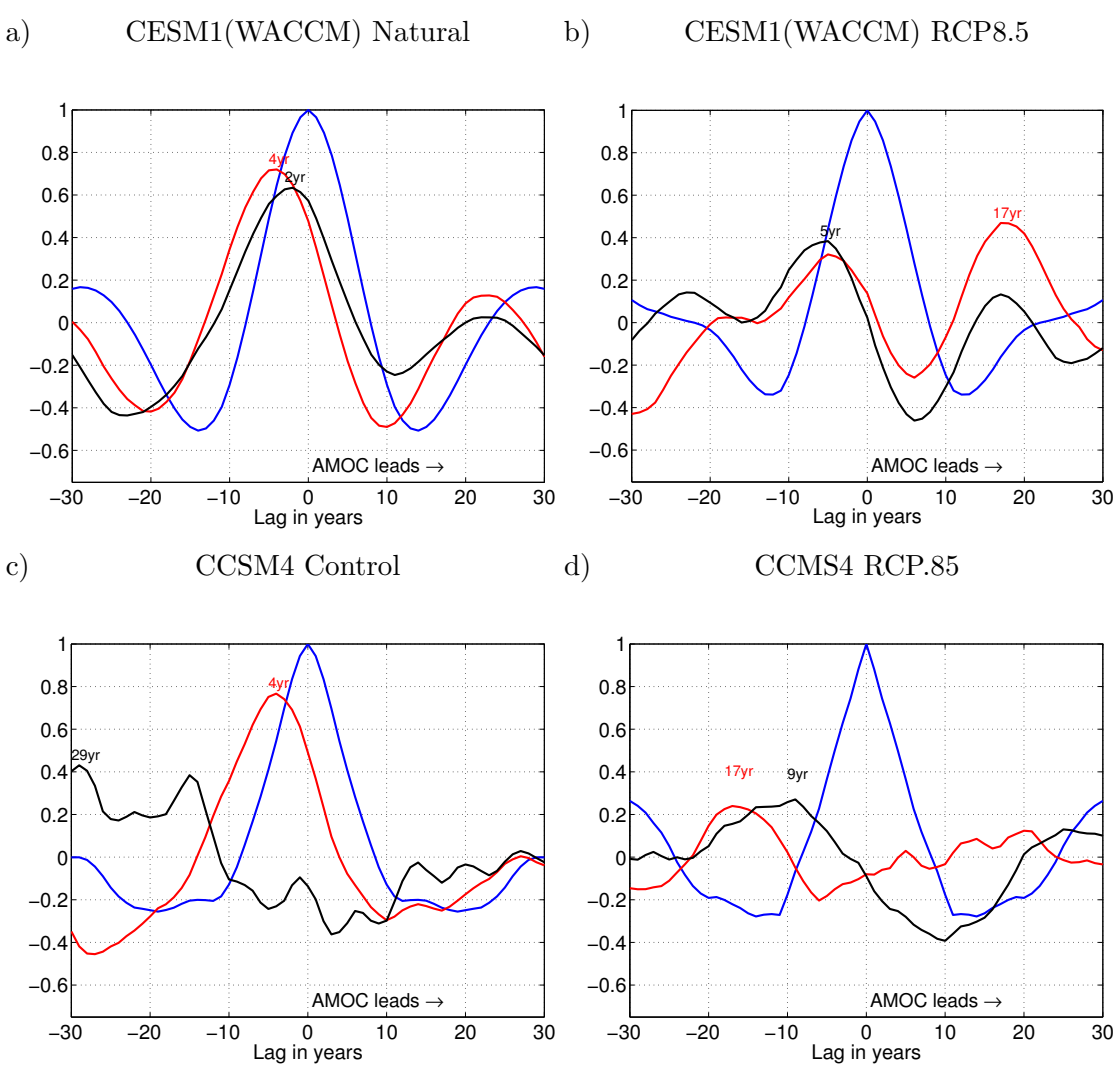

FIGURE 5.13: Lead/Lag auto-correlation of AMOC (blue), cross-correlation of AMOC with NAO (red) and NAM_{10hPa} (black) for a) CESM1(WACCM) Natural, b) CESM1(WACCM) RCP8.5, c) CCSM4 Control, and d) CCSM4 RCP8.5. Lag in [years]. The numbers indicate the lag with the strongest positive correlations. AMOC leads for positive lag.

between the stratosphere, troposphere and NA ocean is influenced by global warming. In CCSM4 Control the signal of the NAM_{10hPa} is not evaluable, neither are the NAO and NAM_{10hPa} signal in CCSM4 RCP8.5 as the correlation with the AMOC is too low. Remarkable is the change of the correlation between AMOC and NAO, that is very high in the Control run and decreases below a correlation coefficient of 0.3 in the RCP8.5 run.

This analysis showed that the influence of the NAM_{10hPa} on the AMOC is not apparent in CCSM4. This was already suggested in the previous section as there was almost no significance found in the relation between MLD and stratospheric polar vortex events.

In CESM1(WACCM), on the other hand, a relation between stratospheric NAM and AMOC can be recognized which is also consistent with the findings in the previous section. Furthermore, both models show a strong connection between NAO and AMOC in the Control/Natural simulation with the NAO leading the AMOC by 4 years. This correlation decreases in the GHG simulation for both models which is consistent with the finding that atmospheric anomalies following a stratospheric polar vortex event are lower under global warming compared to the Control/Natural simulations.

The influence of the NAM_{10hPa} in CESM1(WACCM) is not totally clear as there are differences between the Natural and the RCP8.5 run. In the first case the NAO leads the AMOC, in the second case it is the NAM that leads. This difference is very interesting and further analysis is required to understand the physics behind it.

Chapter 6

Discussion

In this thesis the connection between the winter stratospheric polar vortex and North Atlantic climate variability was investigated using two coupled climate models of the same model family: a high-top, CESM1(WACCM), and a low-top model, CCSM4. To estimate the importance of this connection under global climate change, the RCP8.5 greenhouse gas (GHG) scenario was compared to a scenario with constant GHGs and ozone depleting substances (ODSs) for both models. Stratospheric events were defined using the Northern Annular Mode (NAM) at 10 hPa. Anomalously weak and strong winter polar vortex events were selected and investigated using composite analysis. The downward propagation properties of the different events, their influence on atmospheric and oceanic parameters and their connection to the North Atlantic Oscillation (NAO) was described. In order to analyze the low-frequency dependence between the Atlantic Meridional Overturning Circulation (AMOC) and the NAM/NAO a lead-lag correlation analysis was carried out.

The downward propagation of stratospheric polar vortex anomalies is well captured in CESM1(WACCM), for weak as well as for strong polar vortex events. At 100 hPa, weak and strong vortex events were found to persist for more than 60 days for all cases in CESM1(WACCM). A significant coupling to the surface is missing only in the case of CESM1(WACCM) RCP8.5, for strong polar vortex events. In all other cases the connection between stratosphere and surface is significant and persistent for at least 40 days. This is close to the results from reanalysis data (shown both in this thesis and in *Baldwin* [2001]). In the CCSM4 simulations the downward propagation of stratospheric anomalies

is not well represented. It is missing completely for weak vortex events, and occuring only vaguely for strong vortex events in the Control simulation. Only very few strong vortex events were detected for CCSM4 RCP8.5; therefore the results for these events are difficult to evaluate. Nevertheless, a certain persistence of vortex anomalies at the 100 hPa level is also apparent in the CCSM4 simulations, although it is not as pronounced as in the CESM1(WACCM) simulations. The lower-quality representation of the downward coupling between the stratosphere and troposphere in the low-top model was to be expected as stratospheric dynamics are not well represented in a low-top model. This difference between the low- and high-top models is consistent with a study of *Charlton-Perez et al.* [2013], who investigated about 20 CMIP5 models and found much weaker persistence of negative NAM anomalies in the troposphere in low-top models compared to high-top models. For CCSM4 in particular, *Marsh et al.* [2013] showed that the occurrence of sudden stratospheric warmings (SSWs) is far below the observed frequency, and that the downward propagation of negative NAM anomalies is practically absent in that model.

Since the most pronounced connection between the stratosphere and the surface was found for the CESM1(WACCM) Natural and CESM1(WACCM) RCP8.5 simulations (only for weak vortex events in the latter case), these simulations were also expected to show the largest stratospheric signal on atmospheric and oceanic parameters at the air-sea interface. The composite analysis showed that this assumption was correct. Stratospheric polar vortex events connect well to an NAO-like signal at the surface for these simulations. For weak vortex events a negative NAO-like response was found, whereas for strong vortex events a positive NAO-like response was found. This response could be seen in sea level pressure (SLP), surface wind stress, as well as in surface turbulent heat fluxes. In the low-top model, on the other hand, the SLP anomalies following stratospheric vortex events did not show a signal as close to the NAO as seen in the high-top model. Nevertheless, heat flux and wind stress did show anomalies of the same sign compared to those found in the high-top model simulations. In both models, the anomalies found in SLP, turbulent heat flux and wind stress were generally a bit lower under the global warming scenario compared to the Control/Natural simulations.

To investigate the oceanic response to the NAO-like surface forcing connected to stratospheric polar vortex events the maximum mixed layer depth (MLD) was used. A generally deeper than normal MLD was found following strong vortex events, and vice versa for weak events. In CESM1(WACCM) this signal is strongest in the Labrador Sea, which is a very important region for deep water formation (showed explicitely for CCSM4 by

Danabasoglu et al. [2012a]) and therefore also for the variability of the AMOC. In CCSM4 the anomalies in MLD are restricted to a very small region at the southern edge of the Labrador Sea after strong polar vortex events and are not significant following weak polar vortex events. Since, in CESM1(WACCM), stratospheric events do influence the amount of Labrador Sea deep water formation (indicated by anomalies in MLD in that area) an influence on the variability of the AMOC is very likely in CESM1(WACCM) in contrast to CCSM4, where anomalies in MLD were almost absent.

The NAO-like response, that we found following stratospheric vortex events, was also described for example in *Reichler et al.* [2012], who examined strong vortex events in a low-top coupled GCM control simulation covering 4000 years. They found a surface forcing in SLP, turbulent heat flux and wind stress after the onset of strong polar vortex events that is closer to an NAO-like signal than our results for the low-top model. Additionally, they found outstanding periods marked by very strong or weak vortex events that persisted for several consecutive years, which were statistically connected to an anomaly in the strength of the AMOC. Such a connection could not be found in our study for the low-top model. The lack of MLD anomalies following weak and strong stratospheric polar vortex events in CCSM4 leads to the conclusion that the variability of the AMOC should not be affected by stratospheric events in that model. Though the work presented here did not regard weak and strong vortex events separately (which could be a point of future work), our results are in contrast to *Reichler et al.* [2012] because our work suggests that a low-top model was not able to adequately represent the influence of the stratosphere on the oceanic circulation. But also *Reichler et al.* [2012] clarified that the surface response following strong vortex events is stronger in high-top compared to low-top models.

Other studies have also shown that the connection between the atmosphere and the surface cannot be simulated correctly when stratospheric dynamics are missing. This was shown for example by *Omrani et al.* [2013], who investigated the influence of North Atlantic SST anomalies (captured by the Atlantic Multidecadal Variability - AMV) on the NAO using a low- and a high-top model (with lids at 10 and 0.01 hPa respectively). The low-top model was not able to simulate the NAO response that was observed to follow a positive AMV anomaly, but this response was simulated in the model that could resolve stratospheric dynamics. This corresponds well to our result that the CCSM4 model is unable to significantly connect stratsopheric polar vortex events to anomalies in MLD (and therefore also to AMOC variability), whereas in CESM1(WACCM) this connection

is simulated. Quantifying this stratospheric influence on the AMOC is unfortunately beyond the scope of this work but it would be an interesting topic to address in a future study.

Nevertheless, a simple connection between the NAM and AMOC was drawn by calculating the lead-lag correlation between both indices. The results differ very much between the simulations. In CESM1(WACCM) Natural the AMOC is strongly correlated with the stratospheric NAM when the NAM leads the AMOC by 2 years. In the RCP8.5 simulation, the correlation between NAM and AMOC decreases. For CCSM4 the stratospheric influence can not be seen in the correlation analysis, neither in the Control simulation nor in the GHG run. This was expected due to the lack of downward coupling in the low-top model and the missing stratospheric connection to the MLD. The connection between the NAO and the AMOC on the other hand (also described by a cross-correlation) is very clear: the NAO leads the AMOC by 4 years in CCSM4 Control as well as in CESM1(WACCM) Natural, with a correlation larger 0.7 in both cases. The lag of 4 years is a bit lower compared to the results of *Eden and Willebrand* [2001], who found a delay of 6 to 8 years between NAO and the oceanic response in the North Atlantic circulation. In the GHG simulations the correlations between NAO and AMOC decrease for both models: in CESM1(WACCM), the correlation between the AMOC and the NAO drops even below that between the AMOC and the stratospheric NAM. This change in dependencies under global warming is very interesting and requires further studies to be understood completely. In general, the lower correlation between the NAO/NAM and AMOC under global warming is consistent with our findings that the surface anomalies connected to stratopsheric events are weaker for the GHG runs compared to the Control/Natural runs.

To summarize, it could be shown that there is a surface response following a stratospheric polar vortex event that influences the formation of deep water masses in the Labrador Sea in CESM1(WACCM). This connection was not seen in CCSM4 although even here surface wind stress and heat fluxes deviated significantly from the mean state following a stratospheric event. Although the absolute influence of the stratosphere on the AMOC can not be inferred from the methods used here, including the representation of stratospheric dynamics and interactive chemistry in the model changes the surface behaviour. That was not only shown in the composite analysis but also in the evolution of MLD with time in the Labrador Sea, where CESM1(WACCM) showed a much higher variability in March MLD compared to CCSM4 and a different behaviour with regard to global climate change (Figure 2.14). The effect of global warming on the stratosphere-ocean coupling is

still not understood completely but one can infer from the correlation analysis done in this thesis that global warming could cause a change in the connection between the different compartments of the Earth System, and that a better understanding of these connections, including stratospheric dynamics could improve climate predictions, especially in regards to the strength of the AMOC.

The present study gives a first insight in the dependencies between stratopsheric polar vortex events and anomalies of atmospheric and oceanic parameters at the air-sea interface that influence North Atlantic deep water formation. To explain the differences between the high- and low-top simulations and to better understand the impact of global climate change further analysis regarding the physical processes behind these dependencies is required and will be addressed in future work.

Appendix A

Supplementary Figures

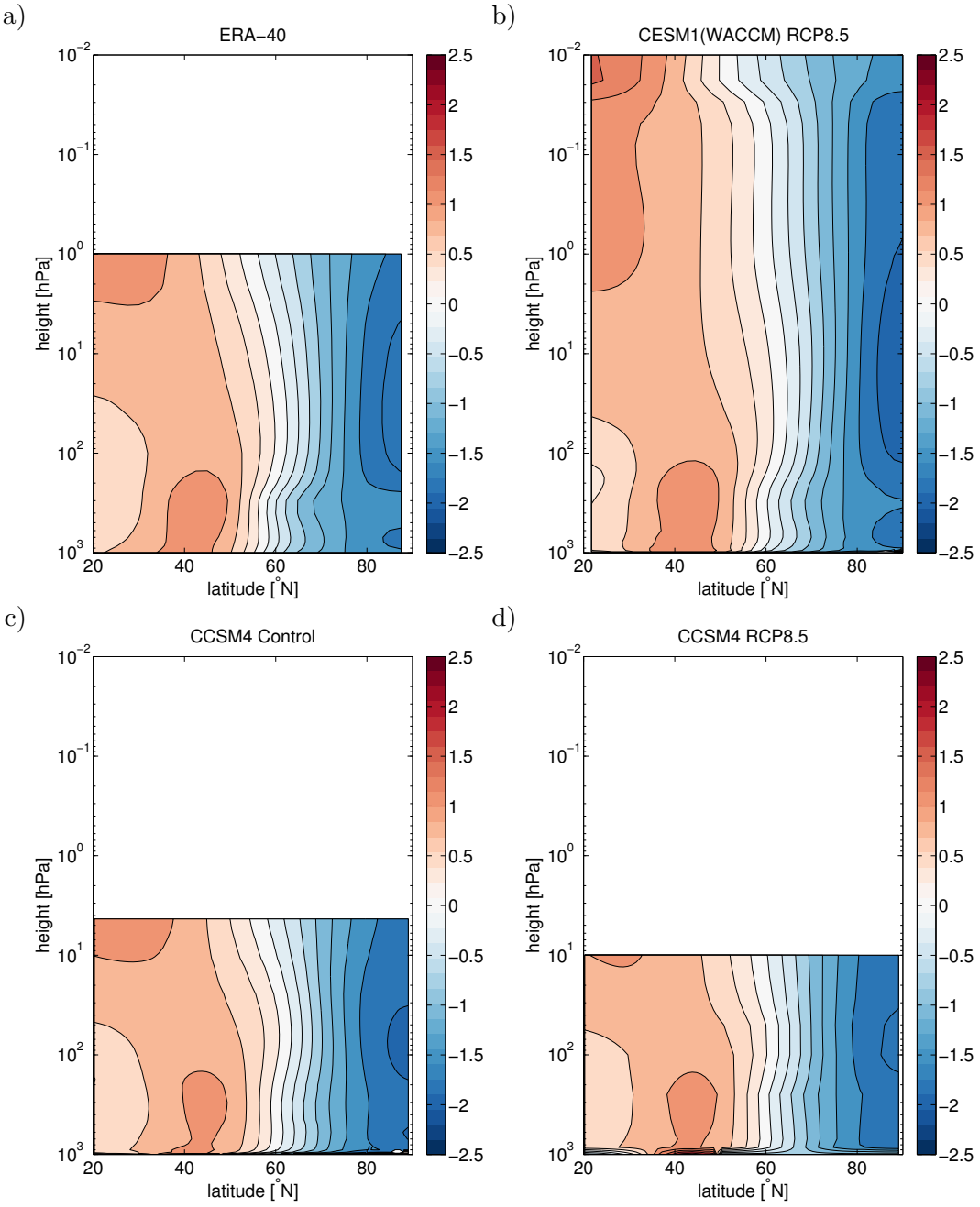

FIGURE A.1: Vertical profile of the Northern Annular Mode in a) ERA-40, b) CESM1(WACCM) RCP8.5, c) CCSM4 RCP8.5 and d) CCSM4 Control. Each level is normalized by its standard deviation. Dimensionless.

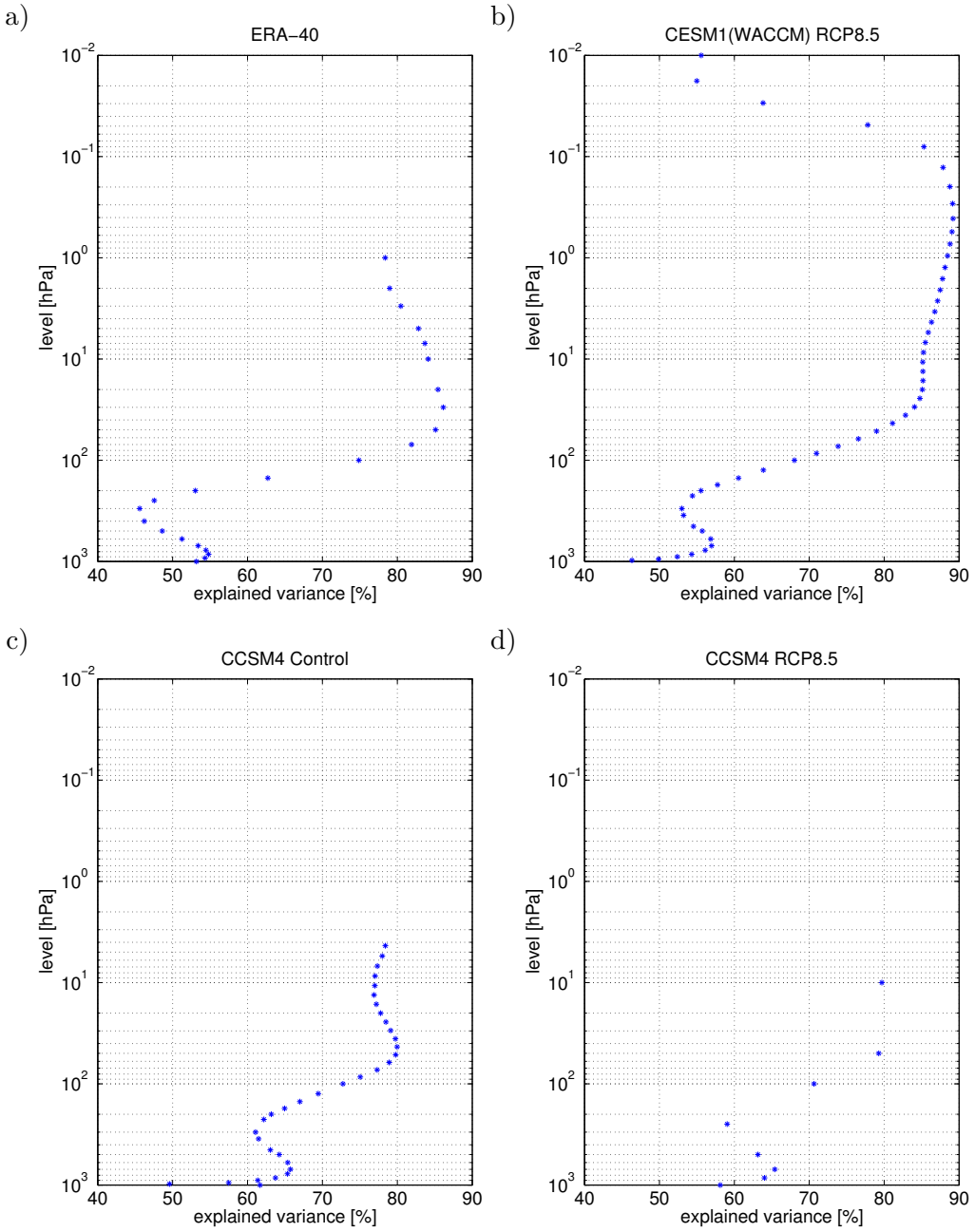

FIGURE A.2: Explained Variance of the Northern Annular Mode for each level in a) ERA-40, b) CESM1(WACCM) RCP8.5, c) CCSM4 RCP8.5 and d) in CCSM4 Control. The explained variance is given in %.

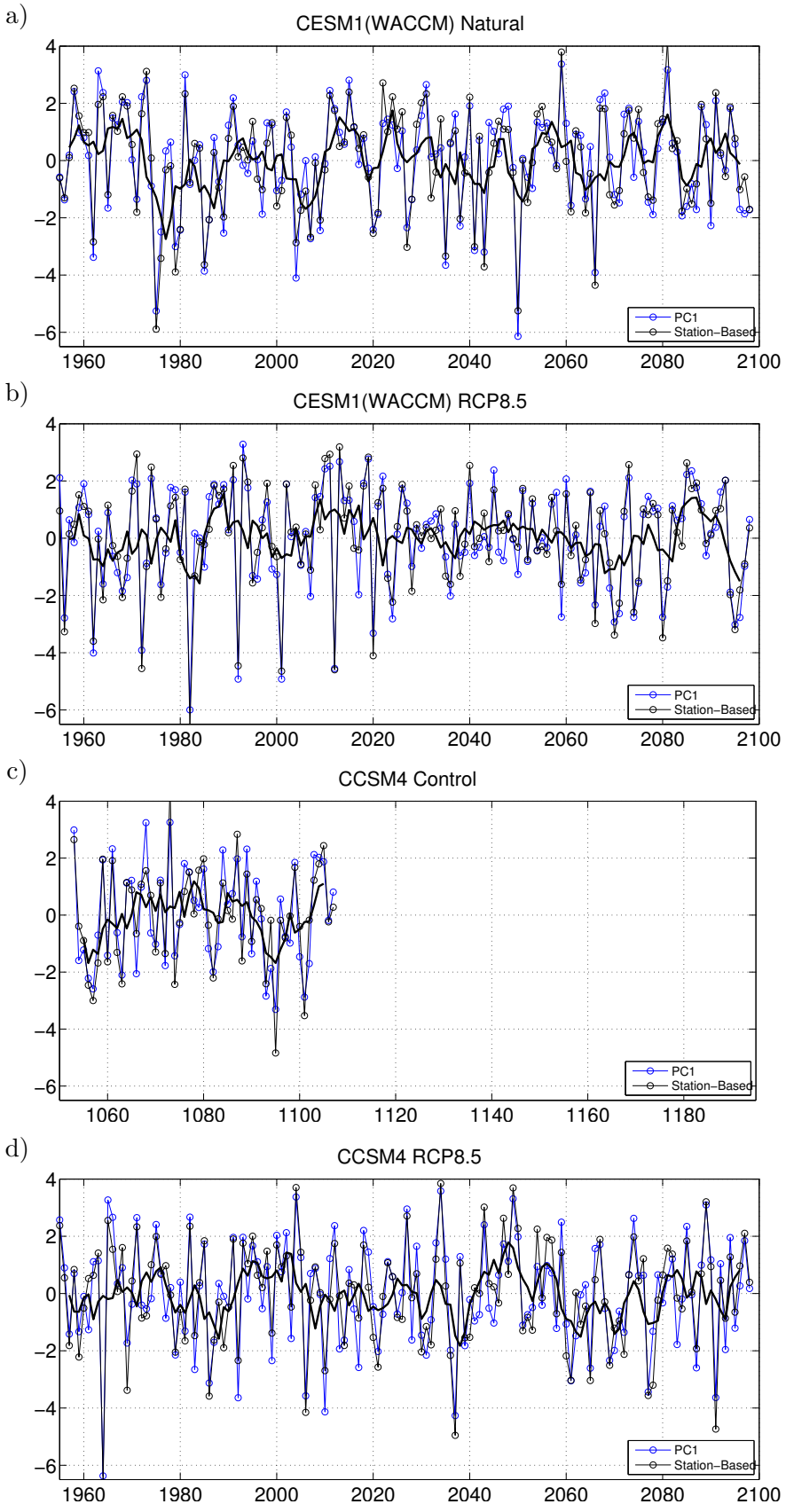

FIGURE A.3: Station-based (black) EOF-based (blue) NAO indices for a) CESM1-WACCM Natural, b) CESM1(WACCM) RCP8.5, c) CCSM4 Control and d) CCSM4 RCP8.5. 5-year running means calculated from station-based indices (bold line).

Bibliography

Alexander, M. A., and C. Deser (1995), A mechanism for the recurrence of wintertime midlatitude SST anomalies, *Journal of Physical Oceanography*, *25*, 122–137.

Andrews, D. G., J. R. Holton, and C. B. Leovy (1987), *Middle atmosphere dynamics*, 489 pp., Academic Press, San Diego, California.

Baldwin, M. P. (2001), Annular modes in global daily surface pressure, *Geophysical Research Letters*, *28*(21).

Baldwin, M. P., and T. J. Dunkerton (1999), Propagation of the Arctic Oscillation from the stratosphere to the troposphere, *Journal of Geophysical Research*, *104*(D24), 30,937–30,946, doi:10.1029/1999JD900445.

Baldwin, M. P., and T. J. Dunkerton (2001), Stratospheric harbingers of anomalous weather regimes., *Science*, *294*, 581–584, doi:10.1126/science.1063315.

Baldwin, M. P., and D. W. J. Thompson (2009), A critical comparison of stratosphere–troposphere coupling indices, *Quarterly Journal of the Royal Meteorological Society*, *135*, 1661–1672, doi:10.1002/qj.

Baldwin, M. P., X. Cheng, and T. J. Dunkerton (1994), Observed correlations between wintermean tropospheric and stratospheric circulation anomalies, *Geophysical Research Letters*, *21*(12), 1141–1144.

Baldwin, M. P., D. B. Stephenson, D. W. J. Thompson, T. J. Dunkerton, A. J. Charlton, and A. O'Neill (2003), Stratospheric memory and skill of extended-range weather forecasts., *Science*, *301*, 636–40, doi:10.1126/science.1087143.

Biastoch, A., C. W. Böning, and J. R. E. Lutjeharms (2008), Agulhas leakage dynamics affects decadal variability in Atlantic overturning circulation., *Nature*, *456*, 489–92, doi:10.1038/nature07426.

Böning, C. W., M. Scheinert, J. Dengg, A. Biastoch, and A. Funk (2006), Decadal variability of subpolar gyre transport and its reverberation in the North Atlantic overturning, *Geophysical Research Letters*, *33*, L21S01, doi:10.1029/2006GL026906.

Boyer, T. P., J. I. Antonov, H. E. Garcia, D. R. Johnson, R. A. Locarnini, A. V. Mishonov, M. T. Pitcher, O. K. Baranova, and I. V. Smolyar (2006), *World Ocean Database 2005*, 190 pp., NOAA Atlas NESDIS 60, U.S. Governement Printing Office, Washington, D.C.

Brasseur, G., and S. Solomon (2005), *Aeronomy of the middle atmosphere: Chemistry and physics of the stratosphere and mesosphere*, 3rd ed., 644 pp., Springer, Dordrecht.

Brewer, A. W. (1949), Evidence for a world circulation provided by the measurements of helium and water vapour distribution in the stratosphere, *Quarterly Journal of the Royal Meteorological Society*, *75*(326), 351–363, doi:10.1002/qj.49707532603.

Broecker, W. S., and T.-H. Peng (1982), *Tracers in the sea*, vol. 47, 690 pp., Eldigio Press, Palisades, New York.

Butchart, N. (2014), The Brewer-Dobson Circulation, *Reviews of Geophysics*, doi:10.1002/2013RG000448.

Carton, J. A., and B. S. Giese (2008), A Reanalysis of Ocean Climate Using Simple Ocean Data Assimilation (SODA), *Monthly Weather Review*, *136*(8), 2999–3017, doi:10.1175/2007MWR1978.1.

Charlton, A. J., and L. M. Polvani (2007), A new look at stratospheric sudden warmings. Part I: Climatology and modeling benchmarks, *Journal of Climate*, *20*, 449–470.

Charlton-Perez, A. J., M. P. Baldwin, T. Birner, R. X. Black, A. H. Butler, N. Calvo, N. A. Davis, E. P. Gerber, N. Gillett, S. Hardiman, J. Kim, K. Krüger, Y.-Y. Lee, E. Manzini, B. A. McDaniel, L. Polvani, T. Reichler, T. A. Shaw, M. Sigmond, S.-W. Son, M. Toohey, L. Wilcox, S. Yoden, B. Christiansen, F. Lott, D. Shindell, S. Yukimoto, and S. Watanabe (2013), On the lack of stratospheric dynamical variability in low-top versions of the CMIP5 models, *Journal of Geophysical Research: Atmospheres*, *118*(6), 2494–2505, doi:10.1002/jgrd.50125.

Charney, J. G., and P. G. Drazin (1961), Propagation of planetary-scale disturbances from the lower into the upper atmosphere, *Journal of Geophysical Research*, *66*(1), 83–109, doi:10.1029/JZ066i001p00083.

Cunningham, S. A., T. Kanzow, D. Rayner, M. O. Baringer, W. E. Johns, J. Marotzke, H. R. Longworth, E. M. Grant, J. J.-M. Hirschi, L. M. Beal, C. S. Meinen, and H. L. Bryden (2007), Temporal variability of the Atlantic meridional overturning circulation at 26.5 degrees N., *Science*, *317*, 935–938, doi:10.1126/science.1141304.

Danabasoglu, G., W. G. Large, J. J. Tribbia, P. R. Gent, B. P. Briegleb, and J. C. McWilliams (2006), Diurnal coupling in the tropical oceans of CCSM3, *Journal of Climate*, *19*, 2347–2365.

Danabasoglu, G., S. G. Yeager, Y.-O. Kwon, J. J. Tribbia, A. S. Phillips, and J. W. Hurrell (2012a), Variability of the Atlantic Meridional Overturning Circulation in CCSM4, *Journal of Climate*, *25*(15), 5153–5172, doi:10.1175/JCLI-D-11-00463.1.

Danabasoglu, G., S. C. Bates, B. P. Briegleb, S. R. Jayne, M. Jochum, W. G. Large, S. Peacock, and S. G. Yeager (2012b), The CCSM4 Ocean Component, *Journal of Climate*, *25*(5), 1361–1389, doi:10.1175/JCLI-D-11-00091.1.

de la Torre, L., R. R. Garcia, D. Barriopedro, and A. Chandran (2012), Climatology and characteristics of stratospheric sudden warmings in the Whole Atmosphere Community Climate Model, *Journal of Geophysical Research*, *117*, D04,110, doi:10.1029/2011JD016840.

Dee, D. P., S. M. Uppala, A. J. Simmons, P. Berrisford, P. Poli, S. Kobayashi, U. Andrae, M. A. Balmaseda, G. Balsamo, P. Bauer, P. Bechtold, A. C. M. Beljaars, L. van de Berg, J. Bidlot, N. Bormann, C. Delsol, R. Dragani, M. Fuentes, A. J. Geer, L. Haimberger, S. B. Healy, H. Hersbach, E. V. Hólm, L. Isaksen, P. Kå llberg, M. Köhler, M. Matricardi, A. P. McNally, B. M. Monge-Sanz, J.-J. Morcrette, B.-K. Park, C. Peubey, P. de Rosnay, C. Tavolato, J.-N. Thépaut, and F. Vitart (2011), The ERA-Interim reanalysis: configuration and performance of the data assimilation system, *Quarterly Journal of the Royal Meteorological Society*, *137*(656), 553–597, doi:10.1002/qj.828.

Dengler, M., J. Fischer, F. A. Schott, and R. Zantopp (2006), Deep Labrador Current and its variability in 1996–2005, *Geophysical Research Letters*, *33*(21), L21S06, doi:10.1029/2006GL026702.

Deser, C., A. S. Phillips, R. a. Tomas, Y. M. Okumura, M. a. Alexander, A. Capotondi, J. D. Scott, Y.-O. Kwon, and M. Ohba (2012), ENSO and Pacific Decadal Variability

in the Community Climate System Model Version 4, *Journal of Climate*, *25*(8), 2622–2651, doi:10.1175/JCLI-D-11-00301.1.

Dobson, G. M. B. (1956), Origin and Distribution of the Polyatomic Molecules in the Atmosphere, *Proceedings of the Royal Society A: Mathematical, Physical and Engineering Sciences*, *236*(1205), 187–193, doi:10.1098/rspa.1956.0127.

Eden, C., and T. Jung (2001), North Atlantic Interdecadal Variability: Oceanic Response to the North Atlantic Oscillation (1865–1997), *Journal of Climate*, *14*(5), 676–691, doi:10.1175/1520-0442(2001)014⟨0676:NAIVOR⟩2.0.CO;2.

Eden, C., and J. Willebrand (2001), Mechanism of interannual to decadal variability of the North Atlantic circulation., *Journal of Climate*, (1994), 2266–2280.

Gent, P. R., G. Danabasoglu, L. J. Donner, M. M. Holland, E. C. Hunke, S. R. Jayne, D. M. Lawrence, R. B. Neale, P. J. Rasch, M. Vertenstein, P. H. Worley, Z.-L. Yang, and M. Zhang (2011), The Community Climate System Model Version 4, *Journal of Climate*, *24*(19), 4973–4991, doi:10.1175/2011JCLI4083.1.

Guemas, V., and D. Salas-Mélia (2007), Simulation of the Atlantic meridional overturning circulation in an atmosphere-ocean global coupled model. Part II: weakening in a climate change experiment: a feedback mechanism, *Climate Dynamics*, *30*(7-8), 831–844, doi:10.1007/s00382-007-0328-8.

Hansen, B., S. Ø sterhus, D. Quadfasel, and W. Turrell (2004), Already the day after tomorrow?, *Science*, *305*(August), 953–954.

Hansen, F., K. Matthes, C. Petrick, and W. Wang (2014), The influence of natural and anthropogenic factors on Major Stratospheric Sudden Warmings, *submitted to Journal of Geophysical Research*, p. 58.

Hines, C. O. (1974), A possible mechanism for the production of sun-weather correlations, *Journal of the Atmospheric Sciences*, *31*, 589–591.

Holton, J. R. (2004), *An introduction to dynamic meteorology*, 4th ed., Elsevier Academic Press, San Diego, California.

Holton, J. R., P. H. Haynes, M. E. McIntyre, A. R. Douglass, R. B. Rood, and L. Pfister (1995), Stratosphere troposphere exchange, *Reviews of Geophysics*, *33*(4), 403–439.

Hurrell, J. W. (1995), Decadal Trends in the North Atlantic Oscillation: Regional Temperatures and Precipitation, *Science*, *269*, 676–679.

Hurrell, J. W., and C. Deser (2010), North Atlantic climate variability: The role of the North Atlantic Oscillation, *Journal of Marine Systems*, *79*(3-4), 231–244, doi:10.1016/j.jmarsys.2009.11.002.

Hurrell, J. W., Y. Kushnir, G. Ottersen, and M. Visbeck (2003), An Overview of the North Atlantic Oscillation, *Geophysical Monograph 134*, pp. 1–35, doi:10.1029/134GM01.

Hurrell, J. W., M. Holland, P. R. Gent, S. Ghan, J. E. Kay, P. J. Kushner, J.-F. Lamarque, W. Large, D. Lawrence, K. Lindsay, W. H. Lipscomb, M. C. Long, N. Mahowald, D. R. Marsh, R. B. Neale, P. Rasch, S. Vavrus, M. Vertenstein, D. Bader, W. Collins, J. Hack, J. Kiehl, and S. Marshall (2013), The Community Earth System Model: A Framework for Collaborative Research, *Bulletin of the American Meteorological Society*, doi:10.1175/BAMS-D-12-00121.

IPCC (2013), *Climate Change 2013: The Physical Science Basis. Contribution of Working Group I to the Fifth Assessment Report of the Intergovernmental Panel on Climate Change*, 1535 pp., Cambridge University Press, Cambridge, United Kingdom and New York, NY, USA.

Kanzow, T., S. A. Cunningham, W. E. Johns, J. J.-M. Hirschi, J. Marotzke, M. O. Baringer, C. S. Meinen, M. P. Chidichimo, C. Atkinson, L. M. Beal, H. L. Bryden, and J. Collins (2010), Seasonal Variability of the Atlantic Meridional Overturning Circulation at 26.5N, *Journal of Climate*, *23*(21), 5678–5698, doi:10.1175/2010JCLI3389.1.

Kushnir, Y. (1994), Interdecadal variations in North Atlantic sea surface temperature and associated atmospheric conditions, *Journal of Climate*, *7*, 141–157.

Labitzke, K., and B. Naujokat (2000), The lower Arctic stratosphere in winter since 1952, *Sparc Newsletter*, *15*, 11–14.

Lean, J., G. Rottman, J. Harder, and G. Kopp (2005), SORCE Contributions to New Understanding of Global Change and Solar Variability, *Solar Physics*, *230*(1-2), 27–53, doi:10.1007/s11207-005-1527-2.

Lozier, M. S. (2012), Overturning in the North Atlantic, *Annual Review of Marine Science*, *4*(1), 291–315, doi:10.1146/annurev-marine-120710-100740.

Lozier, M. S., V. Roussenov, M. S. C. Reed, and R. G. Williams (2010), Opposing decadal changes for the North Atlantic meridional overturning circulation, *Nature Geoscience*, *3*(10), 728–734, doi:10.1038/ngeo947.

Marsh, D. R., M. J. Mills, D. E. Kinnison, J.-F. Lamarque, N. Calvo, and L. M. Polvani (2013), Climate Change from 1850 to 2005 Simulated in CESM1(WACCM), *Journal of Climate*, *26*(19), 7372–7391, doi:10.1175/JCLI-D-12-00558.1.

Marshall, J., and R. Plumb (2008), *Atmosphere, ocean and climate dynamics: an introductory text*, 319 pp., Elsevier Academic Press, San Diego, California.

Marshall, J., and F. Schott (1999), Open ocean convection: Observations, theory, and models, *Reviews of Geophysics*, *37*, 1–64.

McLandress, C., and T. G. Shepherd (2009), Impact of Climate Change on Stratospheric Sudden Warmings as Simulated by the Canadian Middle Atmosphere Model, *Journal of Climate*, *22*(20), 5449–5463, doi:10.1175/2009JCLI3069.1.

Meinshausen, M., S. J. Smith, K. Calvin, J. S. Daniel, M. L. T. Kainuma, J.-F. Lamarque, K. Matsumoto, S. A. Montzka, S. C. B. Raper, K. Riahi, A. Thomson, G. J. M. Velders, and D. P. Vuuren (2011), The RCP greenhouse gas concentrations and their extensions from 1765 to 2300, *Climatic Change*, *109*, 213–241, doi:10.1007/s10584-011-0156-z.

Omrani, N.-E., N. S. Keenlyside, J. Bader, and E. Manzini (2013), Stratosphere key for wintertime atmospheric response to warm Atlantic decadal conditions, *Climate Dynamics*, *42*, 649–663, doi:10.1007/s00382-013-1860-3.

Perlwitz, J., and H.-F. Graf (1995), The statistical connection between tropospheric and stratospheric circulation of the Northern Hemisphere in winter, *Journal of Climate*, *8*, 2281–2295.

Pickart, R. S., F. Straneo, and G. Moore (2003), Is Labrador Sea Water formed in the Irminger basin?, *Deep Sea Research Part I: Oceanographic Research Papers*, *50*(1), 23–52, doi:10.1016/S0967-0637(02)00134-6.

Rayner, D., J. J.-M. Hirschi, T. Kanzow, W. E. Johns, P. G. Wright, E. Frajka-Williams, H. L. Bryden, C. S. Meinen, M. O. Baringer, J. Marotzke, L. M. Beal, and S. A. Cunningham (2011), Monitoring the Atlantic meridional overturning circulation, *Deep*

Sea Research Part II: Topical Studies in Oceanography, *58*(17-18), 1744–1753, doi: 10.1016/j.dsr2.2010.10.056.

Reichler, T., J. Kim, E. Manzini, and J. Kröger (2012), A stratospheric connection to Atlantic climate variability, *Nature Geoscience*, *5*(11), 783–787, doi:10.1038/ngeo1586.

Richardson, P. L. (2008), On the history of meridional overturning circulation schematic diagrams, *Progress in Oceanography*, *76*(4), 466–486, doi:10.1016/j.pocean.2008.01.005.

Scherhag, R. (1952), Die explosionsartige Stratosphären-Erwärmung des Spätwinters 1951/52, *Berichte des Deutschen Wetterdienstes in der US Zone*, *38*.

Schott, F. A., and P. Brandt (2007), Circulation and deep water export of the subpolar North Atlantic during the 1990's, *Geophysical Monograph Series*, *173*, 91–118.

Schott, F. A., L. Stramma, B. S. Giese, and R. Zantopp (2009), Labrador Sea convection and subpolar North Atlantic Deep Water export in the SODA assimilation model, *Deep Sea Research Part I: Oceanographic Research Papers*, *56*(6), 926–938, doi:10.1016/j.dsr. 2009.01.001.

Sutton, R. T., and D. L. R. Hodson (2005), Atlantic Ocean forcing of North American and European summer climate, *Science*, *309*, 115–118, doi:10.1126/science.1109496.

Thompson, D., and J. Wallace (1998), The Arctic Oscillation signature in the wintertime geopotential height and temperature fields, *Geophysical Research Letters*, *25*(9), 1297–1300.

Thompson, D., and J. Wallace (2000), Annular modes in the extratropical circulation. Part I: month-to-month variability*, *Journal of Climate*, *13*, 1000–1016.

Thompson, D. W. J., S. Lee, and M. P. Baldwin (2003), Atmospheric processes governing the northern hemisphere annular mode/North Atlantic oscillation, *Geophysical Monograph 134*, pp. 1–31.

Trenberth, K. E., and J. M. Caron (2001), Estimates of Meridional Atmosphere and Ocean Heat Transports, *Journal of Climate*, *14*(16), 3433–3443, doi:10.1175/1520-0442(2001) 014⟨3433:EOMAAO⟩2.0.CO;2.

Uppala, S. M., P. W. Kå llberg, A. J. Simmons, U. Andrae, V. D. C. Bechtold, M. Fiorino, J. K. Gibson, J. Haseler, A. Hernandez, G. A. Kelly, X. Li, K. Onogi, S. Saarinen, N. Sokka, R. P. Allan, E. Andersson, K. Arpe, M. A. Balmaseda, A. C. M.

Beljaars, L. V. D. Berg, J. Bidlot, N. Bormann, S. Caires, F. Chevallier, A. Dethof, M. Dragosavac, M. Fisher, M. Fuentes, S. Hagemann, E. Hólm, B. J. Hoskins, L. Isaksen, P. A. E. M. Janssen, R. Jenne, A. P. Mcnally, J.-F. Mahfouf, J.-J. Morcrette, N. A. Rayner, R. W. Saunders, P. Simon, A. Sterl, K. E. Trenberth, A. Untch, D. Vasiljevic, P. Viterbo, and J. Woollen (2005), The ERA-40 re-analysis, *Quarterly Journal of the Royal Meteorological Society*, *131*(612), 2961–3012, doi:10.1256/qj.04.176.

Visbeck, M., J. W. Hurrell, L. Polvani, and H. M. Cullen (2001), The North Atlantic Oscillation: past, present, and future., *Proceedings of the National Academy of Sciences of the United States of America*, *98*(23), 12,876–7, doi:10.1073/pnas.231391598.

Visbeck, M., E. P. Chassignet, R. G. Curry, T. L. Delworth, R. R. Dickson, and G. Krahmann (2003), The ocean's response to North Atlantic Oscillation variability, *Geophysical Monograph 134*, pp. 113–145.

Walker, G. T., and E. W. Bliss (1932), World weather, *Memoirs of the Royal Meteorological Society*, *4*(36), 53–84.

Erklärung

Hiermit erkläre ich, dass ich die vorliegende Arbeit selbständig und ohne fremde Hilfe angefertigt und keine anderen als die angegebenen Quellen und Hilfsmittel verwendet habe. Die eingereichte schriftliche Fassung der Arbeit entspricht der auf dem elektronischen Speichermedium (Name der Datei: MA-945327.pdf).

Weiterhin versichere ich, dass diese Arbeit noch nicht als Abschlussarbeit an anderer Stelle vorgelegen hat.

Kiel, den 16.05.2014

Sabine Haase